

A NEW REFERENCE CHEMICAL COMPOSITION FOR TMC-1

P. GRATIER

Laboratoire d'astrophysique de Bordeaux, Univ. Bordeaux, CNRS, B18N, alle Geoffroy Saint-Hilaire, 33615 Pessac, France

AND

L. MAJUMDAR

Laboratoire d'astrophysique de Bordeaux, Univ. Bordeaux, CNRS, B18N, alle Geoffroy Saint-Hilaire, 33615 Pessac, France and
Indian Centre for Space Physics, Chalandika 43, Garia Station Road, Kolkata 700084, India

AND

M. OHISHI

Department of Astronomical Science, The Graduate University for Advanced Studies (SOKENDAI), Osawa 2-21-1, Mitaka, Tokyo
181-8588, Japan
National Astronomical Observatory of Japan, Osawa 2-21-1, Mitaka, Tokyo 181-8588, Japan

AND

E. ROUEFF

LERMA, Observatoire de Paris, PSL Research University, CNRS, UMR8112, Place Janssen, F-92190, Meudon Cedex, France
Sorbonne Universités, UPMC Univ. Paris 6, 4 Place Jussieu, F-75005, Paris, France

AND

J. C. LOISON

Université de Bordeaux, Institut des Sciences Moléculaires, UMR 5255, F-33400 Talence, France

AND

K. M. HICKSON

Université de Bordeaux, Institut des Sciences Moléculaires, UMR 5255, F-33400 Talence, France

AND

V. WAKELAM

Laboratoire d'astrophysique de Bordeaux, Univ. Bordeaux, CNRS, B18N, alle Geoffroy Saint-Hilaire, 33615 Pessac, France

ABSTRACT

Recent detections of complex organic molecules in dark clouds have rekindled interest in the astrochemical modeling of these environments. Because of its relative closeness and rich molecular complexity, TMC-1 has been extensively observed to study the chemical processes taking place in dark clouds. We use local thermodynamical equilibrium radiative transfer modeling coupled with a Bayesian statistical method which takes into account outliers to analyze the data from the Nobeyama spectral survey of TMC-1 between 8 and 50 GHz. We compute the abundance relative to molecular hydrogen of 57 molecules, including 19 isotopologues in TMC-1 along with their associated uncertainty. The new results are in general agreement with previous abundance determination from Ohishi & Kaifu and the values reported in the review from Agúndez & Wakelam. However, in some cases, large opacity and low signal to noise effects allow only upper or lower limits to be derived, respectively.

Subject headings: ISM: abundances — ISM: evolution — astrochemistry — methods: statistical

1. INTRODUCTION

Complex organic molecules (COMs; e.g., CH₃OH, CH₃CHO, HCOOCH₃, CH₃OCH₃, see Herbst & van Dishoeck 2009) were detected in various sources, e.g. hot cores or hot corinos or warm star-forming regions such as SgB2 (Cummins et al. 1986), OMC-1 (Blake et al. 1987), or IRAS 16293-2422 (Bottinelli et al. 2004). Matthews et al. (1985) and Friberg et al. (1988) also detected some of these COMs (CH₃OH and CH₃CHO) in the TMC-1 and L134N dark clouds. Recently, Cernicharo et al. (2012) detected the methoxy radical (CH₃O) in the B1 cold dense core. Bacmann et al. (2012) also reported the detections of a variety of COMs (CH₃OH, CH₃OCH₃, CH₃OCHO, CH₂CO) in the cold prestellar core L1689b along with few more recent detections of additional COMs (C₃O, t-HCOOH) in the L1544 prestellar core reported by Vastel et al. (2014). These detections have triggered a renewed interest in the study of the as-

trochemistry of these environments (Garrod & Herbst 2006; Herbst & Cuppen 2006; Vasyunin & Herbst 2013; Ruaud et al. 2015). Among the different COMs, CH₃OH is the only one for which the production is well understood. Its formation goes through the successive hydrogenation of carbon monoxide accreted from the gas phase on ice mantles of interstellar dust grains (Watanabe & Kouchi 2002). For several other COMs, studies by Vasyunin & Herbst (2013) and Ruaud et al. (2015) have shown that non-thermal desorption processes can bring COMs to the gas phase from the grain surfaces in regions where the grain temperatures remain low ($T_{\text{dust}} < 15$ K) and the UV radiation is also very low ($A_v > 10$) for a standard interstellar radiation field.

Astrochemical models are based on microphysics processes that can be studied in laboratories or computed by quantum chemistry theories. Nevertheless, these models must be benchmarked on template sources that are ex-

tensively studied. TMC-1 is very close (140 pc; Elias 1978; Kenyon et al. 1994) with a very rich molecular composition and has thus been extensively observed to understand dark cloud chemistry. In order to improve astrochemical models, their outputs must be compared to the widest set of observations as possible. Spectral surveys enable the unbiased detection of a large number (several tens) of species, often with many detected lines per species, while at the same time minimizing relative calibration errors. With the advent of new wideband receivers and spectrometers, spectral surveys are *de facto* the default observation mode at millimeter facilities. To interpret this wealth of data, new statistical tools have to be devised.

In this article, we propose to use a Bayesian approach to compute abundance values along with uncertainty estimates associated with all the detected molecules in the Nobeyama spectral survey of TMC-1 from Kaifu et al. (2004).

The paper is organized as follows. We present the observational and spectroscopic data used in Sect 2, the methods to determine abundances in Sect. 3, and the derived values of abundances in Sect. 4. Finally, these results are discussed and compared with previous abundance values from the literature in Sect. 5. The Appendix presents, in detail, the Bayesian statistical method used and the individual results for all molecules.

2. DATA

2.1. Observational data

Kaifu et al. (2004) used the Nobeyama 45m dish between 1984 and 1996 to observe a full spectral survey of the Cyanopolyne peak position of TMC-1 (for the rest of the article, we will use TMC-1 as a shorthand for TMC-1(CP)) between 8.8 and 50 GHz with a spectral resolution of 37 kHz (this corresponds to a velocity resolution ranging from 1.26 km s^{-1} to 0.22 km s^{-1}) with a typical sensitivity of 10 mK per channel.

The observational data from Kaifu et al. (2004) consists of integrated intensities associated with a single (or several in the case of unresolved hyperfine structure) line of a given molecule. These integrated intensities are computed by fitting Gaussian line profiles to the spectral data. No uncertainty is given for these integrated intensities but the authors give a measured line width ΔV and a local noise level per channel σ . From these values, we compute the noise on the integrated intensity, assuming a gaussian profile, using the following formula:

$$\sigma_I = \sqrt{\frac{2\pi}{8 \ln 2}} \sigma \Delta V \simeq 1.064 \sigma \Delta V \quad (1)$$

,where the numerical term comes from the integral of a gaussian function of $FWHM = \Delta V$

The data from Kaifu et al. (2004) take into account the coupling with the source (they assume TMC-1 is a gaussian source of $FWHM 160''$). Thus, the column densities and abundances we compute correspond to this spatial scale.

2.2. Spectroscopic data

Under the local thermal equilibrium hypothesis, integrated intensities are dependent on a set of microphysic parameters: the Einstein coefficients of spontaneous de-excitation between levels i and j : A_{ij} , the degeneracy

of the upper level i , g_i , the energy of the upper level i , E_i , and the partition function $Q(T)$ measuring the number of occupied states at temperature T . These values are available from online databases, mainly the CDMS (Müller et al. 2005) and the JPL Spec databases (Pickett et al. 1998). The online databases often only give values of the partition functions down to a temperature of 9.75 K but the measured excitation temperatures in dark clouds are often lower than that. Using the energy levels E_i and the corresponding level degeneracies g_i , we compute when necessary the values of the partition function at 2.375 and 5 K using the following formula

$$Q(T) = \sum_i g_i \exp^{-\frac{E_i}{kT}}. \quad (2)$$

We systematically check that the value obtained by this sum for 9.75 K is similar to the tabulated value of the databases.

Between these tabulated values, the logarithm of the partition function is interpolated linearly in temperature. The last two columns of Table 2 give the source of the spectroscopic parameters and the lowest temperature for which the partition function values are tabulated in the databases.

3. METHODS

3.1. Local Thermal Equilibrium

We determine the column densities and abundances in the local thermodynamical equilibrium (LTE) hypothesis. For a given molecule, we compute the integrated intensities for each line, using the hypothesis of gaussian opacity profiles as a function of frequency. The modeled opacity is a function of the species column density, excitation temperature, and line width. The integrated intensity is derived from the opacity assuming a temperature of the cosmic microwave background of 2.73 K.

Some lines detected in Kaifu et al. (2004) are attributed to several blended transitions of a given molecule. In this case, we sum the computed intensity for the identified transitions. Following Ohishi & Kaifu (1998), the column density of a species X , noted $[X]$ are converted into abundance assuming a constant molecular hydrogen column density of $N(\text{H}_2) = 10^{22} \text{ cm}^{-2}$:

$$[X] = N(X)/N(\text{H}_2) \quad (3)$$

3.2. Bayesian approach: outlier detection

We devise a Bayesian approach which enables to retrieve the LTE model parameter distributions. The advantages of a Bayesian approach over a more traditional optimization approach are threefold.

1. The full distribution of parameters can be recovered. This means that upper abundance limits in the case of marginal detections and lower abundance limits in the case of highly optically thick lines are readily obtained.
2. Prior knowledge can be included for some parameters. For example, with a single detected line, the abundance can only be constrained by assuming a prior value of the excitation temperature. A Bayesian approach enables us to include a prior *distribution* of excitation temperatures. The derived

abundance then takes into account the prior uncertainty on the knowledge of the excitation temperature.

3. Additional parameters can be added to the model, for example, to identify data points that are outlier to the physical model. These additional parameters are marginalized out in the end to obtain a posterior distribution of the parameters of interest; in our case, the molecular abundances.

For a few of the molecules, some of the integrated intensities were clearly outliers and could not be modeled consistently with the rest of the data set. This can arise when a line has either: (1) erroneous spectroscopic parameters, (2) been misattributed to the modeled species, or (3) when a line from another species is blended with one from the modeled species. The method we have developed automatically takes into account the probability of each data point of being an outlier. This enables us to recover the parameters for the modeled species such as the abundance and excitation temperature in a robust way. Although the method is applied to radiative transfer modeling of molecular lines, it is quite general and can be readily applied to a wide range of problems where outlier detection is needed.

The model parameters are divided into two groups: the first concerning the LTE modeling, and the second concerning the modeling of outliers. The LTE model parameters are the column density N , the excitation temperature T_{ex} , the line width ΔV , and a scatter term σ that enables us to describe both the possible underestimation of the observational uncertainty and the fact that the LTE model is simpler than would be needed to perfectly describe the observations. The outlier model parameters are the two parameters (mean integrated intensity Y_o and dispersion around this mean σ_o) describing the gaussian distribution from which the outliers are supposed to be originating. Additionally, each data point is attributed a binary parameter q_i which can take a value of either 0 if the point is an outlier or 1 if the point is not. There are thus as many q_i as there are data points. A final parameter is P_o the probability that a point is an outlier considering the binomial distribution of the q_i parameters. It is possible to analytically marginalize the q_i parameters while at the same time recovering the posterior probability of a point being an outlier. The full model thus has 10 free parameters and does not become more complicated to solve as the number of data points increase.

The mathematical details of this approach, in particular the expression of the likelihood used, are presented in Appendix A.

When only a single line is detected for a given species, the identification of outliers makes no sense. In this case, the number of parameters is limited to four: N , T_{ex} , ΔV , and $\log \sigma$. Since with only one line the additional scatter parameter is completely unconstrained, an informative prior consisting of a gaussian function of mean -1.2 and standard deviation 0.4 was used. This is the median and sample standard deviation of the values of $\log \sigma$ determined from the 26 species with more than 2 detected lines.

The Bayesian approach requires us to choose prior distributions for all model parameters. Some of them can

be rather uninformative. For example the prior distribution of the logarithm of the column density is chosen to be uniform between 9 and 17 (with the column density in units of cm^{-2}). Similarly, the prior probability of the outliers P_o is chosen as uniform between 0 and 1. Conversely, we use informative priors on two specific parameters. Following previous studies (Ohishi & Kaifu 1998) that found excitation temperatures around 5 K in TMC-1, we use a gaussian prior on T_{ex} of mean 5 K and standard deviation 2 K along with a lower temperature limit of 2.73 K corresponding to the background temperature. Similarly, we choose a gaussian distribution of mean 0.5 km s^{-1} and standard deviation 0.2 km s^{-1} for the prior distribution of line widths. Table 1 summarizes these choices.

4. RESULTS

Table 2 summarizes the derived abundances for observed molecules toward TMC-1 by means of the Bayesian approach. In this table, column (1) is the species name, column (2) is the median value of the abundance along with the associated 68% (1σ) confidence interval, column (3) is similar to column (2) for the excitation temperature, column (4) is the peak signal-to-noise ratio, the ratio between the intensity of the brightest line of each molecule to the noise computed for the fit of this molecule, column (5) is the range of opacities spanned by the lines of a given species, column (6) is the source of the spectroscopic data, and column (7) is the minimum temperature for which the partition functions are tabulated in the spectroscopic databases; below these temperatures, the partition functions are extrapolated according to equation 2. Individual fits to the observed data are shown in Appendix B

4.1. Main isotopes

Figure 1 gives a graphical representation of the computed abundances for the main isotope-bearing molecules.

Three main classes of outcomes can be identified. For some molecules, all observed lines have high opacities, and in these cases only lower limits can be placed on their abundances. This is the case for CS and SO. For other molecules, the signal-to-noise ratio is not sufficient enough to obtain more than an upper limit on the abundances. This is the case for C_2O and OCS. For all other molecules, it is possible to determine an abundance along with an associated uncertainty.

4.2. Isotopologues

Twenty isotopologues are also detected in the Nobeyama survey of TMC-1. We have computed their abundances relative to H_2 and the ratio of the minor isotopologues to the main isotopologues for each molecule. The results are summarized in Fig. 2 and Table 3.

5. DISCUSSION

5.1. Outlier lines

Using the Bayesian approach we have demonstrated that it is possible to identify outliers in the data set: observed line intensities that are not explainable by the global model best fitting the rest of the lines for a given species. Table 4 summarizes the properties of the outlier lines.

TABLE 1
PRIOR PARAMETER DISTRIBUTIONS

Parameter	Distribution	Expression	Lower bound	Upper bound
$\log N$	Uniform	$p(\log N) = [(\log N)_{max} - (\log N)_{min}]^{-1}$	9	17
T_{ex}	Gaussian	$p(T_{ex}) = \mathcal{N}(5, 2)$	2.73	20
ΔV	Gaussian	$p(\Delta V) = \mathcal{N}(0.5, 0.2)$	0	3
$\log \sigma$	Uniform	$p(\log \sigma) = [(\log \sigma)_{max} - (\log \sigma)_{min}]^{-1}$	-3	1
$\log \sigma$	Gaussian ^(a)	$p(\log \sigma) = \mathcal{N}(-1.2, 0.4)$	-3	1
Y_o	Uniform	$p(Y_o) = [(Y_o)_{max} - (Y_o)_{min}]^{-1}$	0	10
$\log \sigma_o$	Uniform	$p(\log \sigma_o) = [(\log \sigma_o)_{max} - (\log \sigma_o)_{min}]^{-1}$	-3	2
$\{q_i\}$	Binomial	$p(\{q_i\}) = \prod_{i=1}^N [1 - P_o]^{q_i} P_o^{[1-q_i]}$		
P_o	Uniform	$p(P_o) = 1$	0	1

(a): The gaussian prior is used when only one line of a given molecule is detected.

TABLE 2
BEST-FIT PARAMETERS BY THE BAYESIAN APPROACH FOR MAIN ISOTOPE-BEARING SPECIES

Species	$\log N^a$ (cm^{-2})	T_{ex} (K)	PSNR	τ range	Number of Transitions	Min Partition Function Temp	Appendix Figure
NH ₃	14.70(-2.33, +0.61)	6.16(-1.92, +1.76)	26.8	0.00 - 0.73	6	9.375†	B1
CH ₃ OH	13.16(-1.79, +0.25)	5.22(-1.43, +1.95)	2.0	0.00 - 0.31	1	9.375†	B2
c-C ₃ H	13.48(-0.05, +0.07)	5.73(-1.29, +1.58)	12.7	0.02 - 0.12	6	9.375†	B3
l-C ₃ H	12.75(-0.03, +0.07)	5.90(-1.40, +1.56)	14.5	0.03 - 0.14	6	9.375	B4
l-C ₃ H ₂	11.77(-1.90, +0.50)	6.02(-1.97, +1.77)	1.6	0.01 - 0.04	4	9.375	B5
c-C ₃ H ₂	13.27(-2.90, +1.13)	5.45(-1.53, +1.86)	6.6	0.07 - 0.59	4	2.725	B6
CH ₃ CCH	14.06(-1.26, +1.16)	5.47(-1.89, +2.03)	2.6	0.08 - 0.39	3	9.375	B9
C ₂ O	< 12.57	5.50(-1.57, +1.71)	0.4	< 0.02	1	9.375†	B10
H ₂ CCN	13.58(-0.34, +0.24)	3.46(-0.35, +1.66)	5.3	0.01 - 1.74	38	9.375	B11
CH ₃ CN	12.61(-0.18, +0.19)	5.04(-1.27, +1.85)	3.2	0.04 - 0.20	5	2.725	B12
H ₂ CCO	12.68(-1.71, +0.35)	9.50(-4.68, +3.46)	1.6	0.01 - 0.01	3	2.725	B13
HNCO	13.03(-0.05, +0.10)	5.26(-1.09, +1.58)	10.5	0.03 - 0.24	5	9.375†	B14
CS	> 13.46	4.45(-0.52, +1.60)	24.2	> 3.96	1	2.725	B15
CH ₃ CHO	12.43(-2.03, +0.31)	5.24(-1.49, +1.80)	1.7	0.04 - 0.04	2	9.375†	B16
HCS ⁺	12.76(-0.38, +0.53)	5.33(-1.74, +1.62)	5.5	0.10 - 3.37	1	9.375	B18
H ₂ CS	13.62(-0.13, +0.53)	5.16(-1.55, +1.55)	7.7	0.26 - 6.74	1	2.725	B21
SO	> 13.67	4.44(-1.21, +2.06)	11.8	> 0.50	1	2.725	B23
C ₄ H	[13.43, 14.94] ^b	4.79(-0.39, +0.62)	26.4	0.03 - 2.78	27	9.375	B24
o-C ₄ H ₂	13.28(-0.30, +0.23)	5.04(-0.77, +1.52)	6.5	0.08 - 0.25	8	9.375	B25
p-C ₄ H ₂	12.42(-0.49, +0.45)	4.63(-1.18, +1.78)	3.6	0.10 - 0.22	4	9.375	B27
C ₃ N	13.55(-0.30, +0.21)	3.31(-0.22, +0.64)	3.6	0.13 - 0.94	12	9.375	B28
HC ₃ N	14.37(-0.06, +0.13)	5.22(-0.58, +0.80)	33.0	0.04 - 19.50	20	2.725	B29
HNC ₃	11.68(-0.18, +0.19)	5.69(-1.67, +1.97)	3.5	0.05 - 0.12	4	9.375†	B30
HCCNC	12.93(-0.11, +0.31)	5.41(-1.45, +1.80)	5.0	0.04 - 0.27	5	9.375†	B31
C ₃ O	11.92(-1.29, +0.25)	5.03(-1.23, +1.77)	1.7	0.04 - 0.04	2	9.375	B37
HC ₃ NH ⁺	11.87(-1.81, +0.45)	5.55(-1.49, +1.85)	1.4	0.01 - 0.01	2	9.375	B38
CH ₂ CHCN	12.81(-0.08, +0.22)	5.00(-1.36, +2.07)	3.9	0.04 - 0.21	12	9.375	B39
HCCCHO	11.26(-1.54, +0.95)	5.29(-1.42, +1.39)	0.7	0.00 - 0.08	1	9.375	B40
C ₂ S	14.01(-0.16, +0.14)	4.19(-0.34, +0.60)	9.9	0.28 - 5.08	8	9.375	B41
OCS	< 13.26	5.27(-1.39, +1.88)	0.7	< 0.06	1	9.375	B42
C ₅ H	12.27(-0.10, +0.12)	4.80(-0.72, +0.94)	4.7	0.03 - 0.05	16	9.375	B43
CH ₃ C ₄ H	13.17(-0.17, +0.23)	6.85(-2.01, +1.68)	2.7	0.01 - 0.04	8	2.725	B44
CH ₃ C ₃ N	11.99(-0.17, +0.18)	6.26(-1.71, +1.63)	2.8	0.01 - 0.05	8	2.725	B45
C ₃ S	13.14(-0.11, +0.16)	5.19(-0.70, +0.90)	7.4	0.22 - 0.83	7	2.725	B46
C ₆ H	12.74(-0.05, +0.04)	5.95(-0.45, +0.35)	6.1	0.04 - 0.09	42	9.375	B47
HC ₅ N	13.77(-0.09, +0.10)	6.39(-0.51, +0.54)	9.5	0.20 - 2.33	16	9.375	B48
HC ₇ N	13.66(-0.10, +0.14)	6.14(-0.41, +0.32)	14.3	0.04 - 3.52	34	9.375	B56
HC ₉ N	13.02(-0.06, +0.06)	8.51(-1.15, +1.07)	4.6	0.00 - 0.03	16	9.375	B57

Spectroscopic data from the CDMS database except for species marked by a † which are from form the JPL database. (a): The abundance $[X]$ can be derived using $N(X)/N(H_2)$ with $N(H_2) = 10^{22} cm^{-2}$

(b): Values in bracket are the 1σ confidence interval. See the text for details concerning these specific molecules.

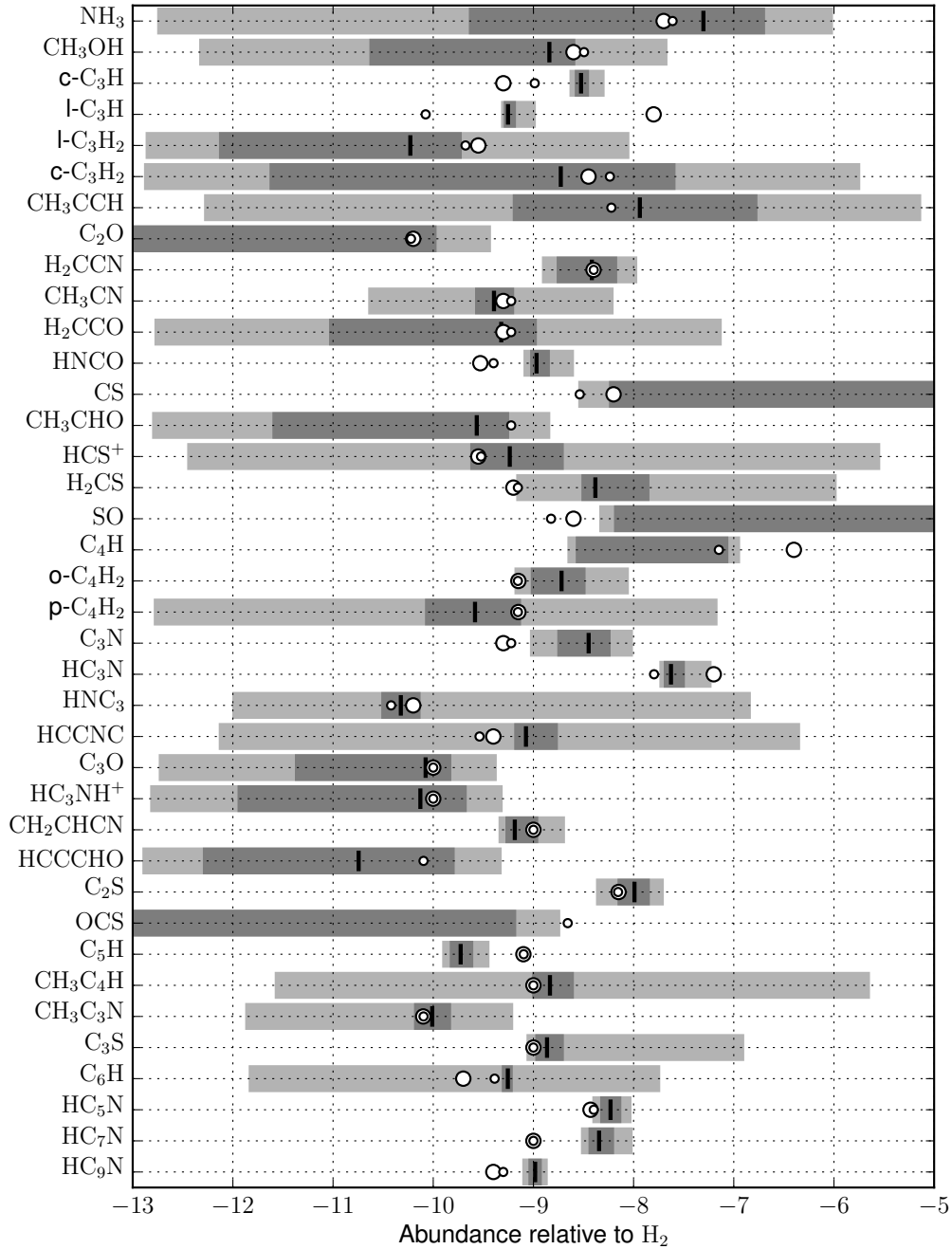


FIG. 1.— Graphical representation of the computed abundances of molecules in TMC-1. The thick black vertical lines are the medians of the abundance distributions, while the dark (resp. light) gray rectangles represent the 68% and 95% confidence intervals, respectively. Large open circles are the values presented in Ohishi & Kaifu (1998), while smaller open circles are the values compiled in Agúndez & Wakelam (2013)

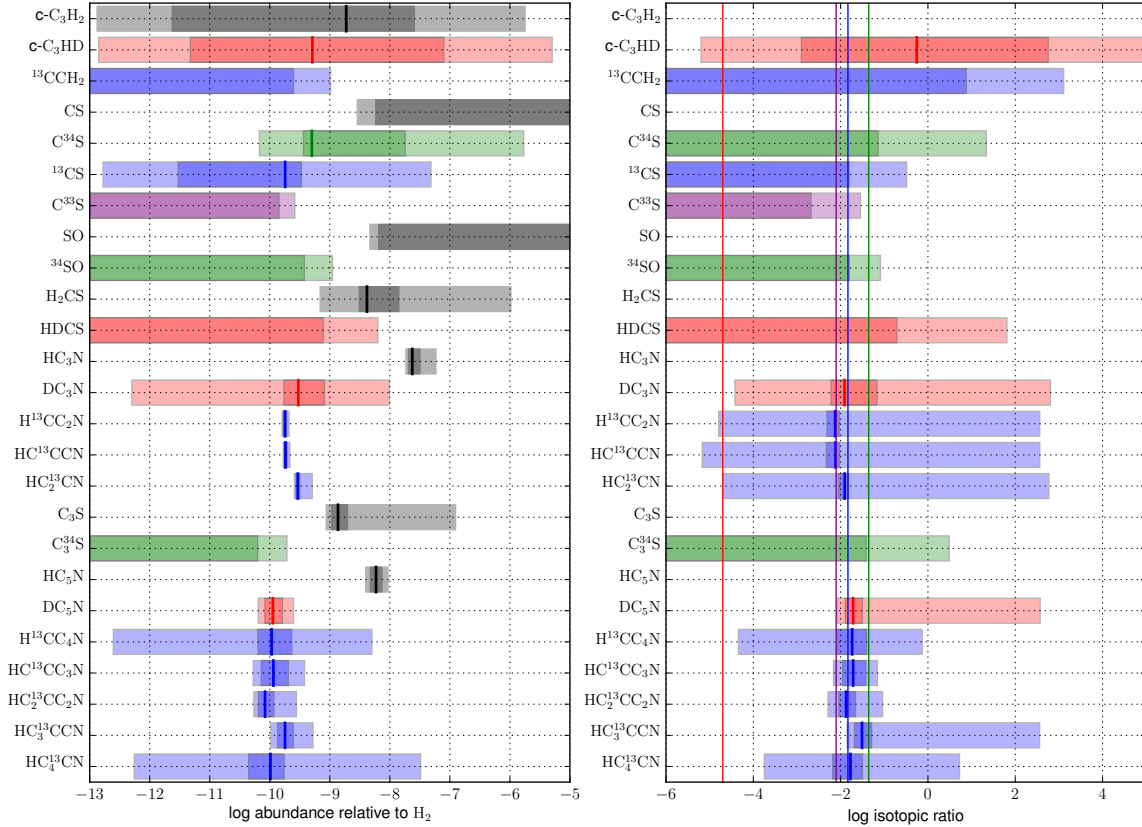


FIG. 2.— Graphical representation of the computed abundances of isotopologues in TMC-1. The left plot shows the computed abundances with the same definition of the shading as for Fig. 1. The right plot shows the ratios of the isotopologue to the molecule with the main isotope. Species are color coded, with main isotopologues in black, isotopologues of deuterium in red, isotopologues of ^{13}C in blue, isotopologues of ^{34}S in green, and isotopologues of ^{33}S in purple. The solid vertical lines spanning the full height of the plot correspond to constant values of the isotopic ratio of $\text{D}/\text{H} = 2 \times 10^{-5}$, $^{13}\text{C}/^{12}\text{C} = 1/68$, $^{34}\text{S}/^{32}\text{S} = 4.4 \times 10^{-2}$, $^{33}\text{S}/^{32}\text{S} = 7.9 \times 10^{-3}$.

TABLE 3
BEST-FIT PARAMETERS BY THE BAYESIAN APPROACH FOR RARER ISOTOPE-BEARING SPECIES

Species	$\log N^a$ (cm^{-2})	T_{ex} (K)	PSNR	τ range	Number of Transitions	Min Partition Function Temp	Appendix Figure
$^{13}\text{CCH}_2$	< 13.01	$5.31(-1.49, +1.69)$	0.9	< 0.04	2	9.375	B7
$c\text{-C}_3\text{HD}$	$12.71(-2.03, +2.19)$	$5.23(-1.91, +2.13)$	2.0	$0.11 - 0.28$	4	9.375	B8
^{13}CS	$12.26(-1.78, +0.27)$	$5.30(-1.66, +1.99)$	2.3	$0.00 - 0.51$	1	9.375	B17
C^{33}S	< 12.42	$5.22(-1.40, +1.52)$	1.2	< 0.02	1	9.375	B19
C^{34}S	$12.70(-0.14, +1.55)$	$4.94(-1.61, +1.91)$	6.9	$0.40 - 546.68$	1	9.375	B20
HDCS	< 13.80	$5.21(-1.57, +2.00)$	1.5	< 0.41	1	9.375	B22
^{34}SO	< 13.04	$5.35(-1.55, +1.93)$	1.1	< 0.08	1	9.375	B26
DC_3N	$12.47(-0.24, +0.44)$	$5.53(-1.66, +1.90)$	4.3	$0.01 - 0.28$	5	9.375	B35
$\text{H}^{13}\text{CC}_2\text{N}$	$12.25(-0.03, +0.03)$	$6.54(-1.07, +1.32)$	14.6	$0.01 - 0.15$	6	9.375	B36
HC^{13}CCN	$12.26(-0.02, +0.02)$	$5.38(-0.64, +0.57)$	20.6	$0.02 - 0.20$	6	9.375	B32
$\text{HC}_2^{13}\text{CN}$	$12.47(-0.03, +0.03)$	$5.90(-0.93, +1.29)$	11.5	$0.03 - 0.21$	6	9.375	B34
DC_5N	$12.05(-0.13, +0.16)$	$5.80(-0.85, +0.96)$	6.5	$0.02 - 0.04$	6	9.375	B50
$\text{H}^{13}\text{CC}_4\text{N}$	$12.03(-0.23, +0.34)$	$6.31(-1.55, +1.66)$	3.8	$0.02 - 0.03$	3	9.375	B51
$\text{HC}^{13}\text{CC}_3\text{N}$	$12.06(-0.20, +0.25)$	$4.03(-0.58, +0.99)$	6.9	$0.03 - 0.08$	4	9.375	B53
$\text{HC}_2^{13}\text{CC}_2\text{N}$	$11.92(-0.11, +0.15)$	$5.49(-1.05, +1.09)$	4.8	$0.02 - 0.04$	6	9.375	B52
$\text{HC}_3^{13}\text{CCN}$	$12.25(-0.12, +0.14)$	$4.38(-0.45, +0.49)$	6.7	$0.03 - 0.12$	6	9.375	B54
$\text{HC}_4^{13}\text{CN}$	$12.01(-0.36, +0.23)$	$5.61(-1.33, +1.56)$	2.7	$0.03 - 0.04$	5	9.375	B49

(a): the abundance $[X]$ can be derived using $N(X)/N(\text{H}_2)$ with $N(\text{H}_2) = 10^{22} \text{cm}^{-2}$
Spectroscopic data from the CDMS database.

Two molecules stand out in the outlier detection scheme, H_2CCN and C_3N . In both cases, about half of the observed intensities are not compatible with the best-fit model (see Figures B11 and B28 respectively). With so many outlier lines, the problem cannot arise solely from observational effects (possible blended or mis-attributed lines). The origin of the issue is possibly the values of the spectroscopic catalogs such as erroneous normalized intensities or level degeneracies (the spectroscopy data for H_2CCN is only available from CDMS, while the same dataset is present and identical both in CDMS and JPL catalogs for C_3N).

In these two cases, the outlier detection scheme is not used. The simpler model with just the three LTE parameters (N , T_{ex} and ΔV) and a scatter term is used as described in Sect. 3.2 for the case when only a single line of a molecule is detected. The sampling method adjusts by increasing the scatter error added in quadrature to the observational uncertainty to encompass all observed points at the expense of a larger uncertainty on the other parameters, in particular the column density and thus the abundance.

5.2. Comparison with previous abundance determination

The derived column densities and abundances for these molecules were published in Ohishi et al. (1992) and Ohishi & Kaifu (1998) which have been used since as references for abundances in TMC-1 and by extension for dark clouds in general. In Ohishi & Kaifu (1998), the derived abundances have no associated uncertainty estimates and the authors, while discussing the advantage of having detected lines for some species spanning a wide range of opacities, do not discuss the possible effect of high opacity or low signal-to-noise detection on the molecular abundances, especially for species where the number of detected lines is low (some species have only one detected line).

Ohishi & Kaifu (1998) have used the data later published in Kaifu et al. (2004) to compute the abundances of observed species. Since the local thermal equilibrium approach is used in both our study and theirs, the main difference should arise from the spectrometric data used and from the fact that our Bayesian approach enables us to compute uncertainties on the abundances and even upper or lower limits when the signal to noise ratio is too low or the opacity is too large for all detected lines of a given species. In Figure 1, the values from Ohishi & Kaifu (1998) are shown as large white circles. Agúndez & Wakelam (2013) made a review of the literature to identify molecular abundances in TMC-1. The results they compiled appear as small circles in Fig. 1. Most of the previously determined abundances fall within the 95% (2σ) confidence interval of our Bayesian method. We now discuss notable differences, i.e. species where the old values fall outside our 95% confidence interval. Most of the abundance determination in Ohishi & Kaifu (1998) were carried out without taking into account the hyperfine splitting of the observations. This can lead to biased results when opacities vary across the hyperfine components.

5.2.1. Polyynes

C_6H has a similar abundance as the one derived by Ohishi & Kaifu (1998). C_5H has a new abundance that is lower by about an order of magnitude from previous values. The value we compute for linear C_3H falls between the values of Ohishi & Kaifu (1998) and Agúndez & Wakelam (2013). The value reported for this species in Agúndez & Wakelam (2013) comes from IRAM 30m millimeter observations (Fossé et al. 2001). The difference of a factor of two in beam size between the observations could explain the abundance difference. Cyclic C_3H is found to be about three times more abundant.

The case of C_4H is particular because of the electronic structure of this radical. Previous studies (Woon 1995; Mazzotti et al. 2011) have established that C_4H presents two low-lying electronic states of $^2\Sigma^+$ and $^2\Pi$ symmetries. The experimental spectra of C_4H are consistent with the ground state $^2\Sigma^+$ (Dismuke et al. 1975; Gottlieb et al. 1983; Shen et al. 1990). Recently, Senent & Hochlaf (2010) confirmed that C_4H radical presents two electronic states $^2\Sigma^+$ and $^2\Pi$ which are near degenerate. Their computation confirms that the ground electronic state of C_4H radical is $^2\Sigma^+$, which agrees with the findings of electron paramagnetic resonance (EPR) by Dismuke et al. (1975). Their computation also confirms the short gap between the two low-lying electronic states. They have found that they are around 9 cm^{-1} and 2800 cm^{-1} at the (R)CCSD(T) and CASSCF levels of quantum chemical theory. The dipole moment is specific to each electronic state but since the two electronic states are very close to each other and the molecule is not static, the motion will cause electronic states to mix. However, since the concept of an average dipole moment for a mixed state is not well defined, this issue needs more studies from both the theoretical and experimental points of view.

The CDMS database gives a dipole value of 0.870 Debye, which corresponds to the electronic ground state of the molecule. The computed dipole value for the $^2\Pi$ electronic state is 4.3 Debye (Senent & Hochlaf 2010). Nevertheless, in Tab. 2 and Figure 1 we show the full range of abundances permitted by any value of the dipole moment between the values computed for the $^2\Sigma^+$ and $^2\Pi$ states.

In the optically thin regime, the column density scales as the square of the dipole. Thus, once the correct dipole moment of C_4H has been determined, an updated value of the abundance can be approximated using the following expression:

$$N(\text{C}_4\text{H})_D = \left(\frac{D}{4.3}\right)^2 N(\text{C}_4\text{H})_{4.3} \quad (4)$$

where $N(\text{C}_4\text{H})_D$ is the column density considering a dipole moment of value D and $N(\text{C}_4\text{H})_{4.3} = 3 \times 10^{13}\text{ cm}^{-2}$ the column density considering a dipole moment of value 4.3 Debye.

Of the detected molecules which possess distinct ortho and para states, only C_4H_2 has a number of detected lines (12) that is large enough that the abundances of the ortho and para forms can be determined independently. The median ortho-to-para abundance ratio is found to be around 6, but this ratio is highly uncertain with a one sigma confidence interval ranging from 1.7 to 70. The two ortho and para abundances bracket the abundance previously determined by Ohishi & Kaifu (1998).

TABLE 4
LIST OF LINES THAT HAVE AN OUTLIER PROBABILITY LARGER THAN 0.75.

Species	Transition	Observed Frequency (MHz)	Outlier Probability	Modeled Intensity (K km s ⁻¹)	Observed Intensity (K km s ⁻¹)
HC ₃ N	$J' - J'', F' - F'' = 1-0, 2-1$	9098.329	0.90	1.3 ± 0.1	2.638 ± 0.020
HC ₃ N	$J' - J'', F' - F'' = 5-4, 6-5 \text{ \& } 5-4 \text{ \& } 4-3$	45490.332	0.93	7.2 ± 0.4	5.239 ± 0.020
HC ₇ N	$J' - J'' = 11-10$	12407.995	0.999	0.56 ± 0.25	0.228 ± 0.009
HC ₇ N	$J' - J'' = 12-11$	13535.999	0.999	0.58 ± 0.24	0.212 ± 0.011
C ₄ H	$N' - N'', J' - J'', F' - F'' = 4-3, 9/2-7/2, 4-3$	38049.629	0.94	0.58 ± 0.24	0.212 ± 0.011

5.2.2. Cyanopolyynes

Cyanopolyynes are abundant in TMC-1 with the largest cyanopolyyne present in the interstellar medium, HC₁₁N first detected there by Bell et al. (1997). Our new results are comparable with previous abundance determinations in Ohishi & Kaifu (1998) except for HC₇N and HC₉N which we find to be about three times more abundant than was determined by Ohishi & Kaifu (1998). C₃N is found to be six times more abundant but our derived abundance remains very uncertain (see Sect. 5.1)

5.2.3. Other molecules

HNCO is more abundant by a factor of 3.

5.3. Isotopic ratios

5.3.1. Sulfur

For the two minor isotopes of sulfur ³³S and ³⁴S, only upper limits to the ratio can be computed. This arises because, for SO and CS, the main isotopologues have only lower limits to their abundances because of the high opacity of their lines. In the case of C₃S, it is because only an upper limit on the abundance of the ³⁴S isotopologue itself can be computed because of the low signal-to-noise ratio of the observed line. The derived upper limits are in agreement with the cosmic abundance ratios of ³⁴S/³²S = 4.4×10^{-2} , ³³S/³²S = 7.9×10^{-3} (Berglund & Wieser 2011).

5.3.2. Carbon

The overall median value of ¹²C/¹³C considering all the ¹³C bearing molecules, is 66. For the three ¹³C isotopologues of HC₃N, the median ratio is 130 with values ranging from 80 to 133. For the five ¹³C isotopologues of HC₅N, the median ratio is 54 with values ranging from 32 to 75. Recently, Taniguchi et al. (2016) have observed ¹³C isotopes of HC₅N towards TMC-1. Our computed column densities tend to be somewhat larger than the ones they derive although within the 1 σ interval we estimate.

The upper limits on the carbon isotopic ratios for the two molecules ¹³CS and ¹³CCH₂ are compatible with the typical value of 68 assumed in the ISM (Milam et al. 2005).

5.3.3. Hydrogen

In the observed sample, only three molecules have measured H/D ratios: DC₃N (H/D = 81(-68,+82)), DC₅N (H/D = 52(-20,+26)) and c-C₃HD, with an additional upper limit on HDCS. Excluding c-C₃HD which is very uncertain, the average H/D ratio is 64. Due to differences in zero level energy, molecules tend to be enriched in deuterium in cold ISM conditions (Albertsson et al. 2013). The value we derive are typical of those found in the cold dense ISM.

6. SUMMARY

In this work, we have developed a statistical Bayesian method to determine the abundance of molecules in the interstellar medium in the presence of possible outlier points. This method has been used on previously published data from a spectral survey of TMC-1 by the Nobeyama Observatory. We derive a new reference set of abundances for TMC-1 which will be used to benchmark the chemistry of dark clouds.

Based on observations carried out with the Nobeyama Radio Observatory. The Nobeyama Radio Observatory is an open-use facility for mm-wave astronomy, and is being operated under the National Astronomical Observatory of Japan (NAOJ). P.G., L.M., and V.W. thanks ERC starting grant (3DICE, grant agreement 336474) for funding during this work. P.G.'s current postdoctoral position is funded by the INSU/CNRS. V.W and J.-C.L. acknowledge the French PCMI for funding of their research.

Facilities: National Astronomical Observatory of Japan (NAOJ) 45m Radio Telescope at Nobeyama Radio Observatory.

APPENDIX

BAYESIAN METHOD: DETECTING OUTLIERS

In the Bayesian framework, the posterior $p(\theta|D)$ distribution is obtained using Bayes' equation by multiplying the prior distribution $p(\theta)$ by the likelihood $p(D|\theta)$.

$$p(\theta|D) \propto p(\theta)p(D|\theta) \quad (\text{A1})$$

Here θ is a vector of the parameters describing the model and D is the set of observed data points.

We have devised a method that enables the automatic mitigation of outlier points. This method was inspired by the discussions in Hogg et al. (2010) and Foreman-Mackey (2014) concerning the detection of outliers. The likelihood is constructed by considering two generative models, one for the data points that follow the model and the second one for the outlier points.

The likelihood for the non-outliers points $p_m(\{y_i\}_{i=1}^N|N, \Delta V, T_{\text{ex}}, \sigma)$ is constructed assuming that the observed uncertainties for point i are generated from a gaussian of standard deviation σ_{y_i} . To explain the additional scatter around the modeled data, an additional noise term σ is added in quadrature to the observed uncertainties. We make the hypothesis that the outlier points come from a gaussian distribution of mean Y_o and dispersion σ_o . The corresponding likelihood is written as $p_o(\{y_i\}_{i=1}^N|Y_o, \sigma_o, I)$ in the following equations. Each data point is associated with a number q_i which can be either 0 if the point is an outlier and 1 if it is not. We add an additional parameter P_o representing the overall probability of the data points of being outliers.

Making the hypothesis of independent observations, the full likelihood is obtained by multiplying the individual points' likelihood values. Numerically, we consider the logarithm of the likelihood function.

$$\begin{aligned}
\mathcal{L} &= p(D|\theta) \\
\mathcal{L} &= p(\{y_i\}_{i=1}^N|N, \Delta V, T_{\text{ex}}, \sigma, \{q_i\}_{i=1}^N, Y_o, \sigma_o, I) \\
\mathcal{L} &= \prod_{i=1}^N [p_m(\{y_i\}_{i=1}^N|N, \Delta V, T_{\text{ex}}, \sigma)]^{q_i} \times [p_o(\{y_i\}_{i=1}^N|Y_o, \sigma_o, I)]^{[1-q_i]} \\
\mathcal{L} &= \prod_{i=1}^N \left[\frac{1}{\sqrt{2\pi} [\sigma_{y_i}^2 + \sigma^2]} \exp\left(-\frac{[y_i - W_i(N, \Delta V, T_{\text{ex}})]^2}{2 [\sigma_{y_i}^2 + \sigma^2]}\right) \right]^{q_i} \\
&\quad \times \left[\frac{1}{\sqrt{2\pi} [\sigma_{y_i}^2 + \sigma^2 + \sigma_o^2]} \exp\left(-\frac{[y_i - Y_o]^2}{2 [\sigma_{y_i}^2 + \sigma^2 + \sigma_o^2]}\right) \right]^{[1-q_i]}
\end{aligned} \tag{A2}$$

The total number of parameters is thus $K+7$ where K is the number of observed lines. $N, \Delta V, T_{\text{ex}}, \sigma, \{q_i\}_{i=1}^K, P_o, Y_o, \sigma_o$

By specifying a prior for the q_i parameters, it is possible to marginalize them out analytically. The marginalization can be written:

$$p(y_i|\theta, \sigma_{y_i}) = \sum_{q_i} \prod_{i=1}^N p(q_i) p(y_i|\theta, \sigma_{y_i}, q_i) \tag{A3}$$

where the sum is over all the possible permutations of the q_i flags.

Assuming the following prior for q_i :

$$p(q_i) = \begin{cases} P_o & \text{if } q_i = 0 \\ 1 - P_o & \text{if } q_i = 1 \end{cases}$$

where P_o is the prior probability that a point is draw from the outlier distribution. It is then possible to marginalize out the q_i and obtain the following likelihood:

$$\mathcal{L} = \prod_{i=1}^N [(1 - P_o)p_m(\{y_i\}_{i=1}^N|N, \Delta V, T_{\text{ex}}, \sigma) + P_o p_o(\{y_i\}_{i=1}^N|Y_o, \sigma_o, I)] \tag{A4}$$

It is also possible to obtain the individual posterior distributions of each $p(q_i|y)$ which is the probability that a point is either an outlier or not. For each data point i , this probability is written

$$p(q_i|y) = \int p(q_i, \theta|y) d\theta = \int p(q_i|\theta, y) p(\theta|y) d\theta \tag{A5}$$

where y has been simplified to signify $\{y_i\}_{i=1}^N$.

Since establishing an analytical formulation of the posterior distribution is intractable, the posterior distribution is obtained by numerically sampling the posterior distribution using an MCMC algorithm. We use the affine invariant ensemble sampling method developed by Goodman & Weare (2010) in its Python implementation EMCEE (Foreman-Mackey et al. 2013). This sampling method uses an ensemble of walkers which sample simultaneously the posterior distribution. The number of walker has been kept fixed at 100.

For each molecule, the sampling is run during a burnin time of about 10,000 steps at the end of which the convergence of the ensemble of chains is checked by plotting the running mean of each parameter.

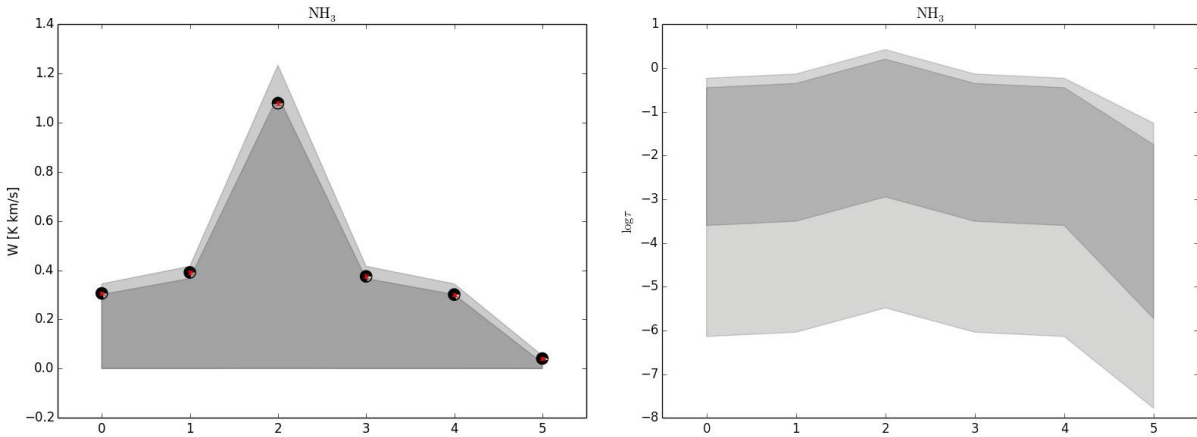
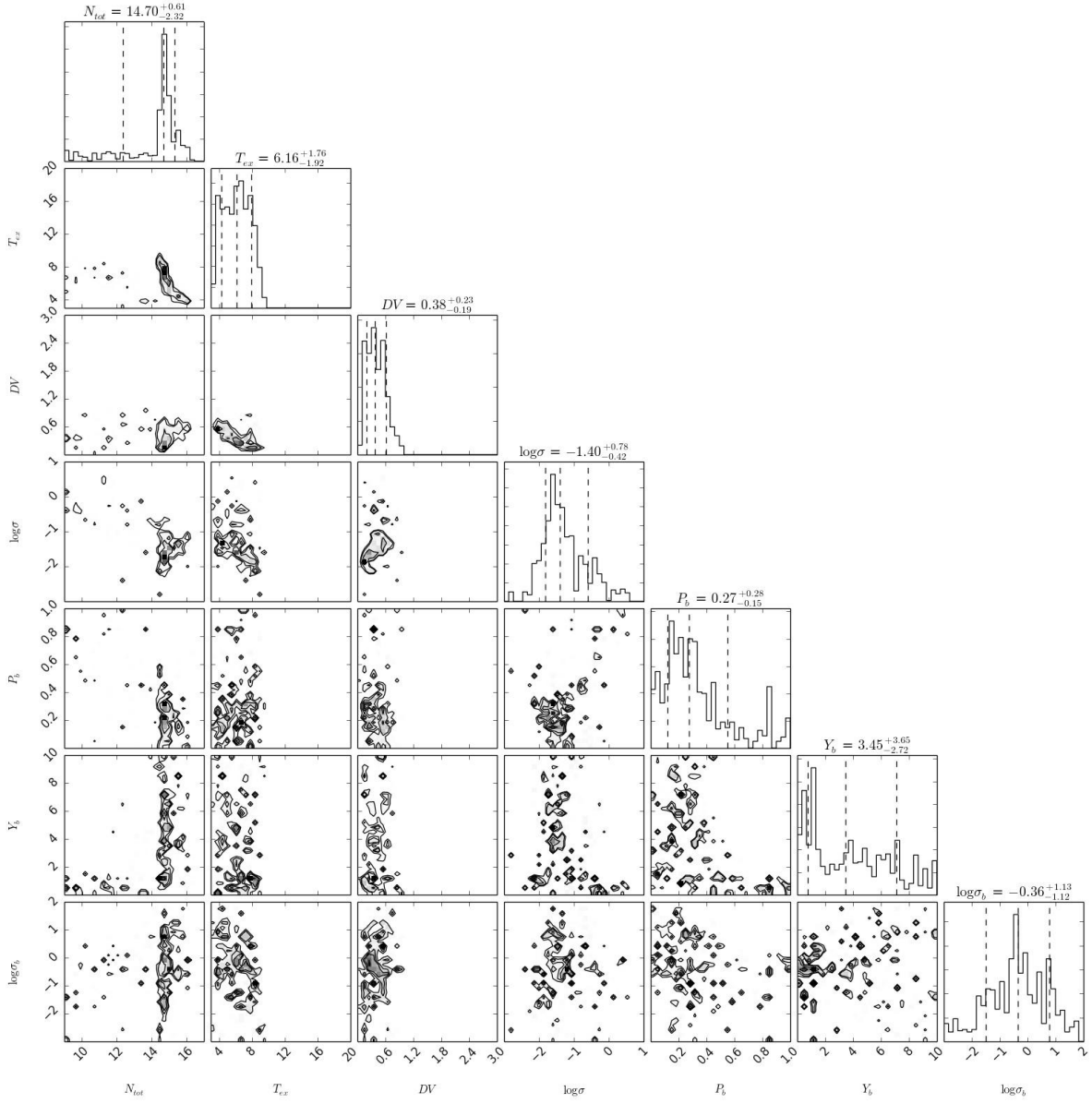
A final run of 100 steps yields 100,000 points from which the histograms of the marginalized distribution and the two parameter correlations can be plotted.

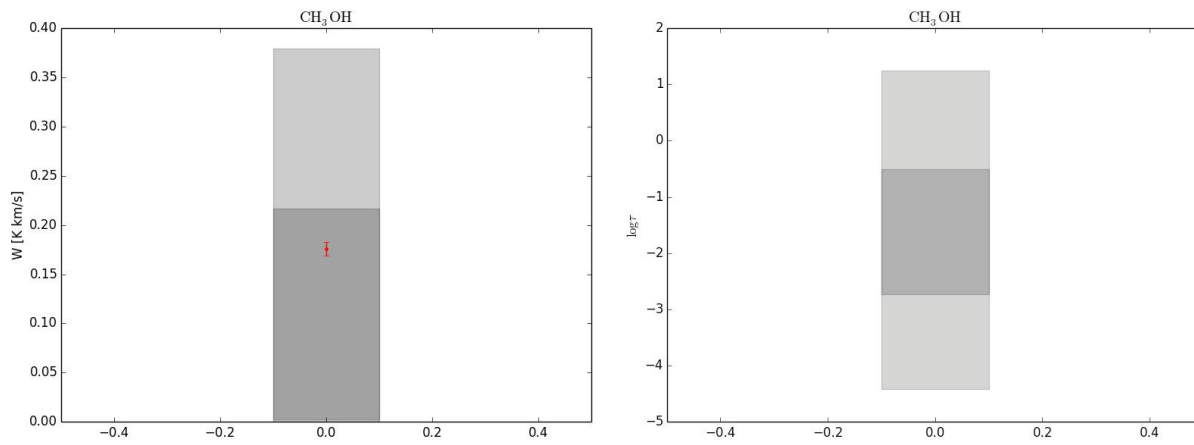
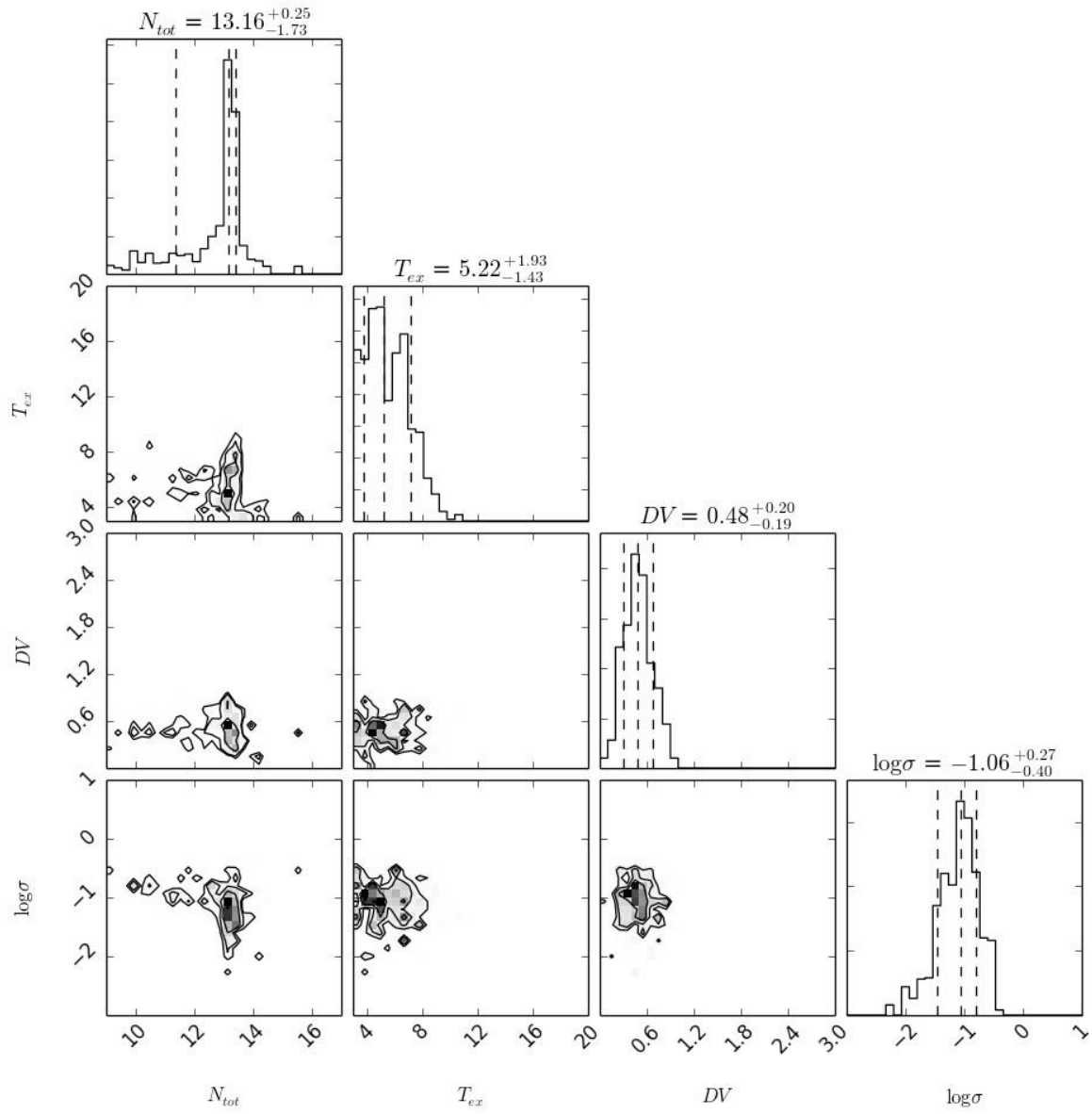
FIGURES

The following set of figures synthesize the results of the Bayesian method for each species. The top triangle plot shows the marginalized posterior distributions of each model parameters along with the median and 16th and 84th percentiles. The set of two-dimension histogram in the lower triangle of the matrix of plot are useful to identify possible correlations between parameters.

In the bottom left, a comparison to the observations is plotted, shown with red error bars, and the modeled integrated intensities for each lines of a given species. The indices in abscissa correspond to the line identifications from Kaifu et al. (2004) in order of increasing frequency. The modeled intensity distribution is represented by the gray intervals corresponding to 68% and 95% of the samples. The outlier probability for each point is represented by the ratio of the white to black surface of each data point. When at least one point has a probability of being an outlier larger than 50%, the 1 sigma interval of the gaussian function that describe the outlier distribution is shown in light blue.

On the bottom right is plotted the distribution of the base 10 logarithm of opacities for each line of a given species is plotted. Again, the gray intervals represent 68% and 95% of the samples.

FIG. B1.— NH_3

FIG. B2.— CH_3OH

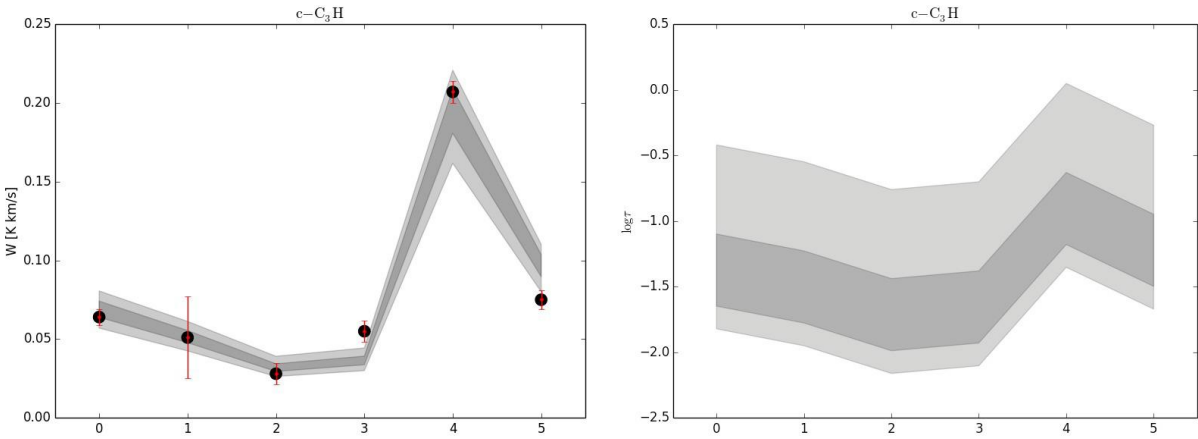
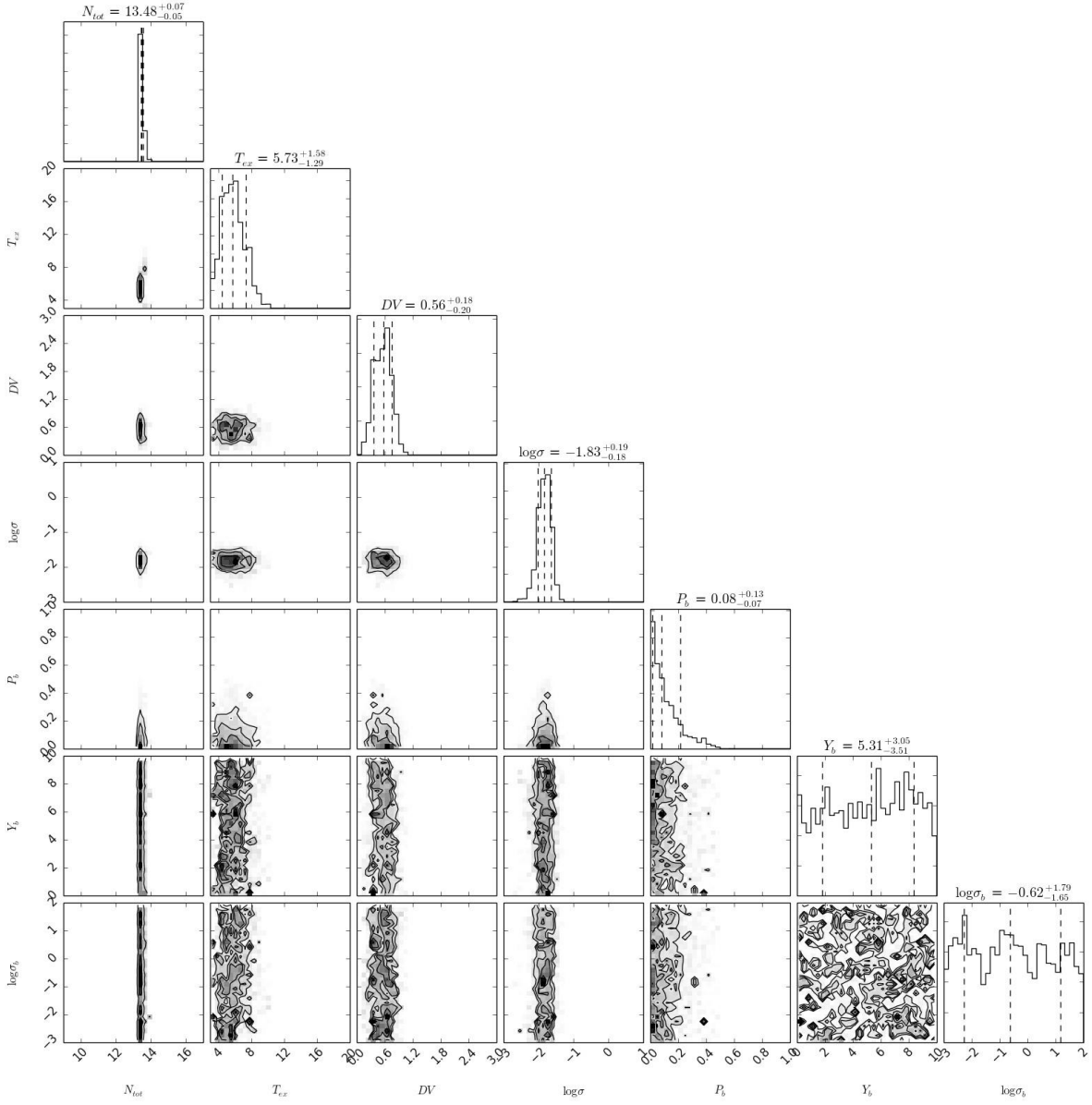
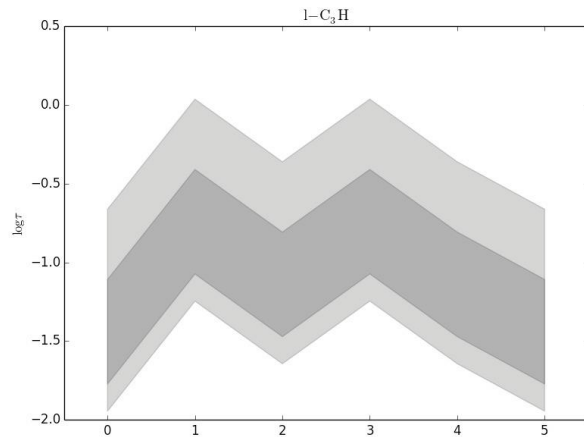
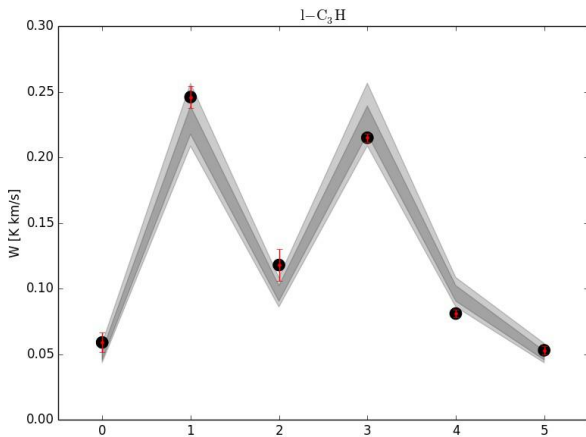
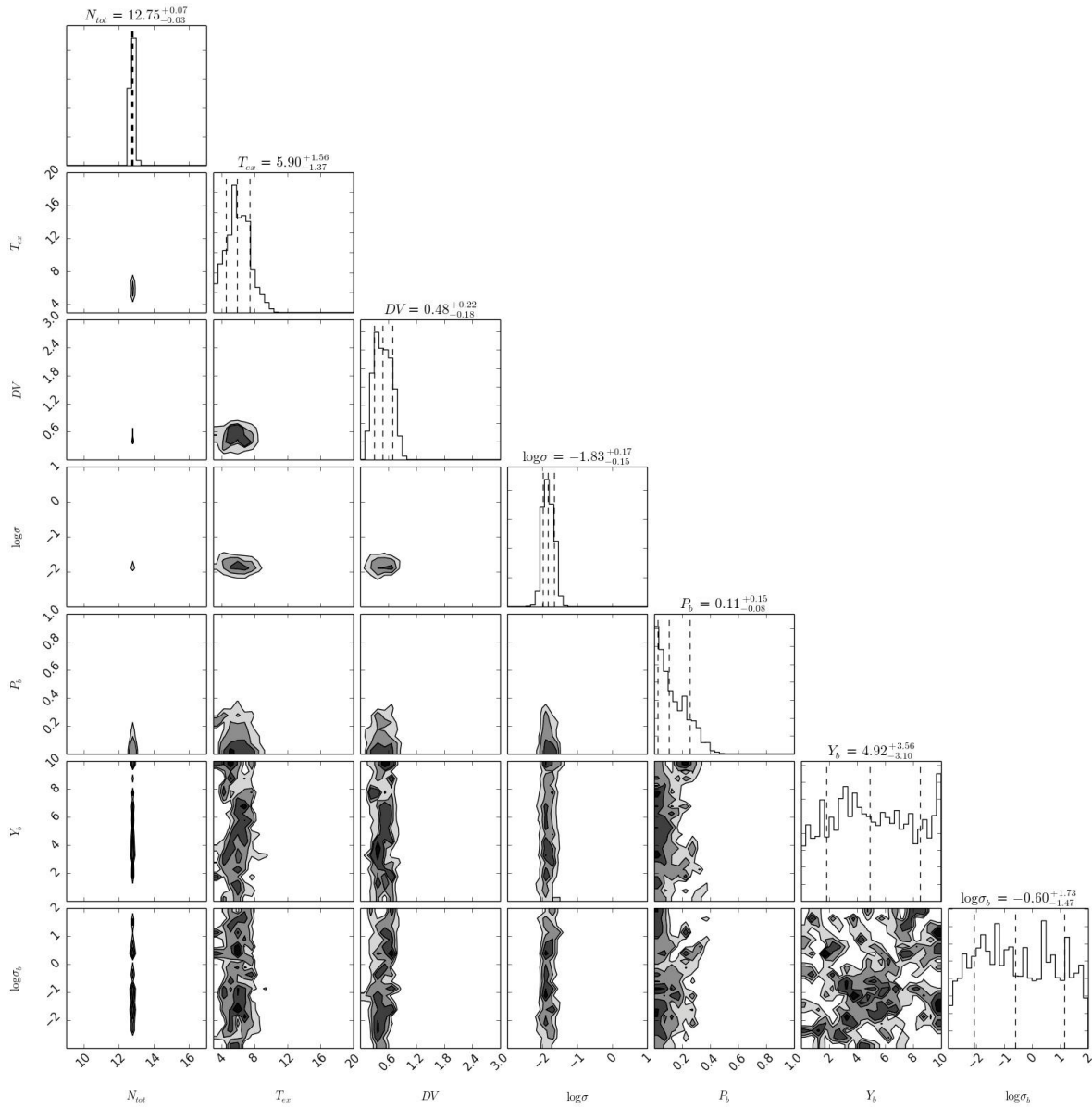


FIG. B3.— $c\text{-C}_3\text{H}$

FIG. B4.— 1-C₃H

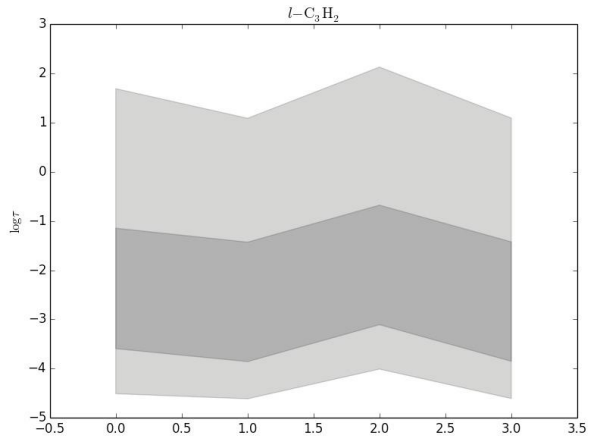
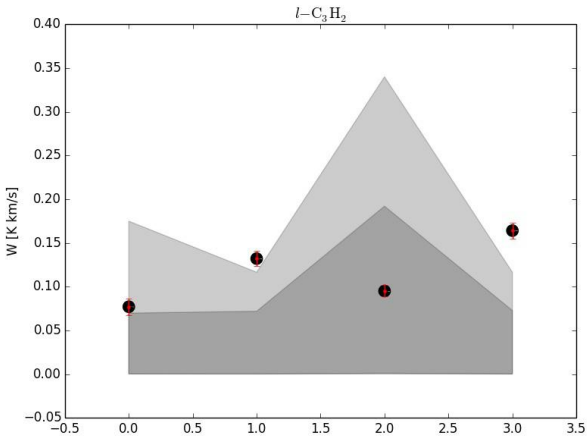
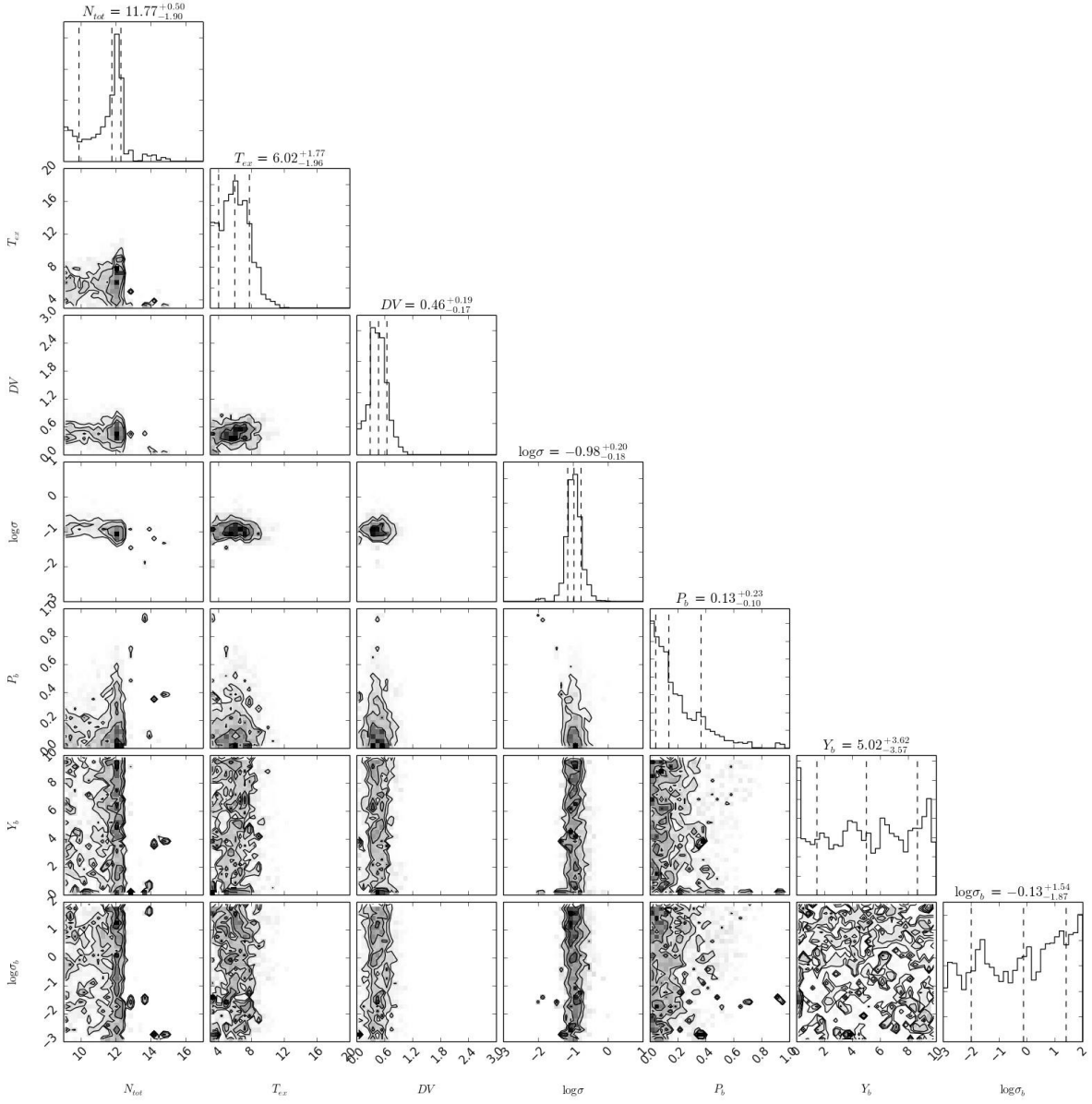
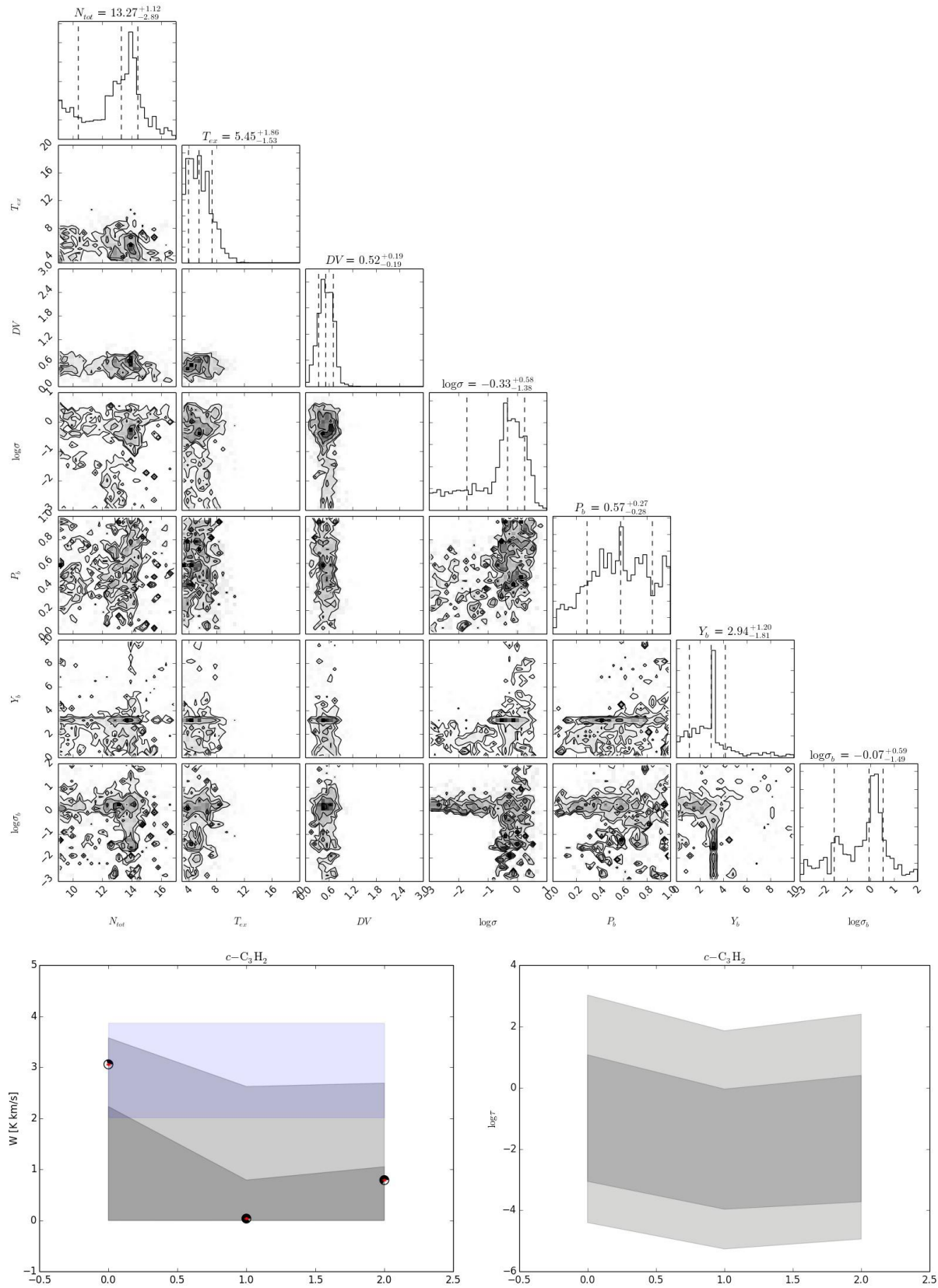
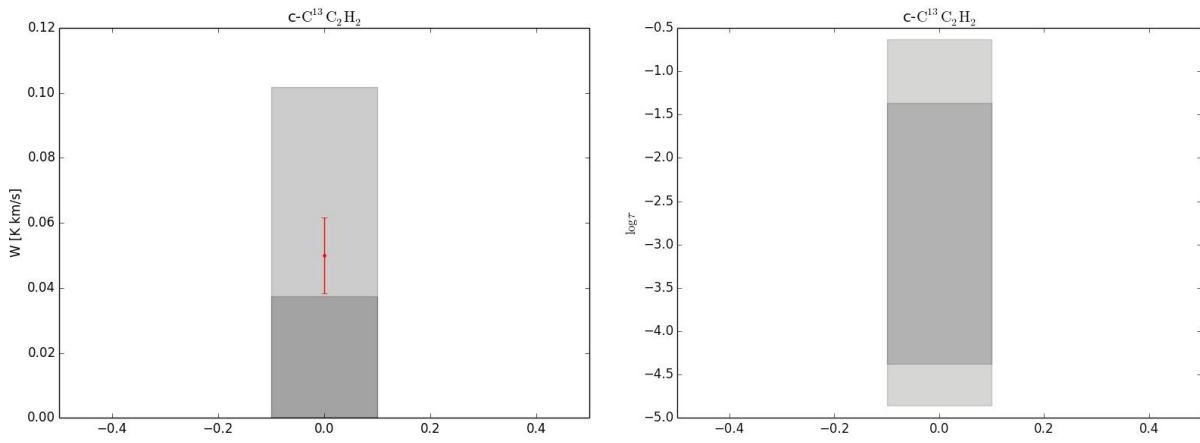
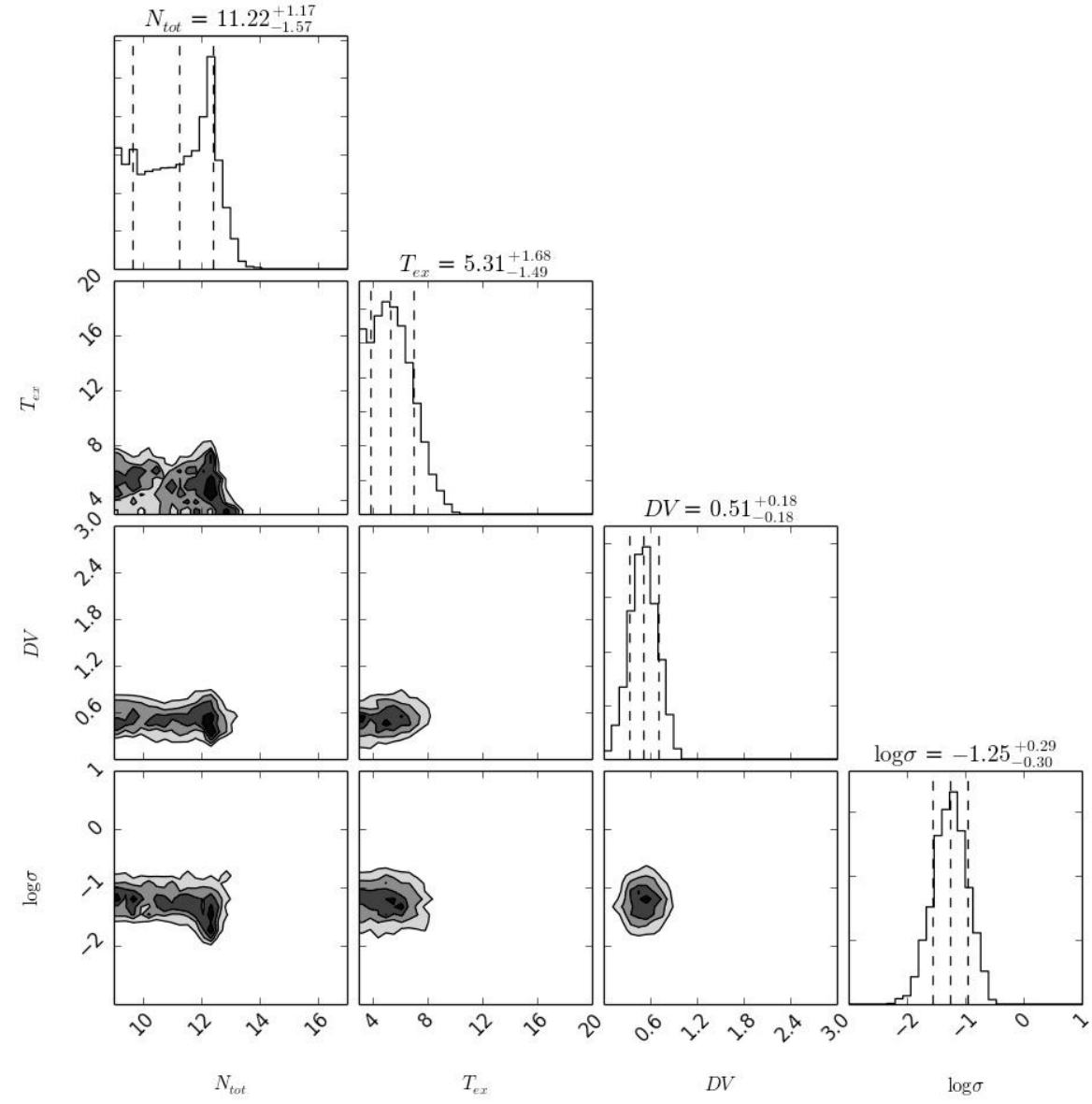
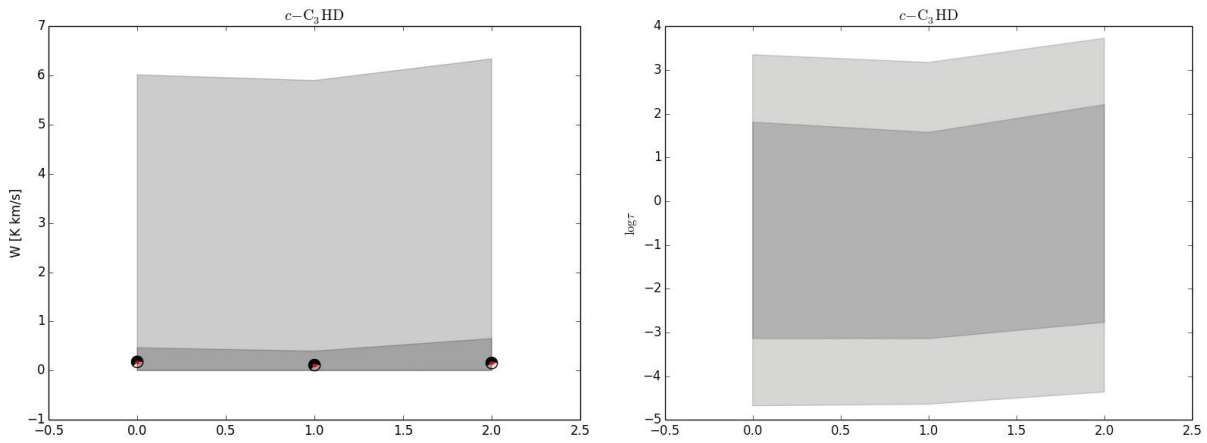
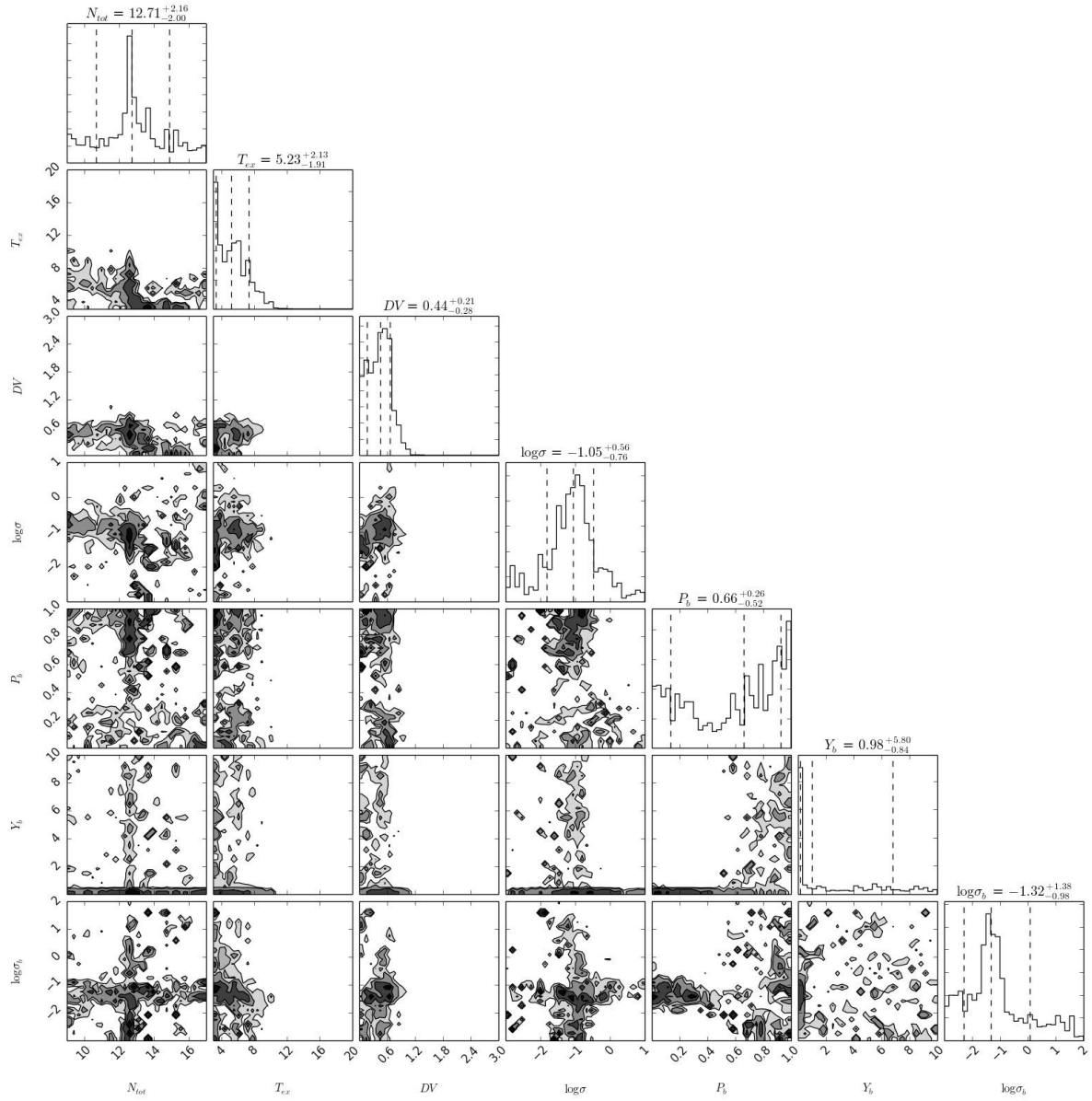


FIG. B5.— $l\text{-C}_3\text{H}_2$

FIG. B6.— $c\text{-C}_3\text{H}_2$

FIG. B7.— $^{13}\text{CCH}_2$

FIG. B8.— $c\text{-C}_3\text{HD}$

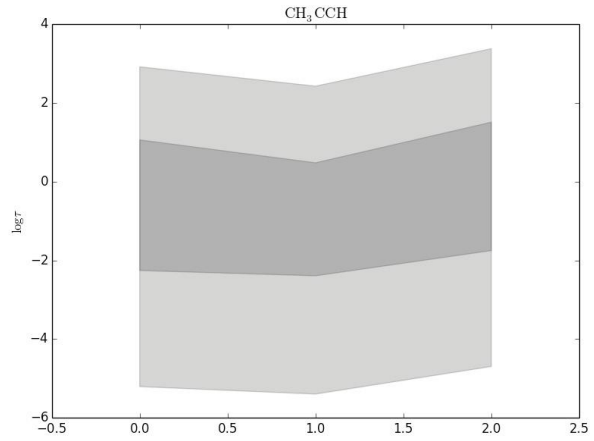
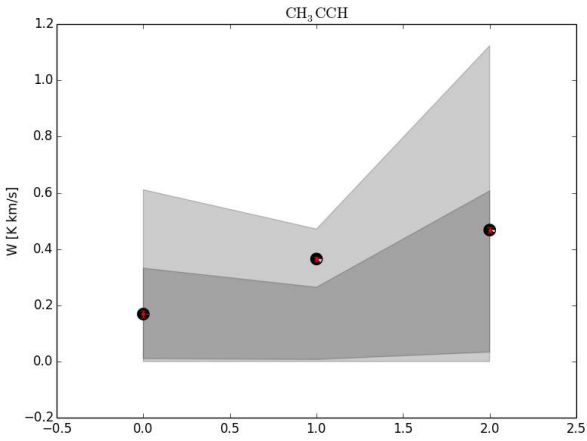
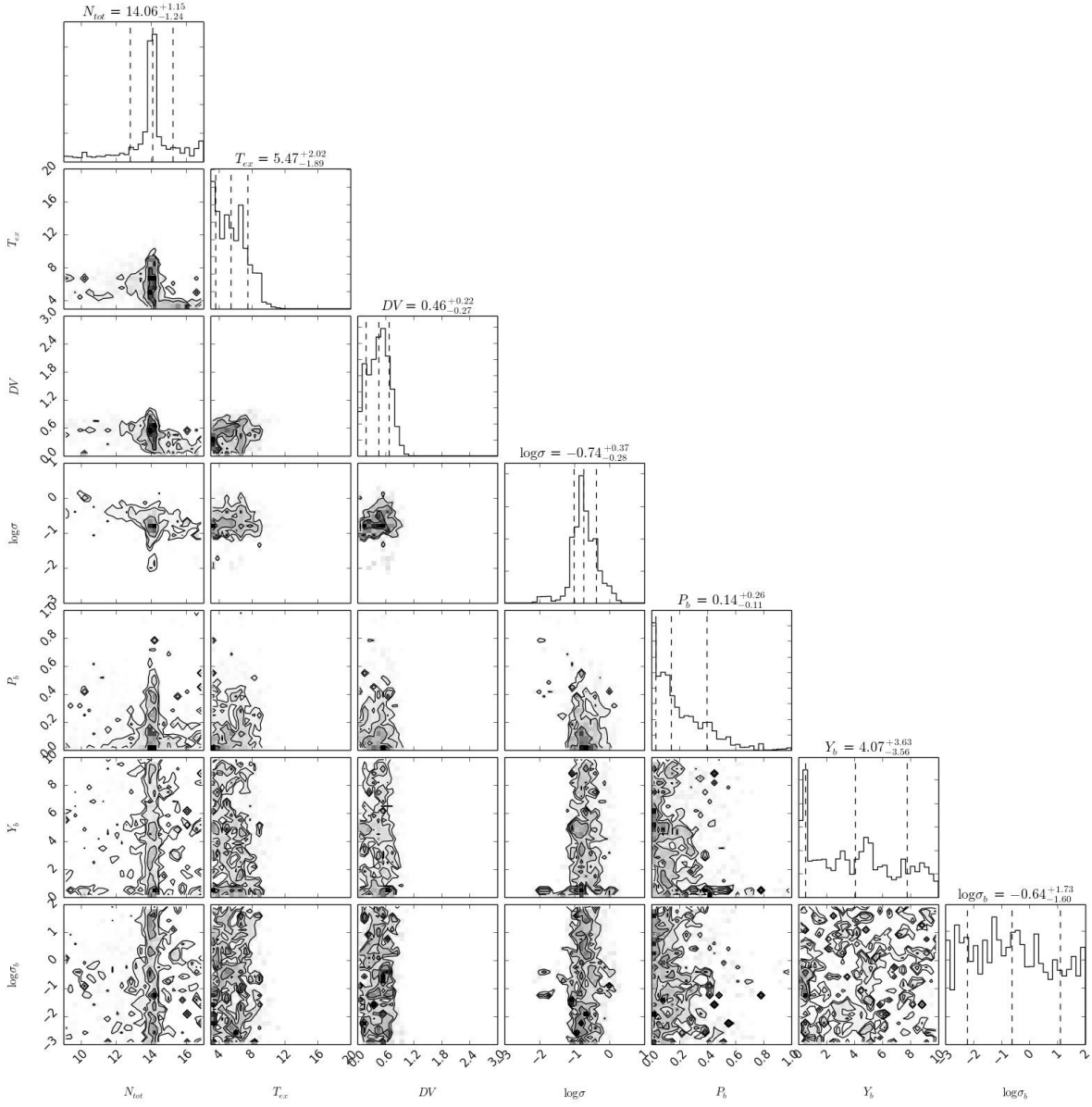
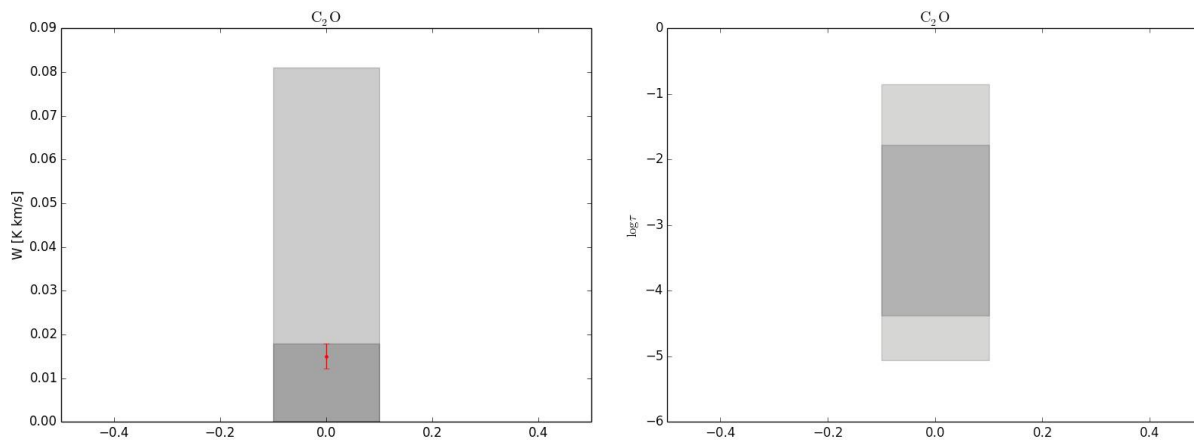
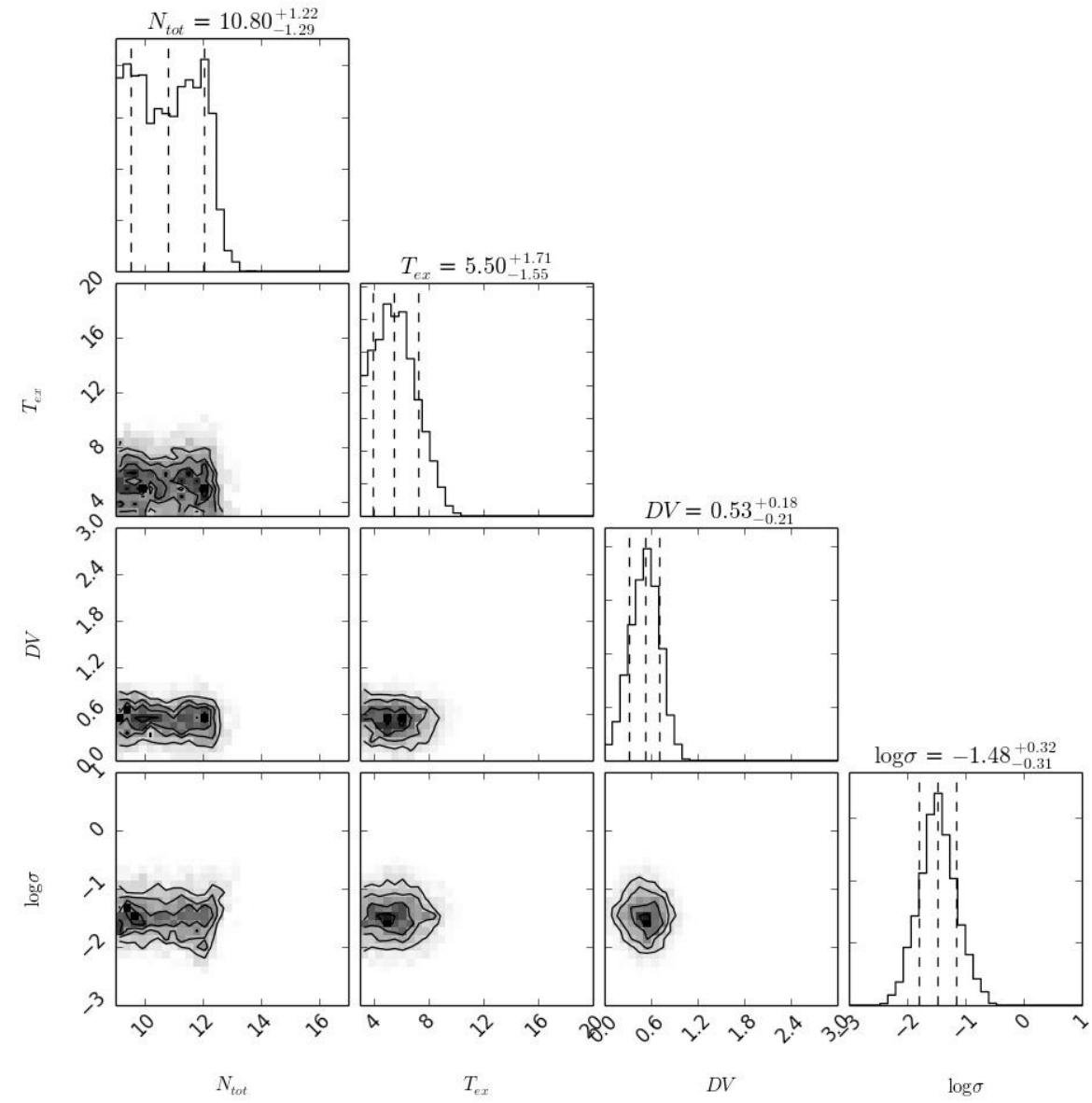


FIG. B9.— CH₃CCH

FIG. B10.— C_2O

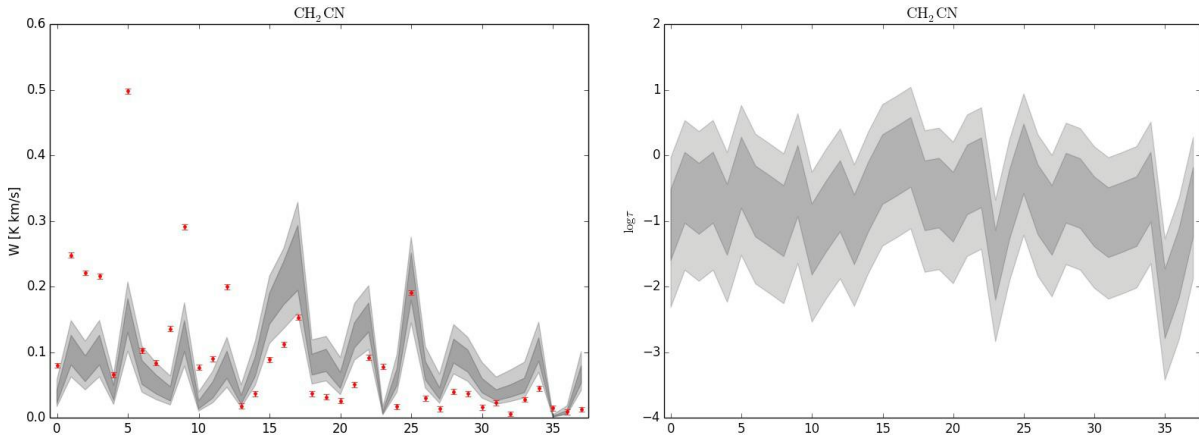
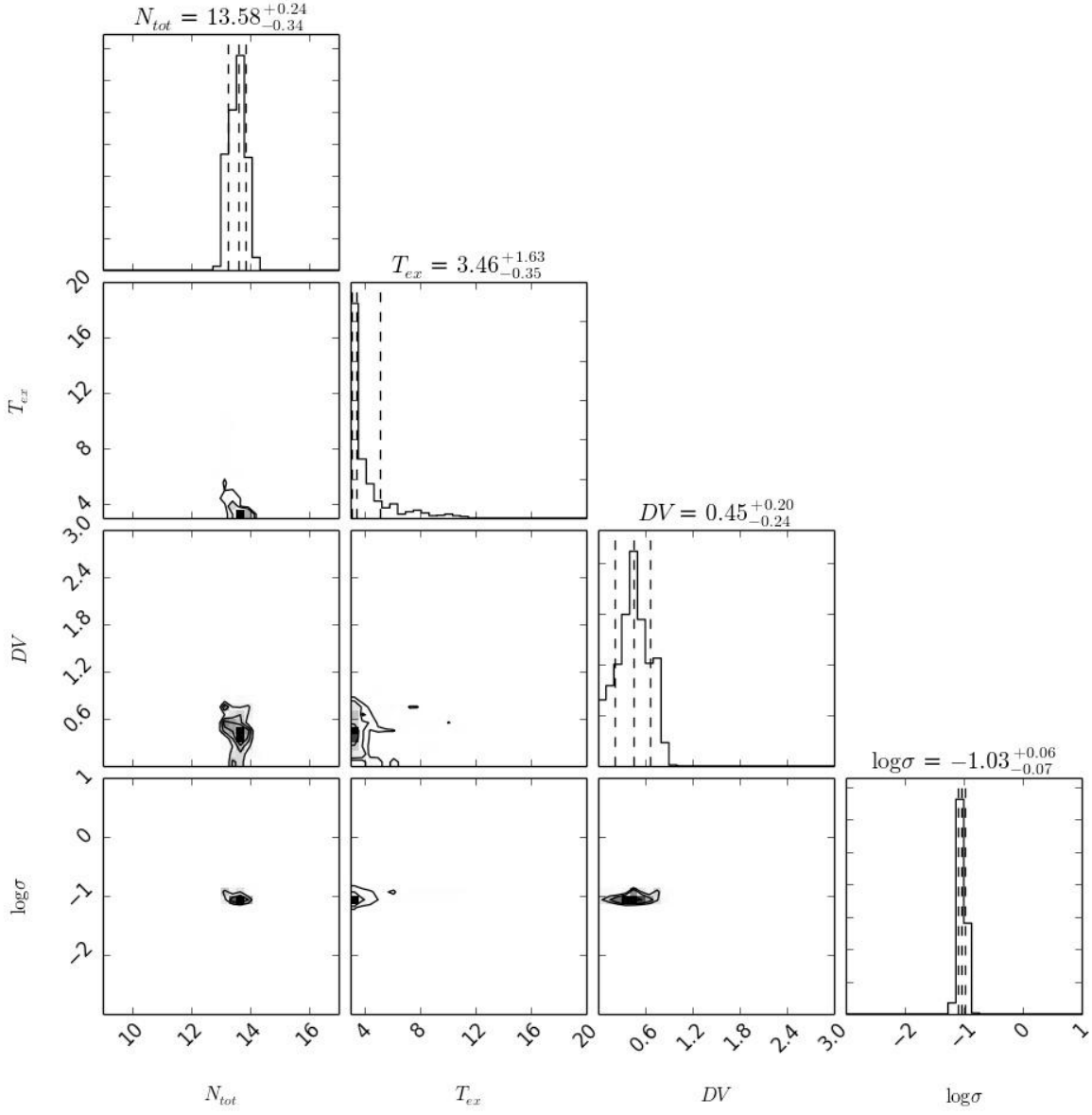
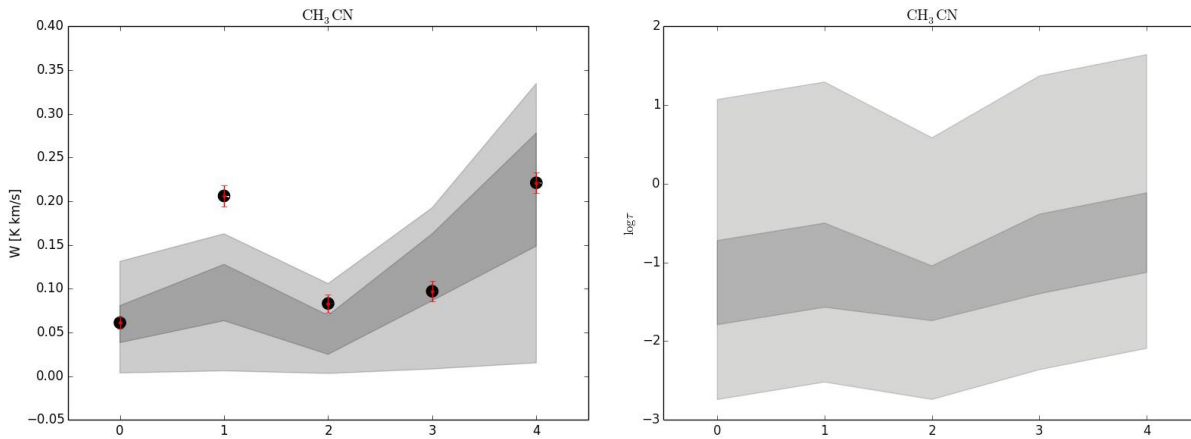
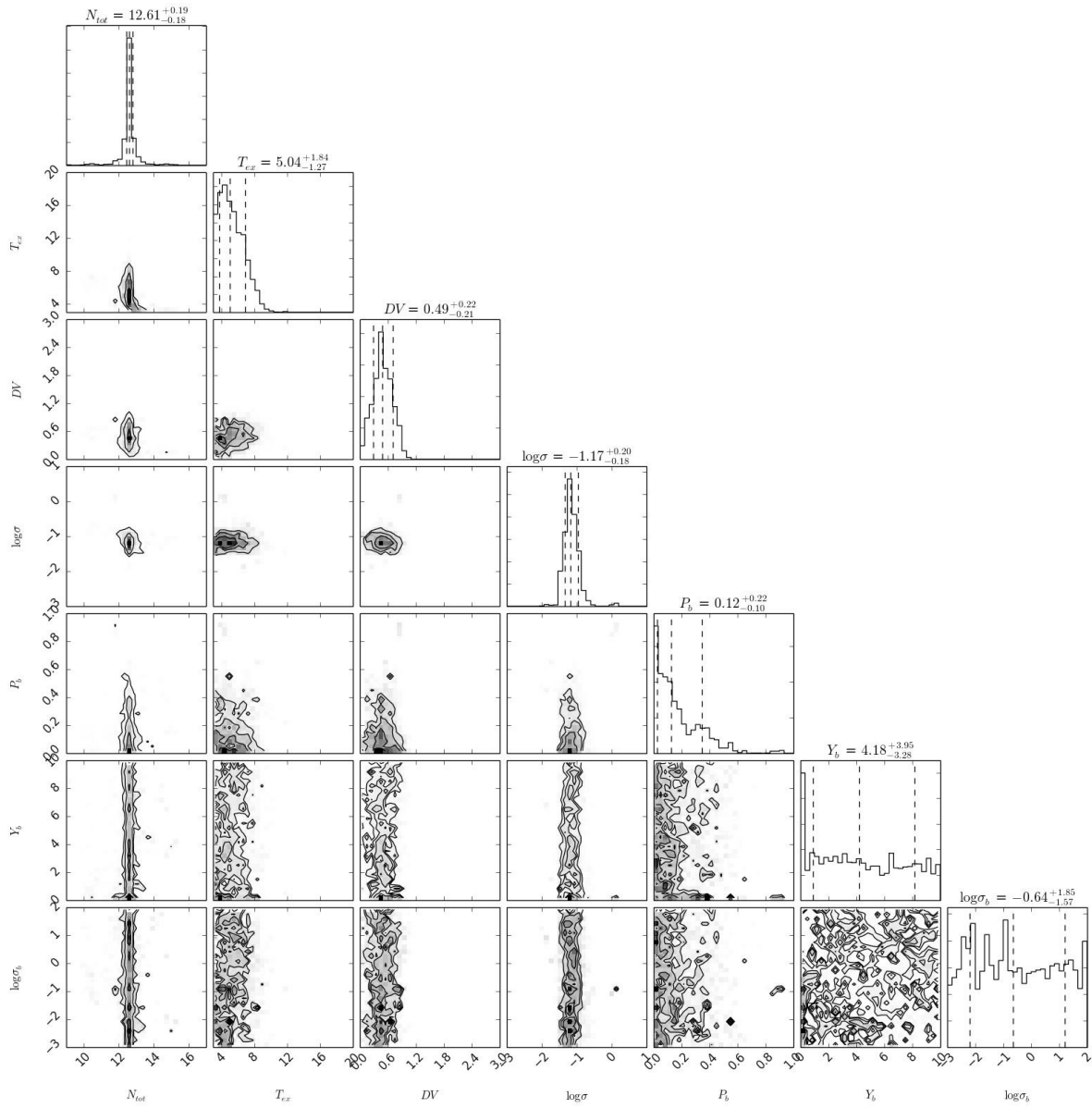


FIG. B11.— H_2CCN

FIG. B12.— CH_3CN

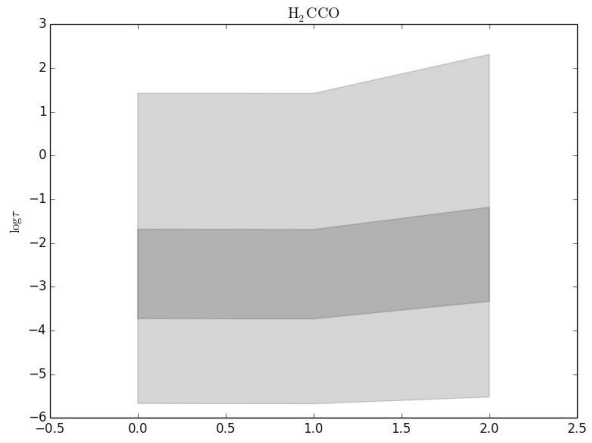
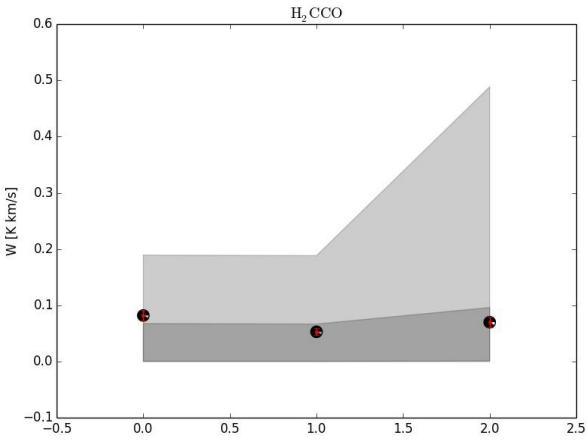
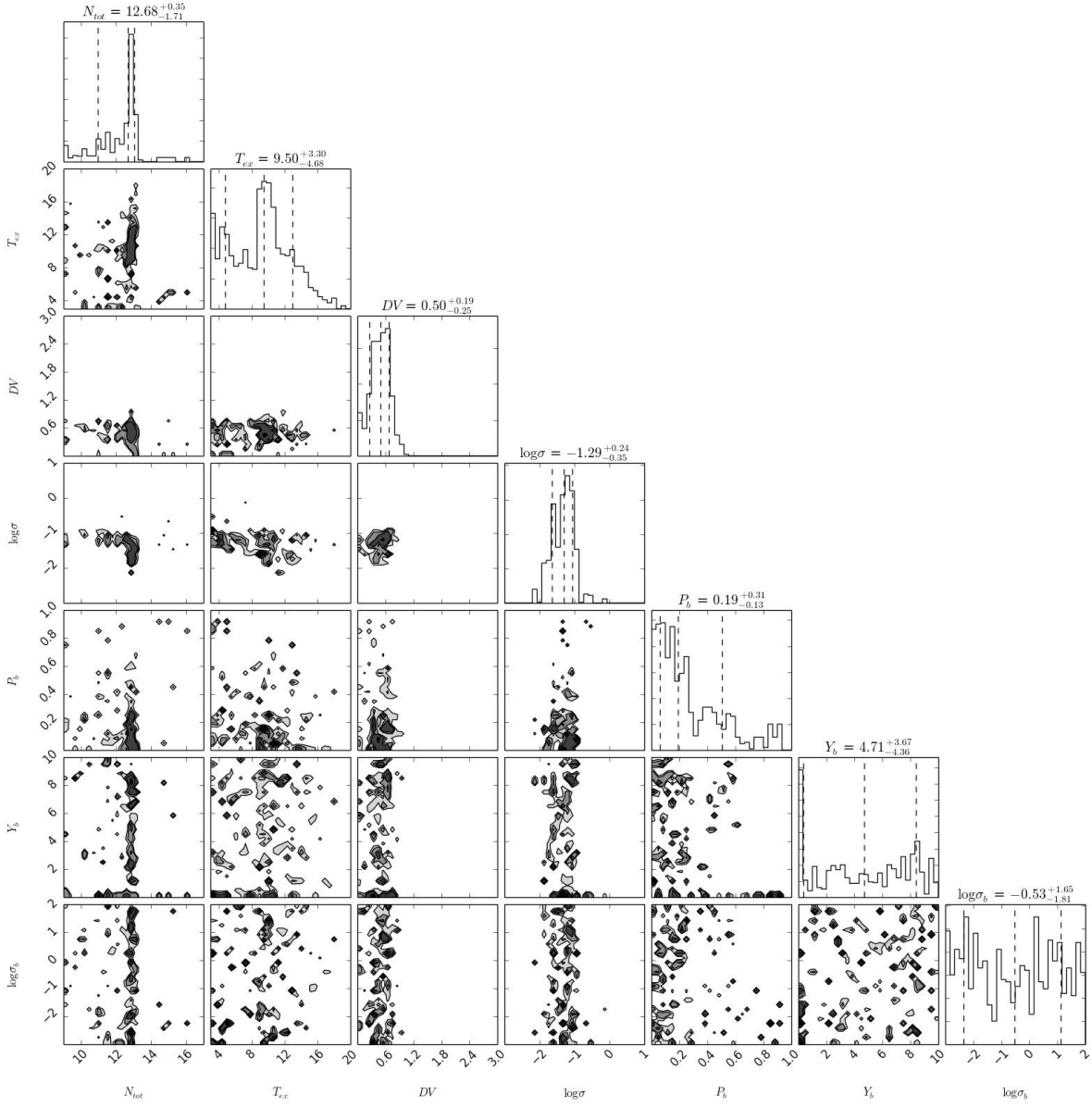


FIG. B13.— H₂CCO

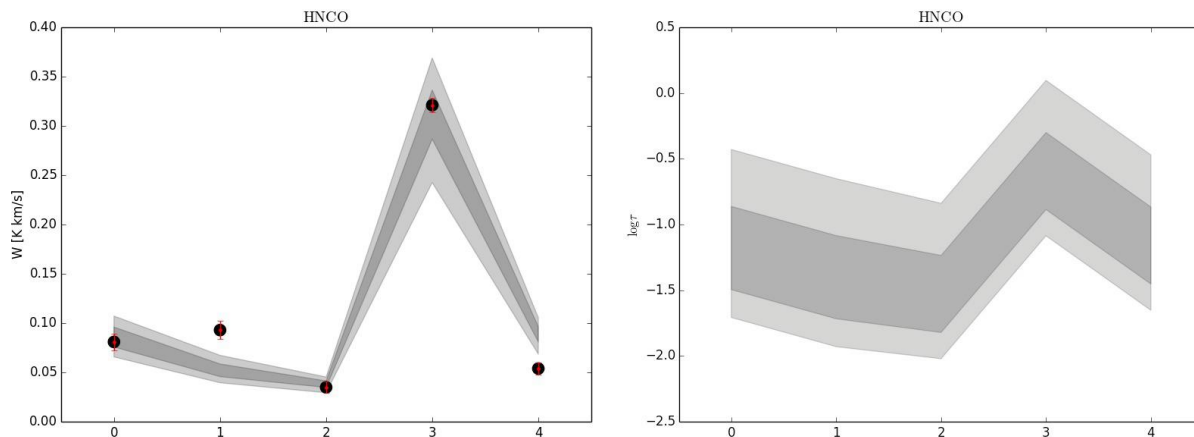
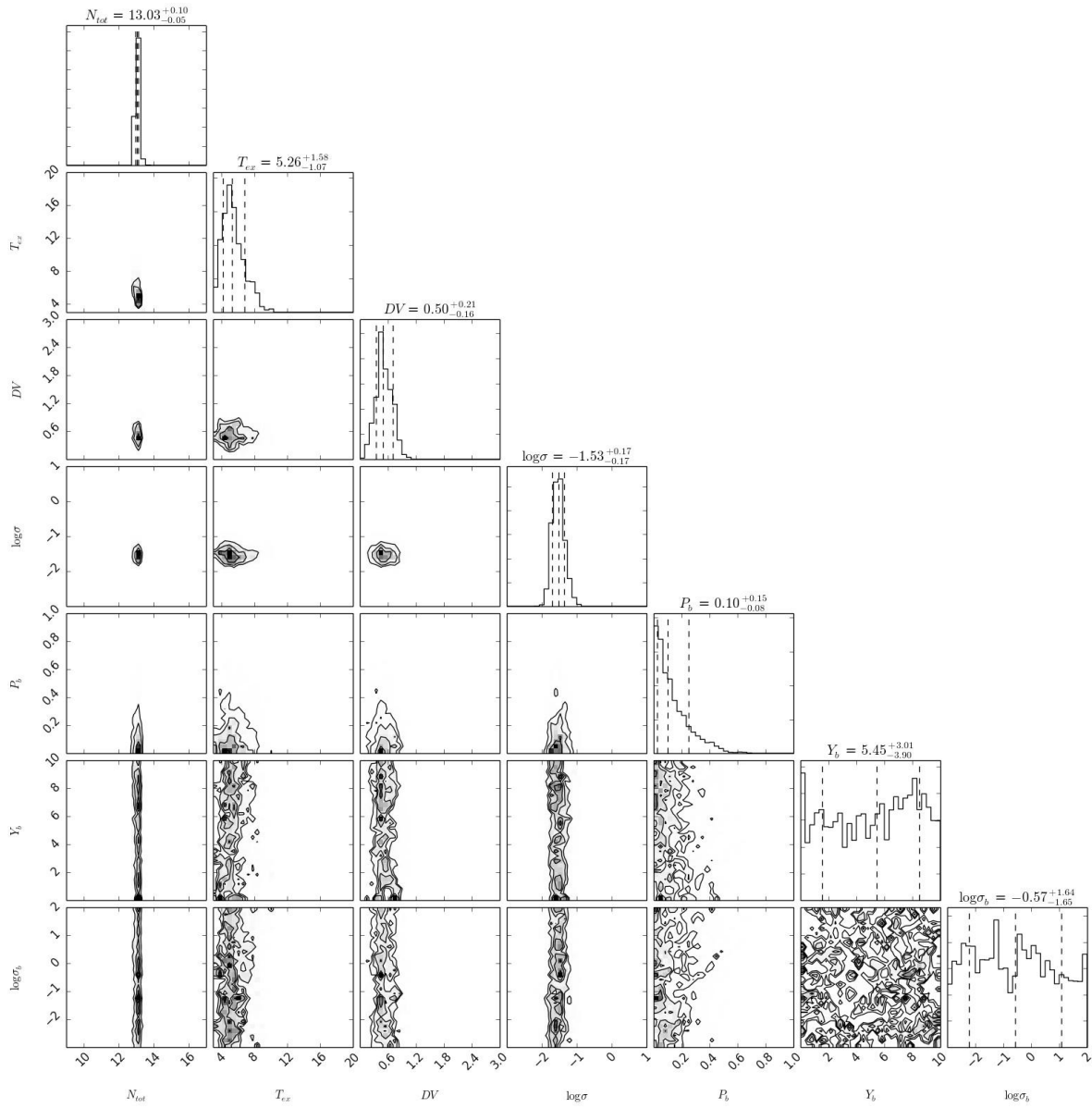


FIG. B14.— HNC/O

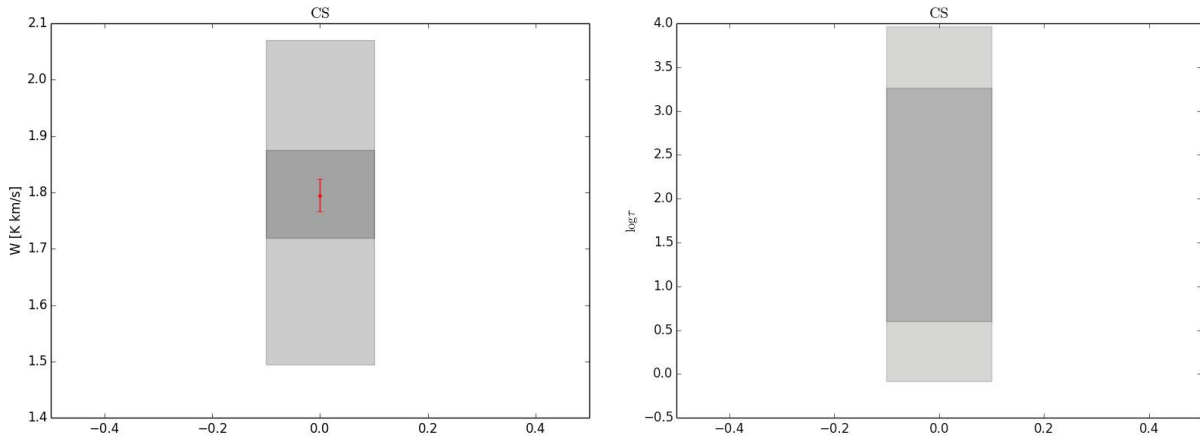
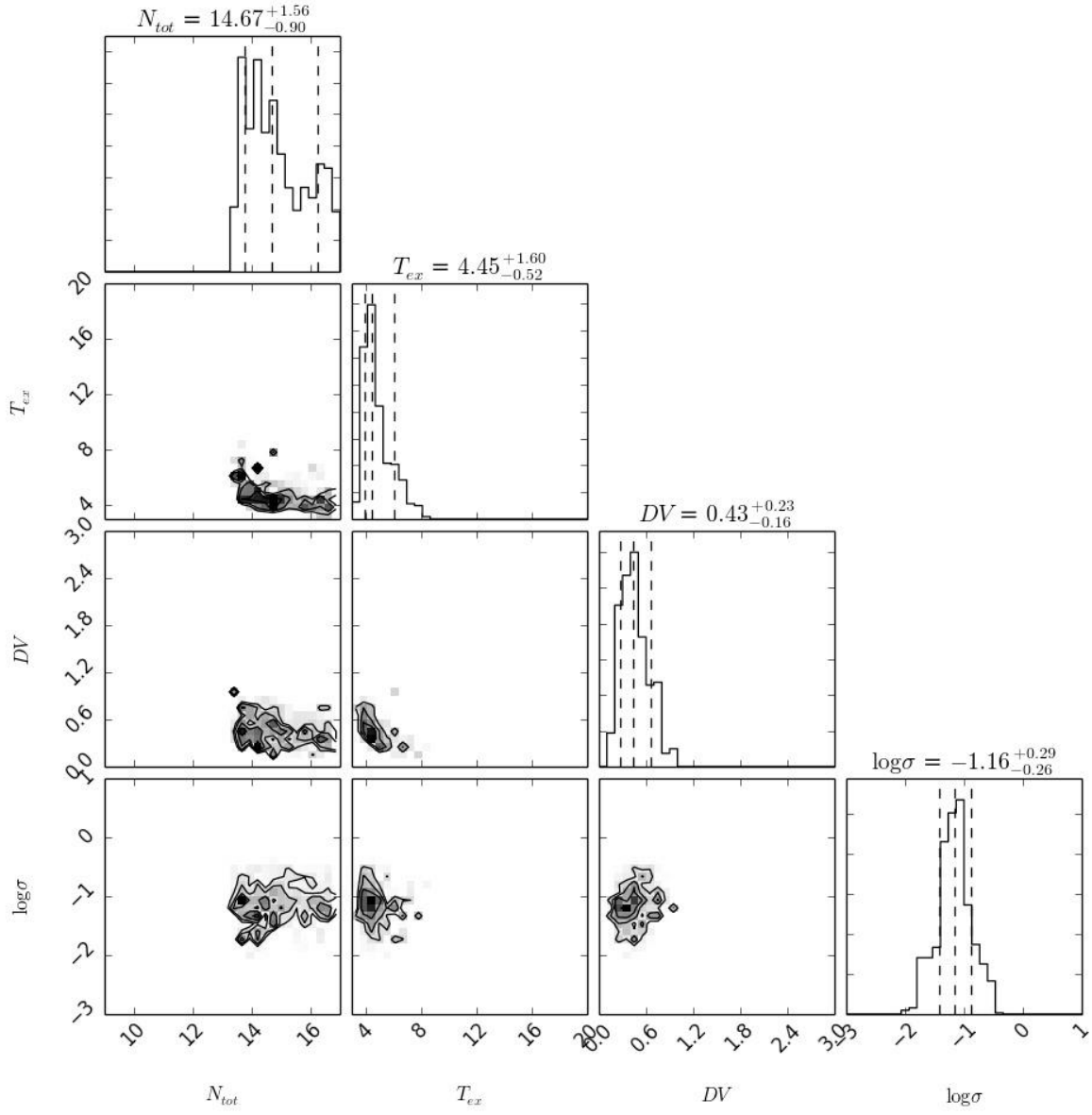
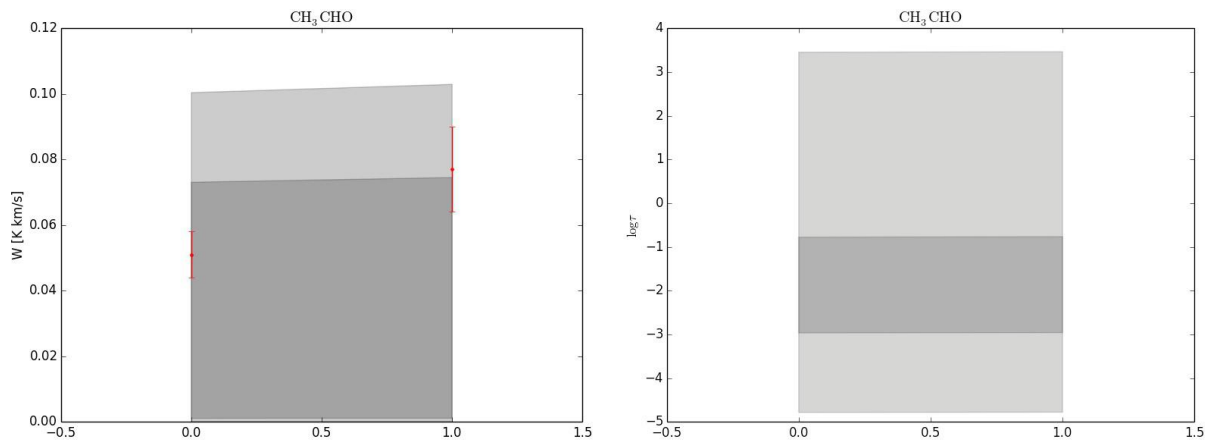
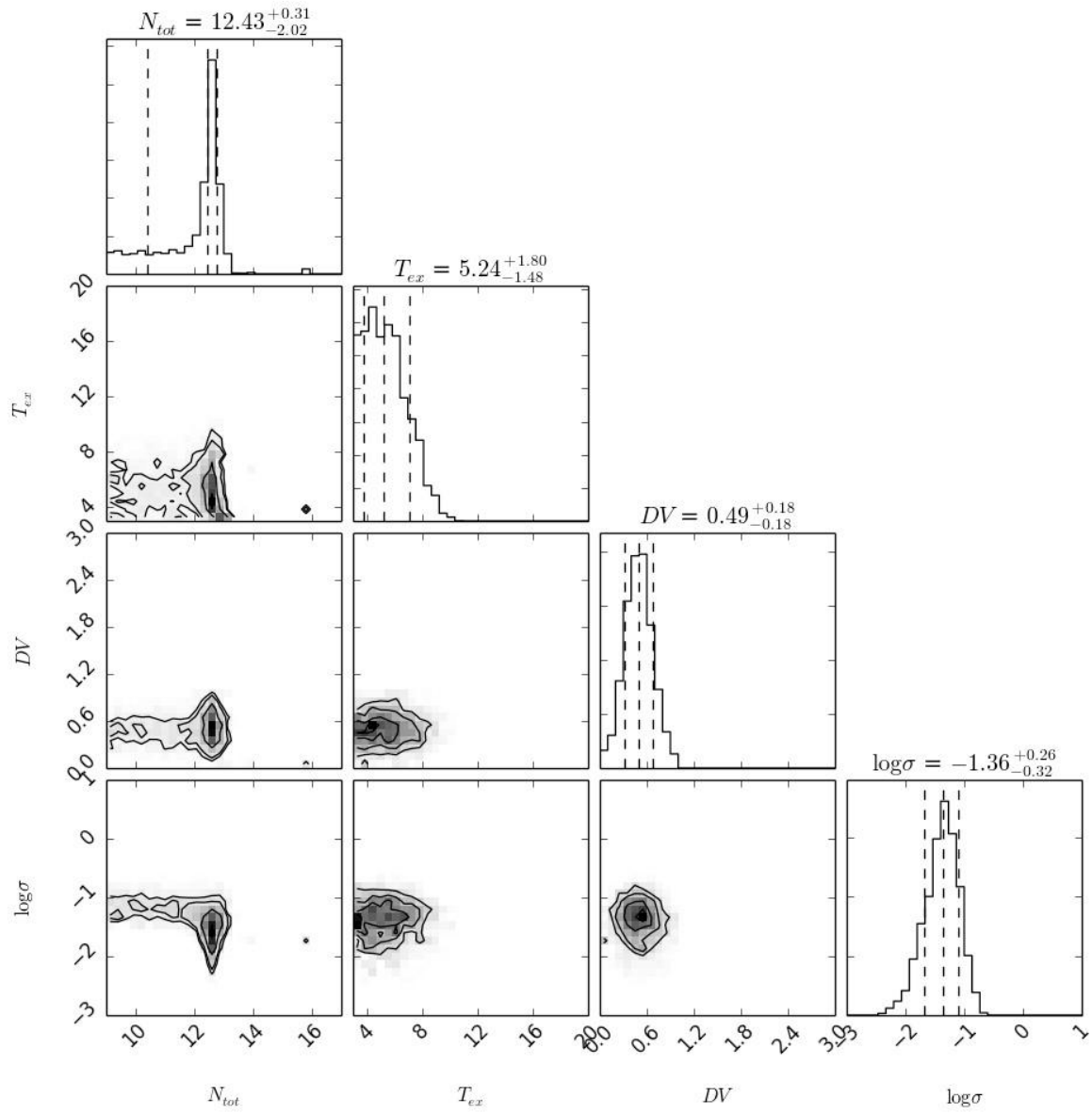


FIG. B15.— CS

FIG. B16.— CH_3CHO

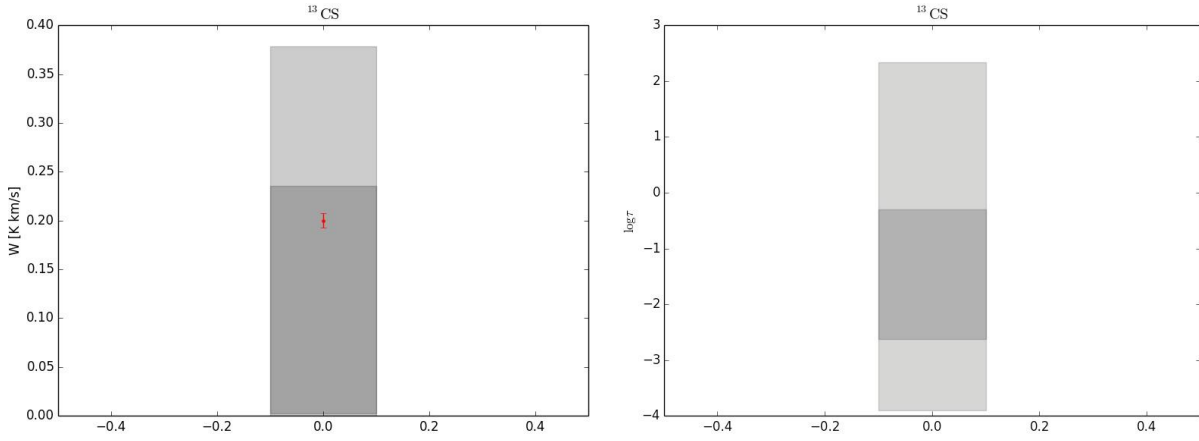
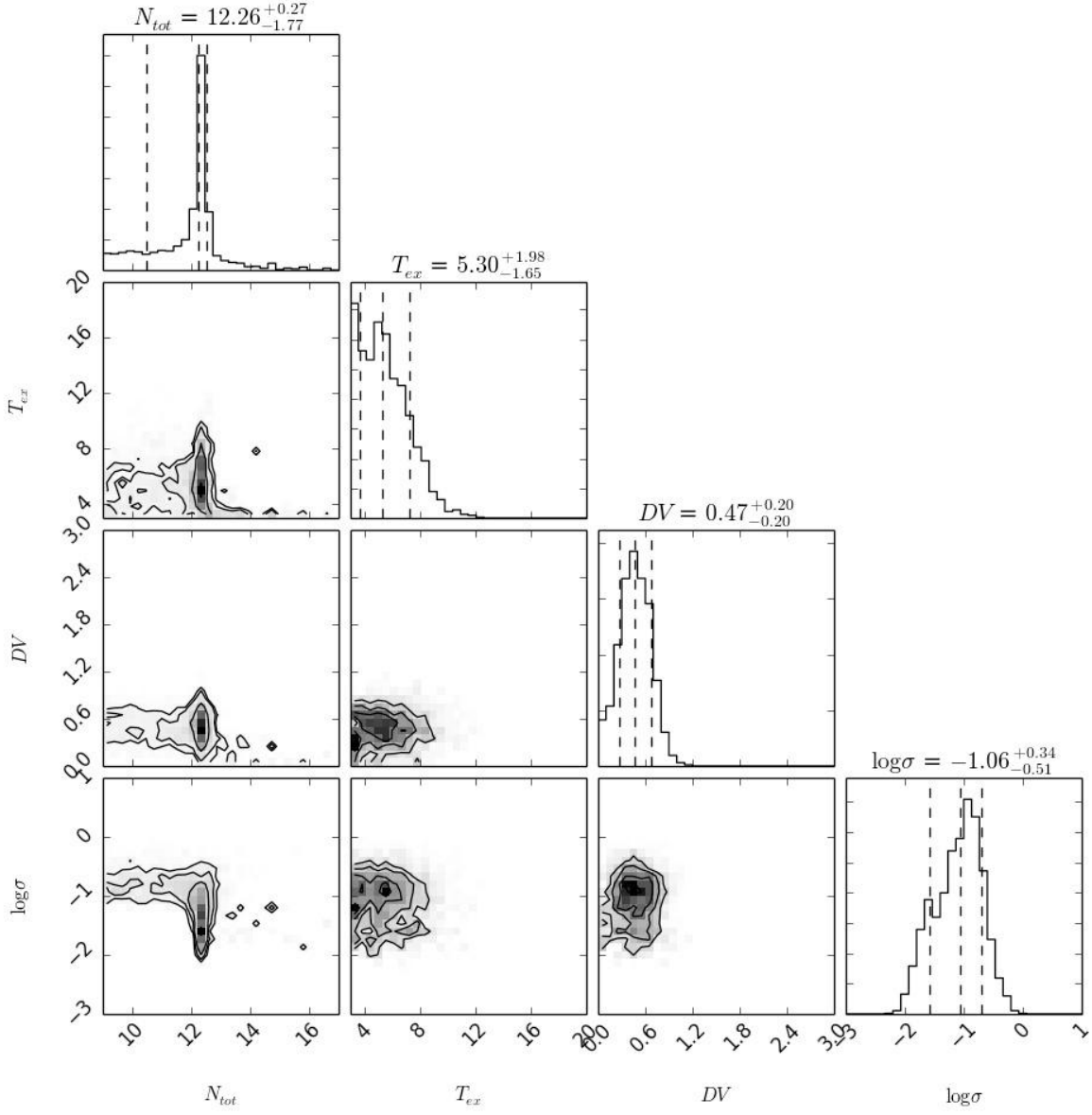
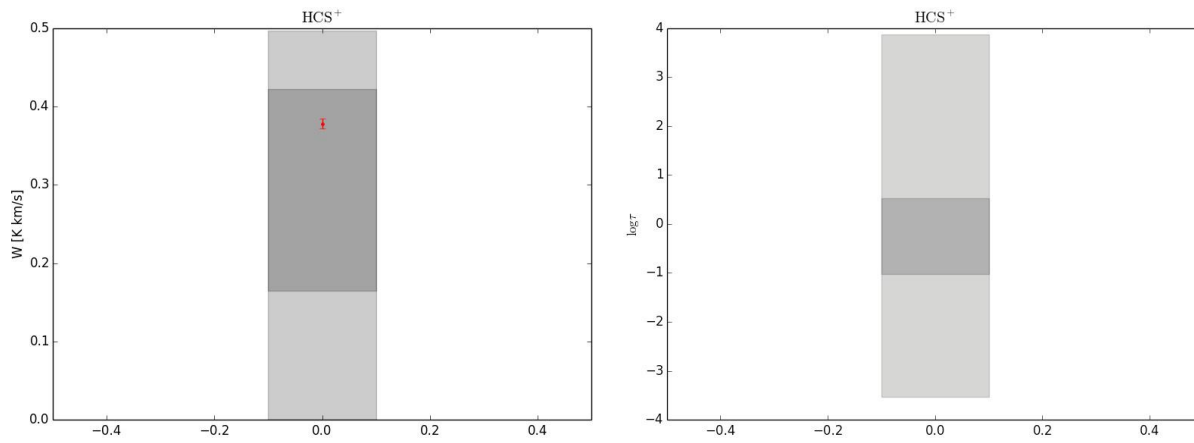
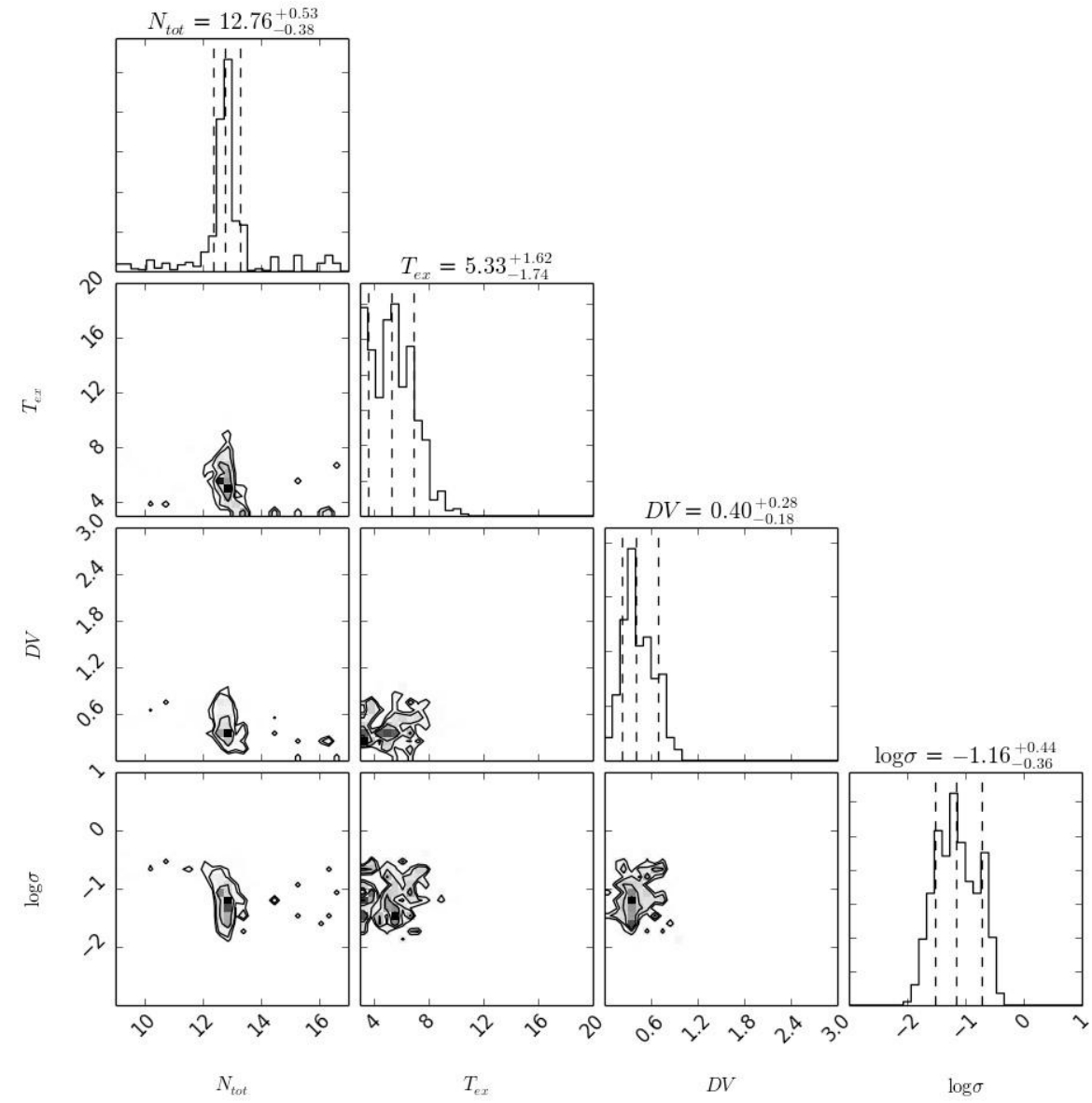


FIG. B17.— ^{13}CS

FIG. B18.— HCS⁺

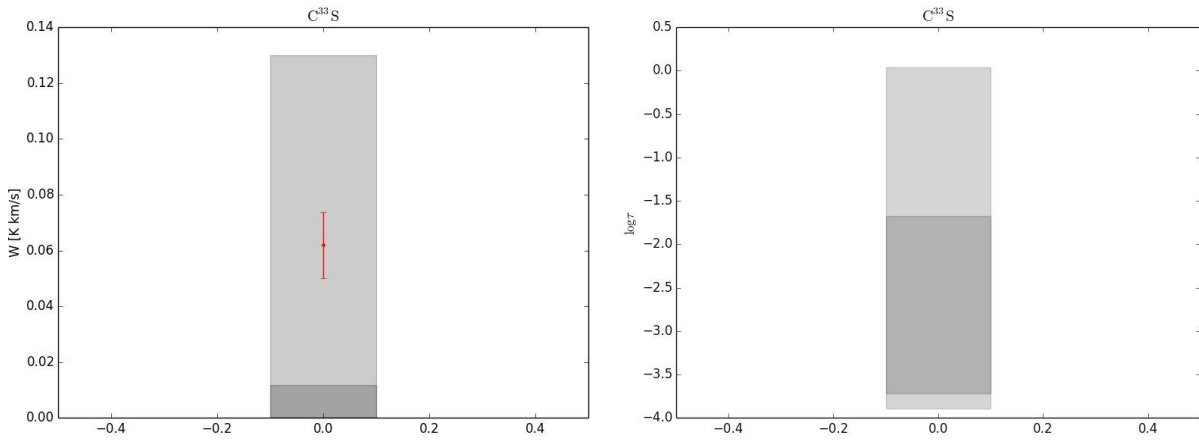
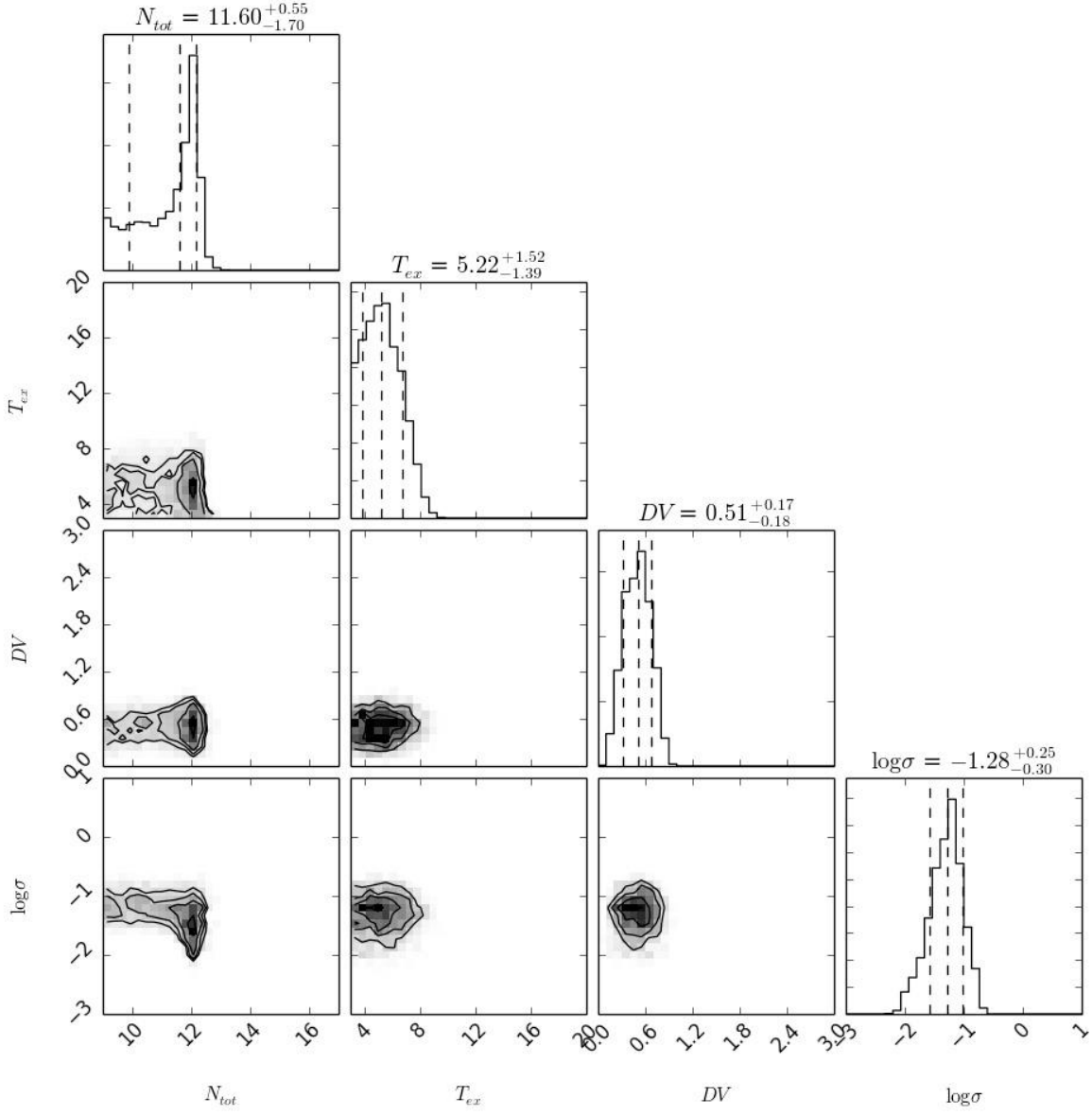
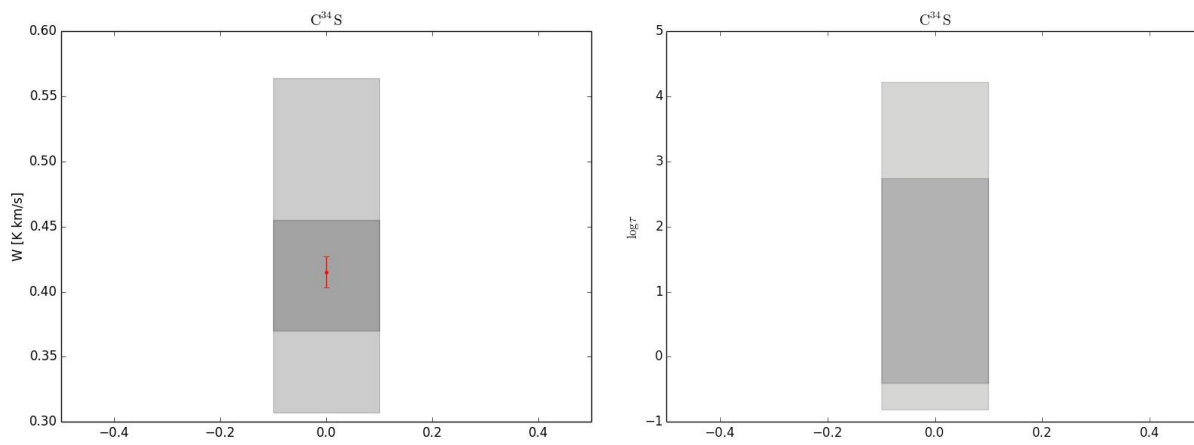
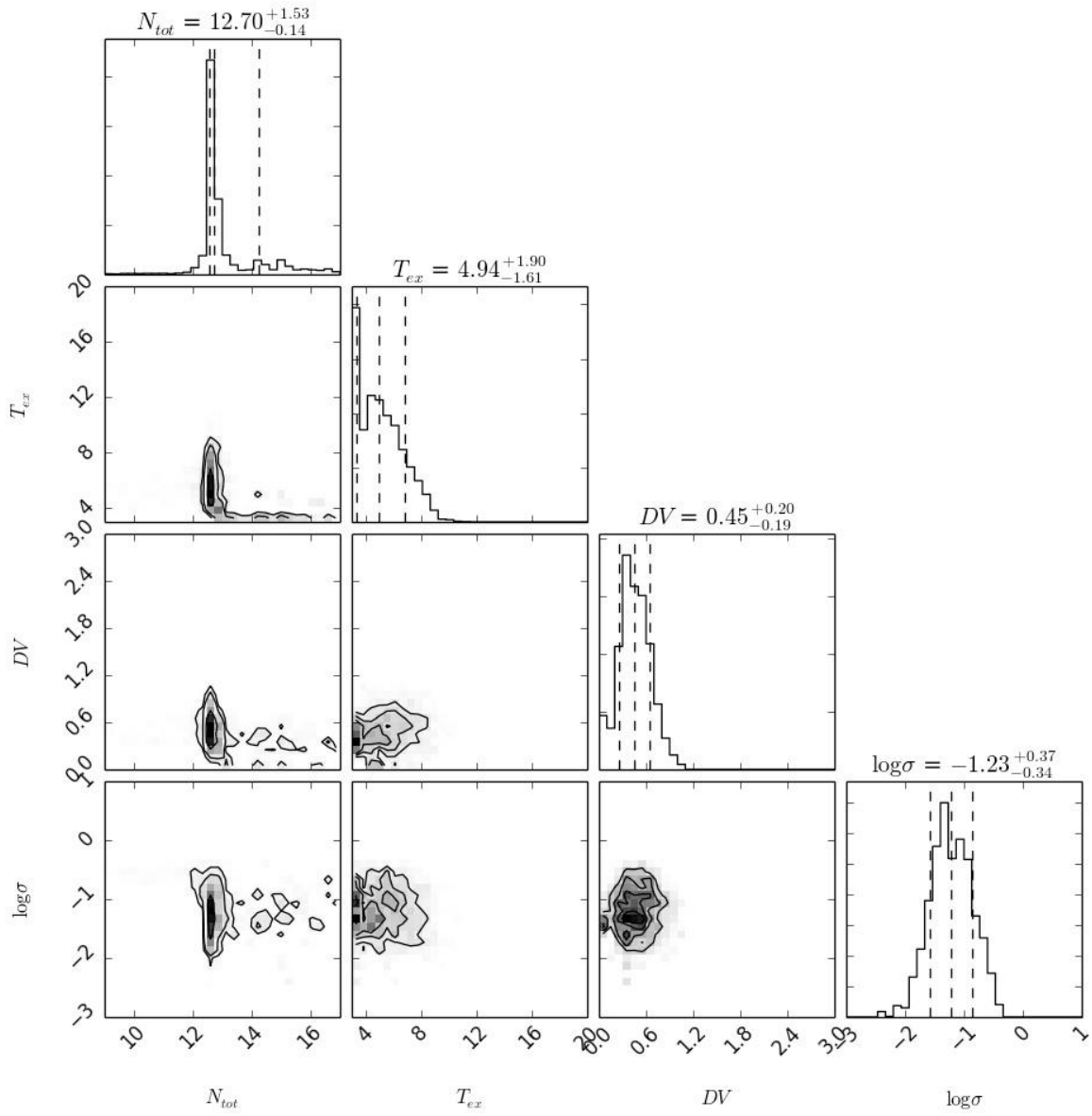
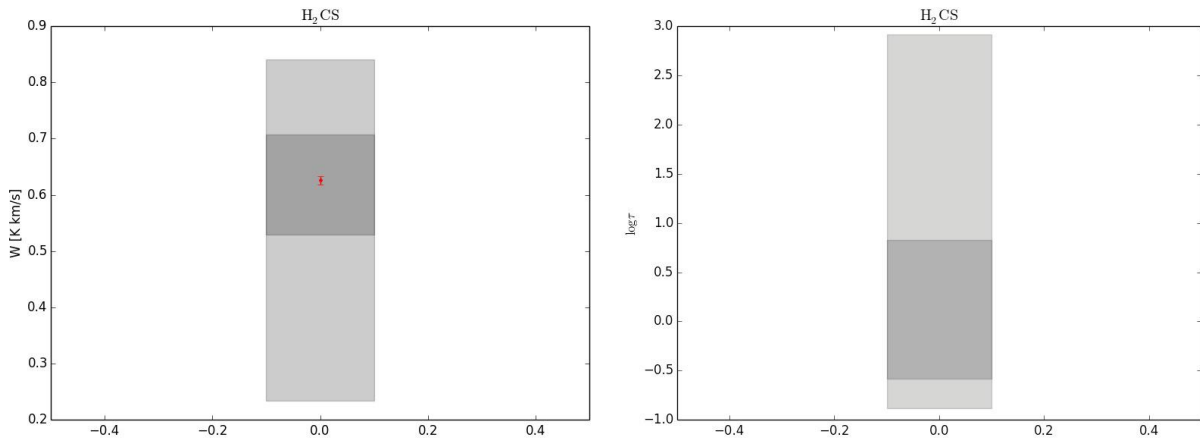
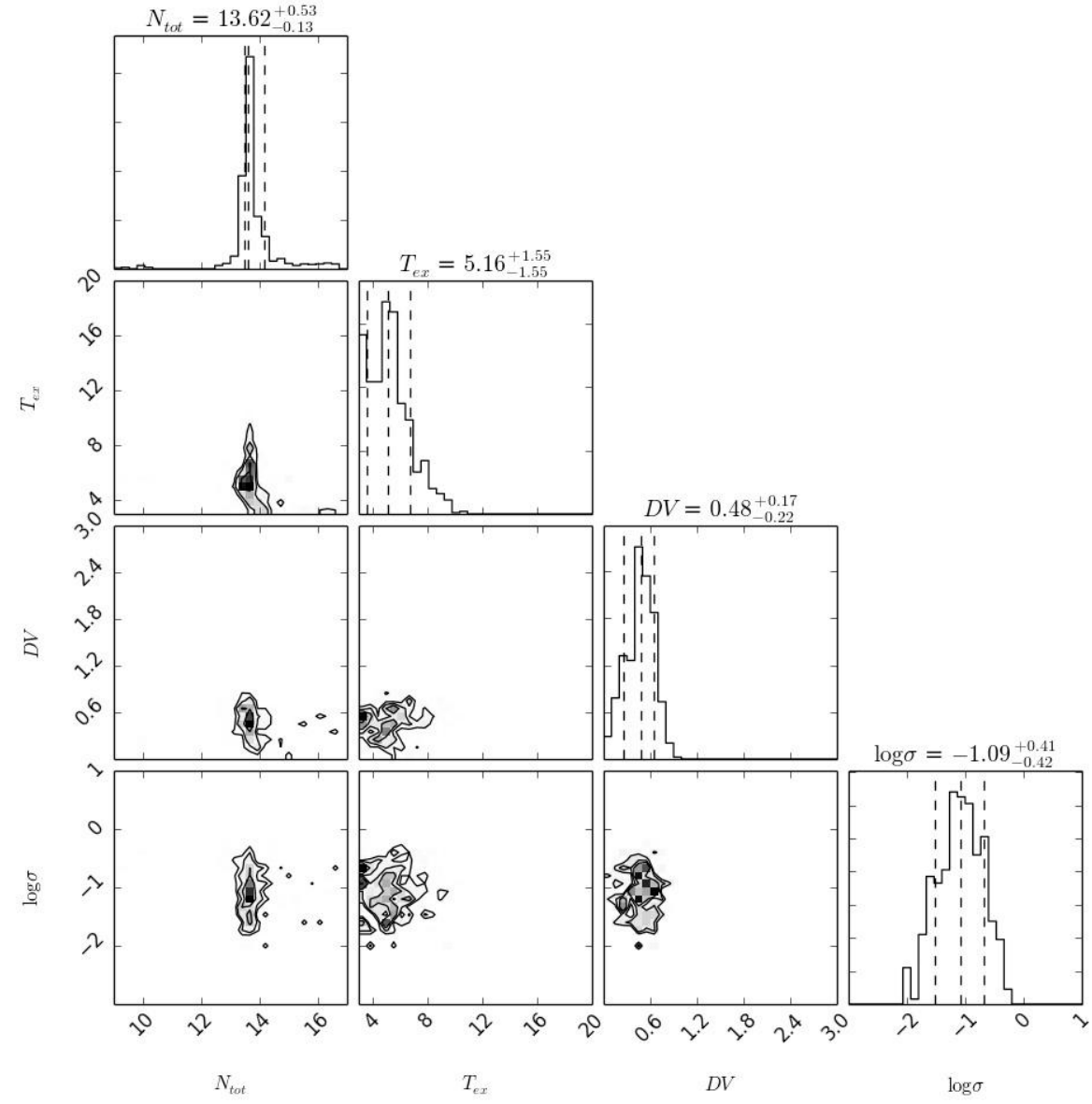


FIG. B19.— $C^{33}S$

FIG. B20.— $C^{34}S$

FIG. B21.— H_2CS

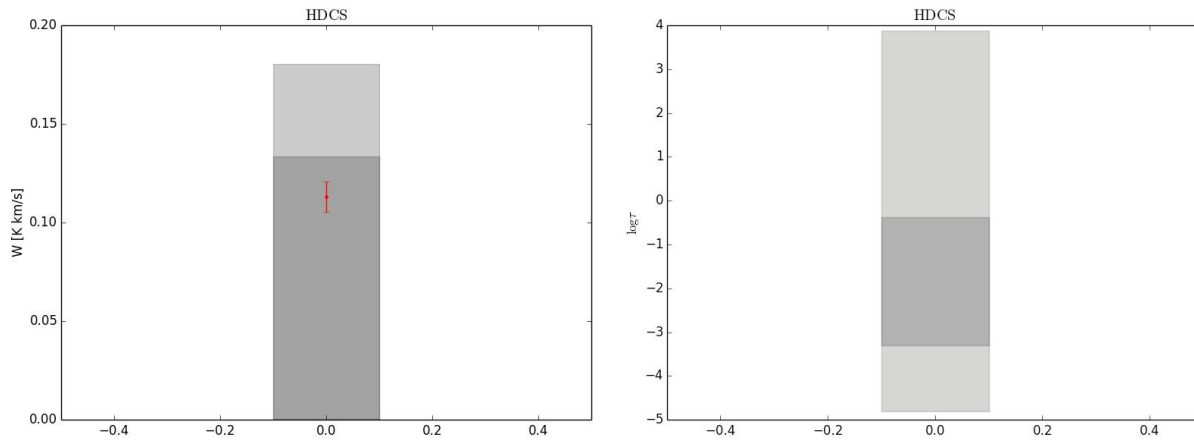
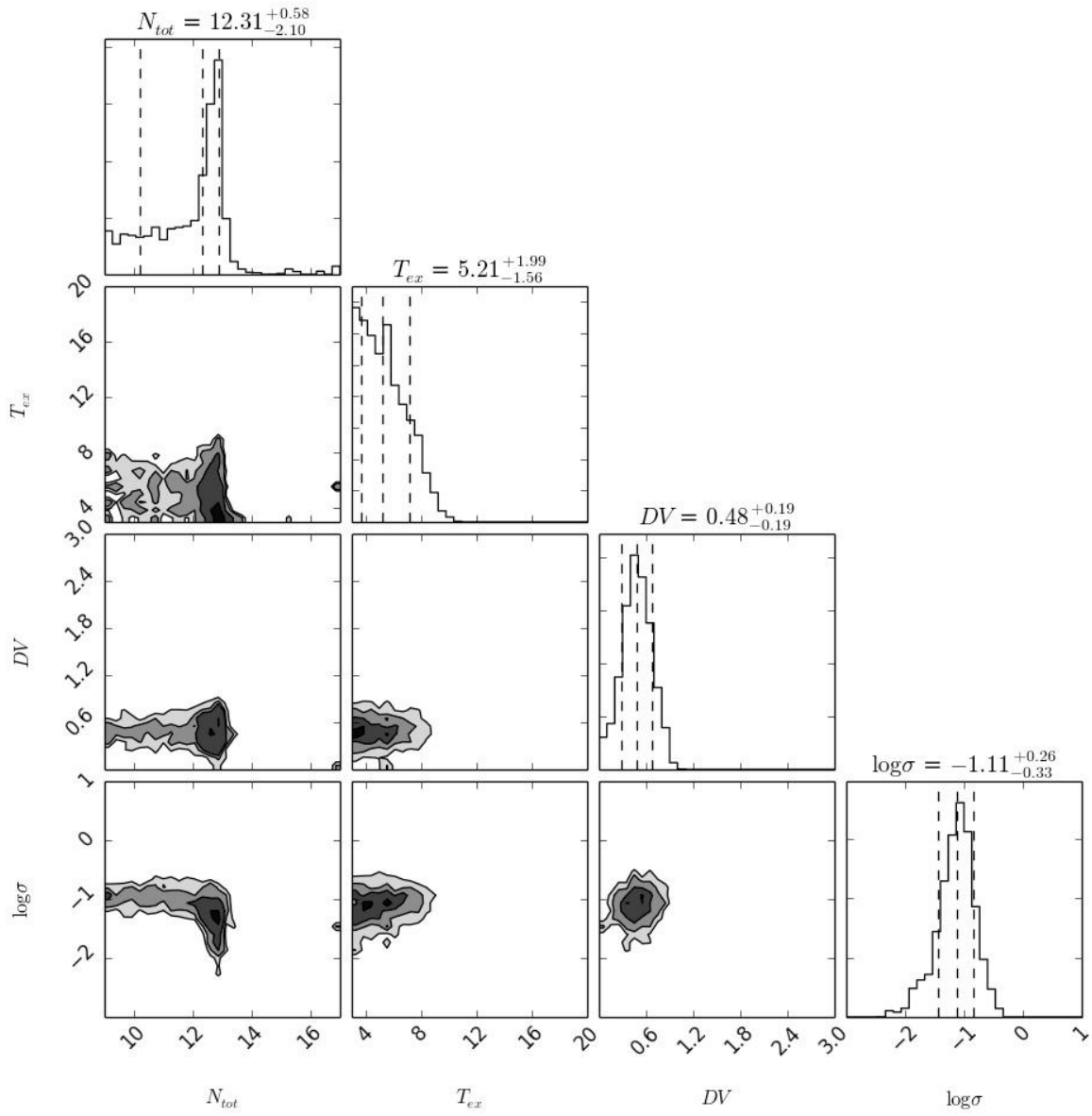


FIG. B22.— HDCS

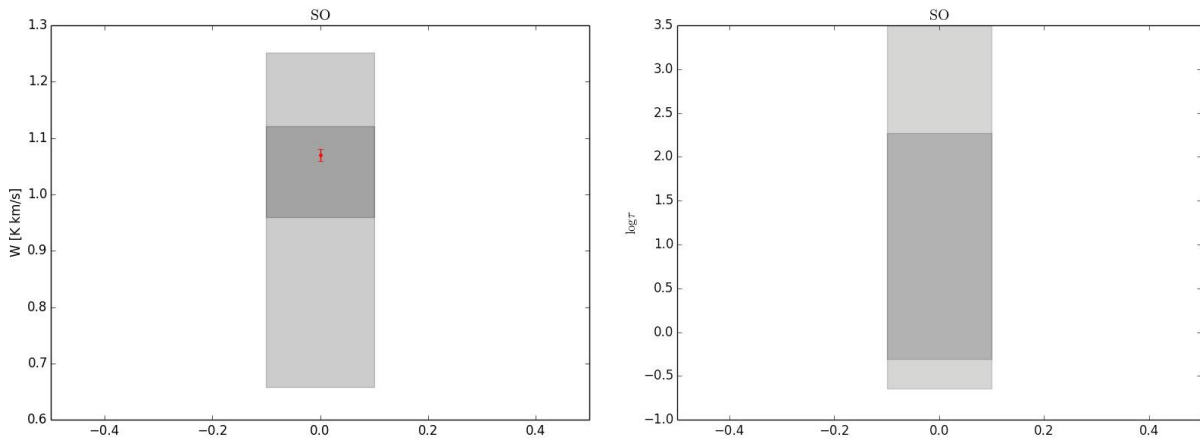
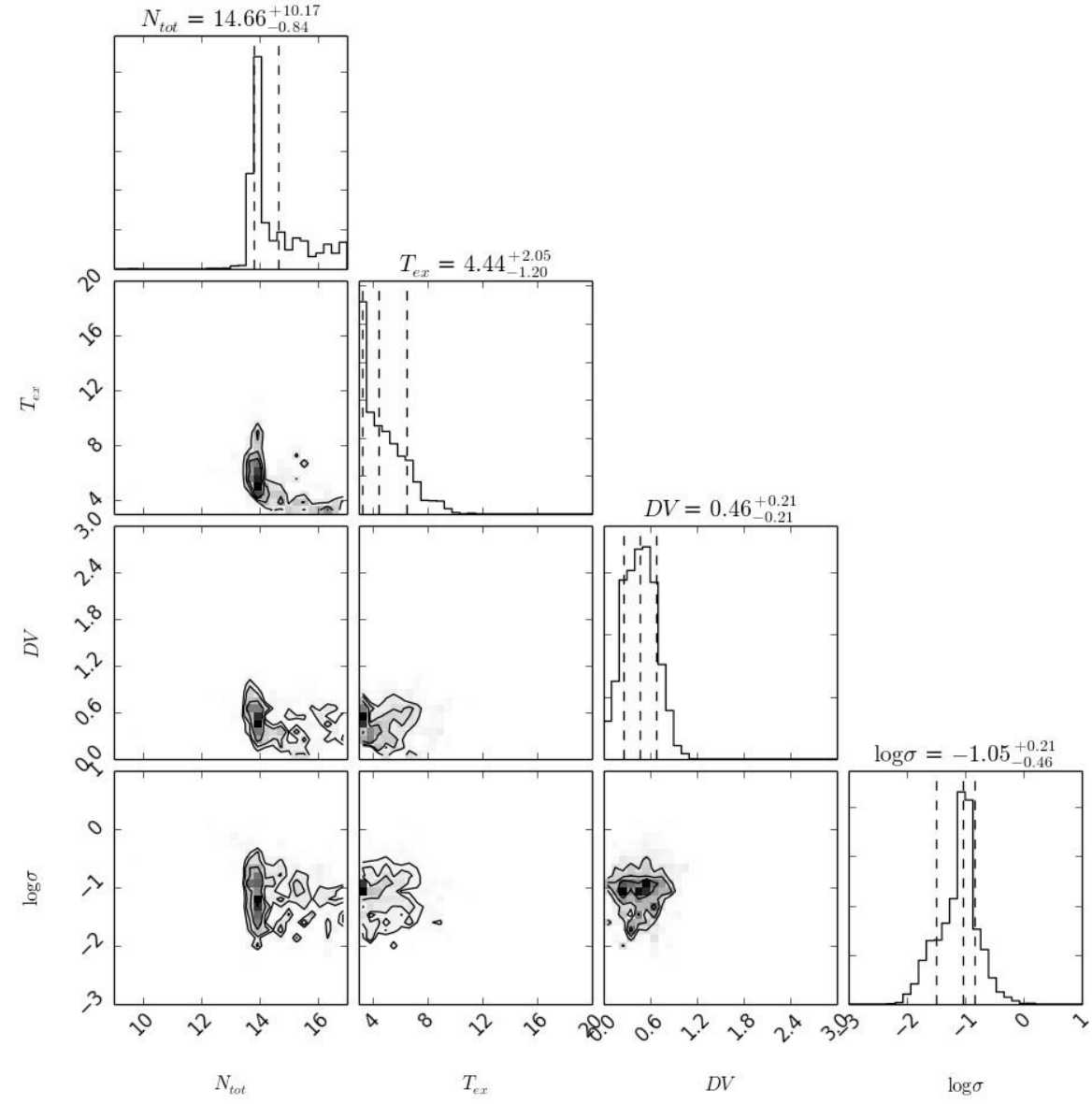
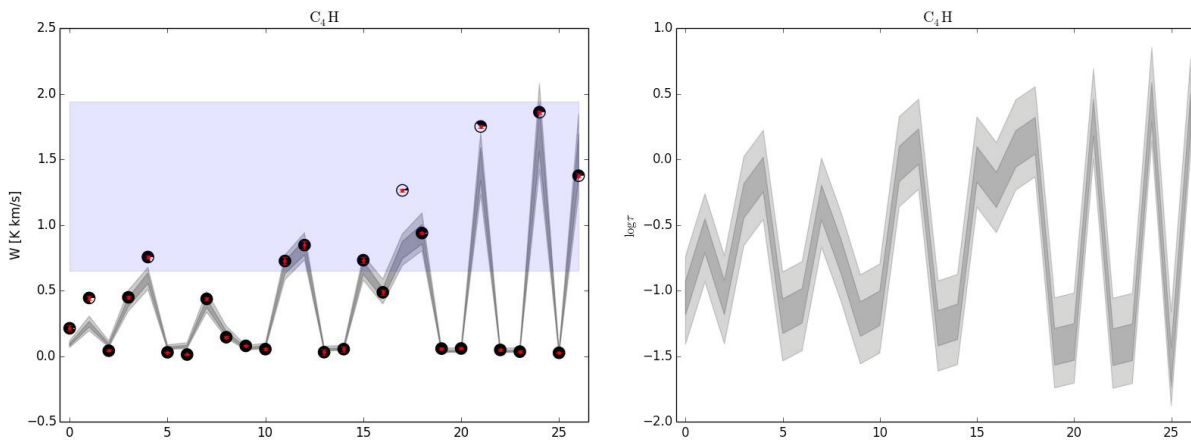
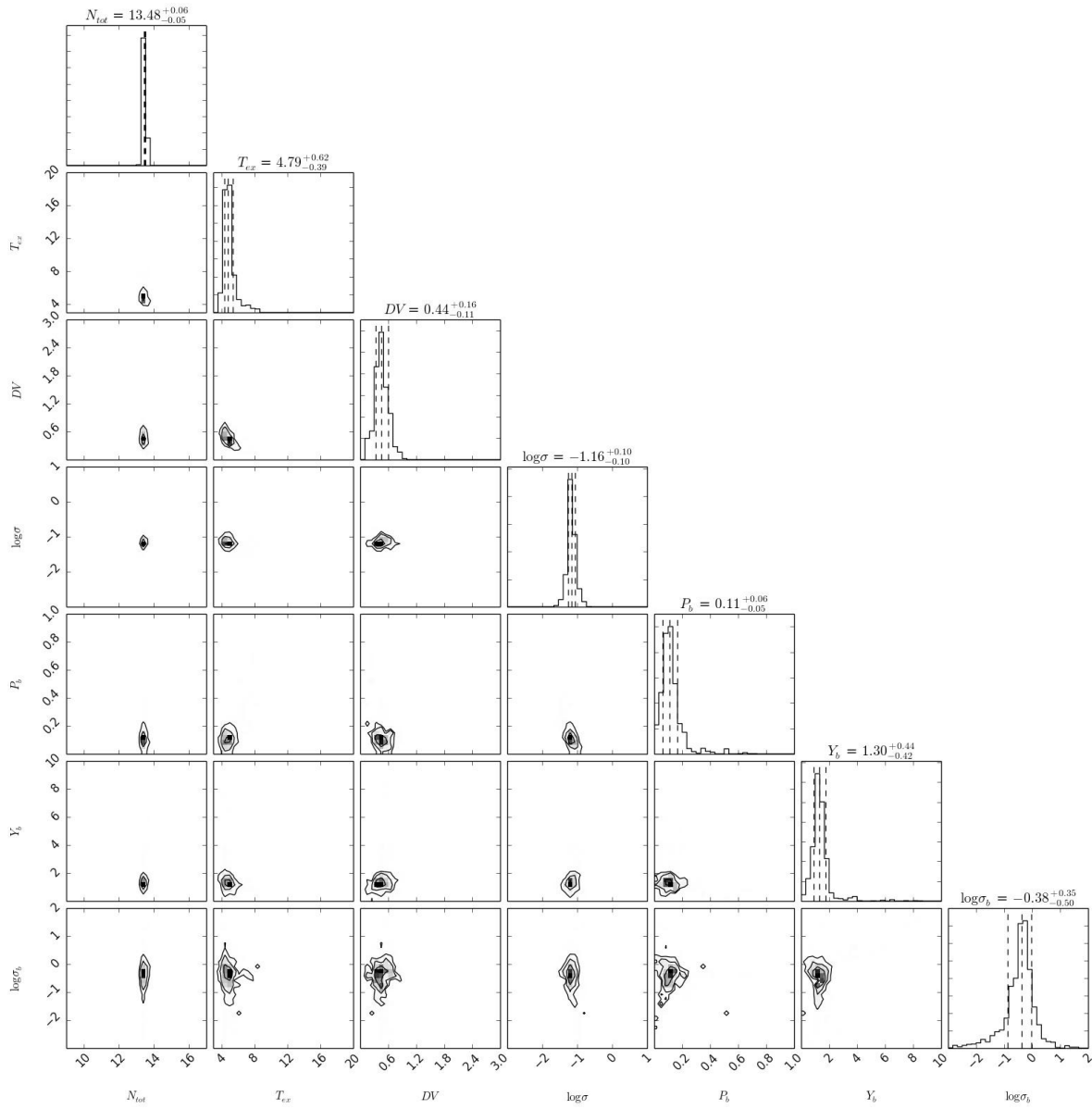


FIG. B23.— SO

FIG. B24.— C_4H

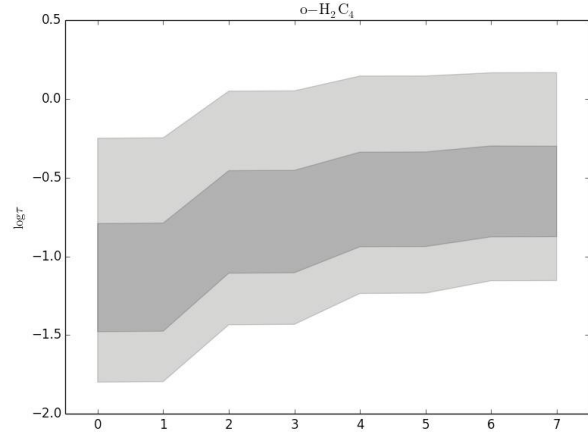
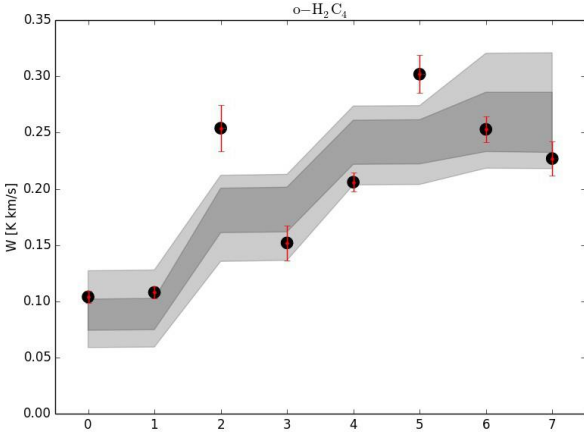
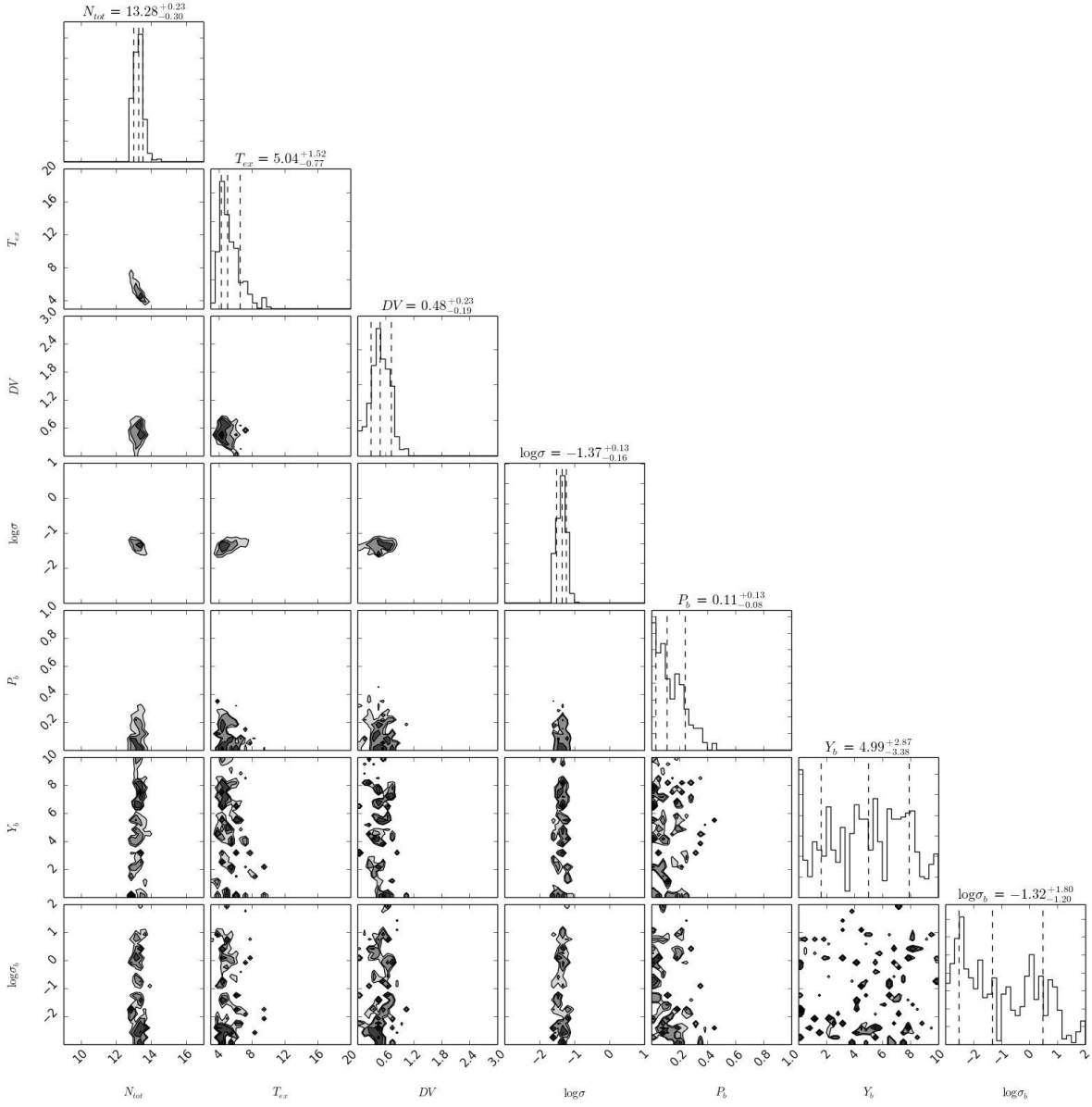
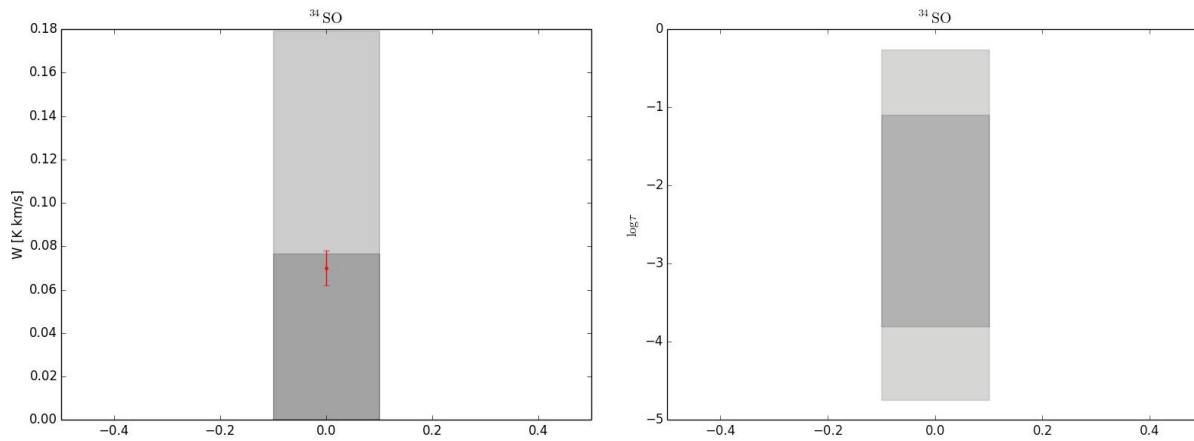
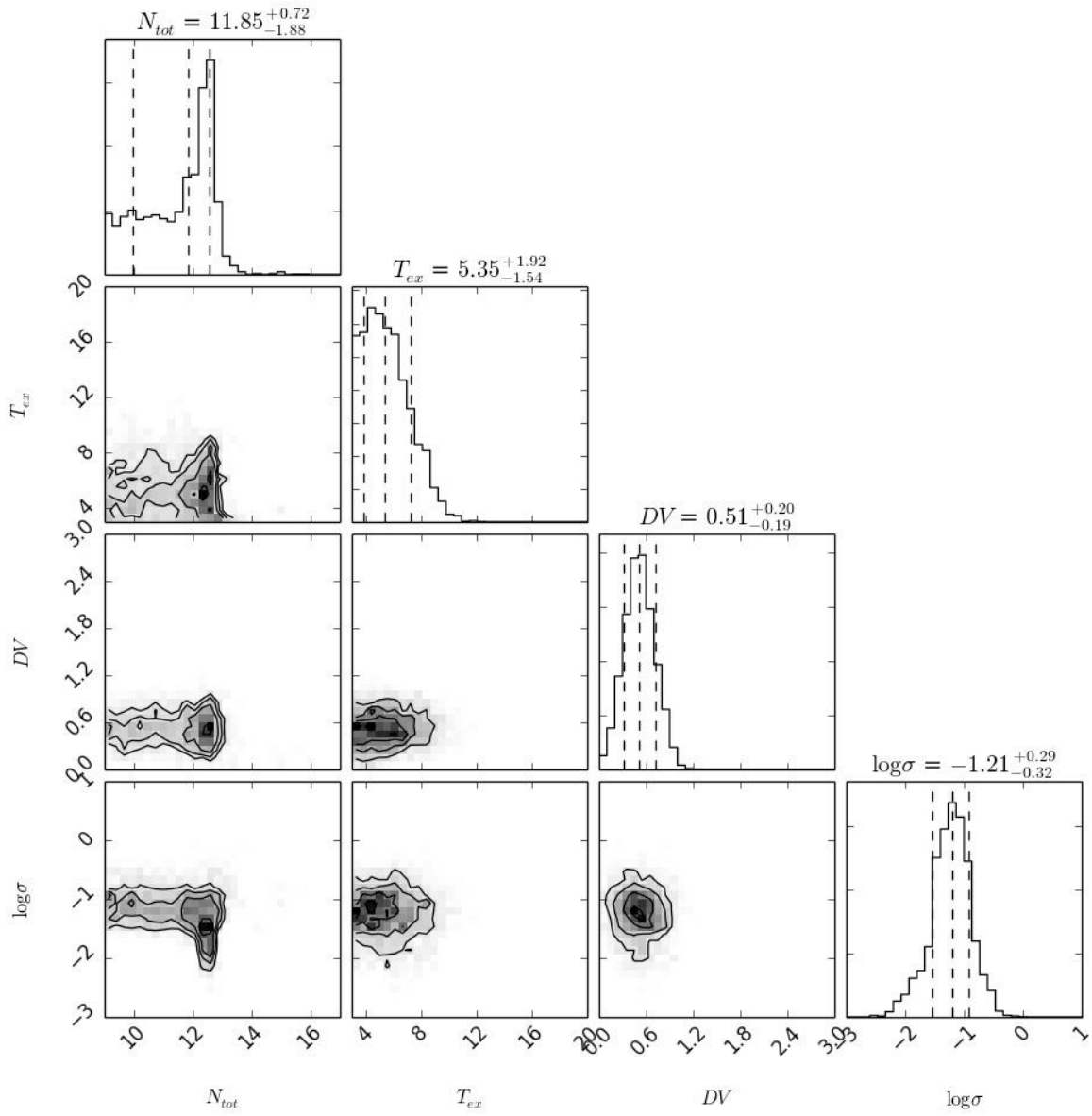
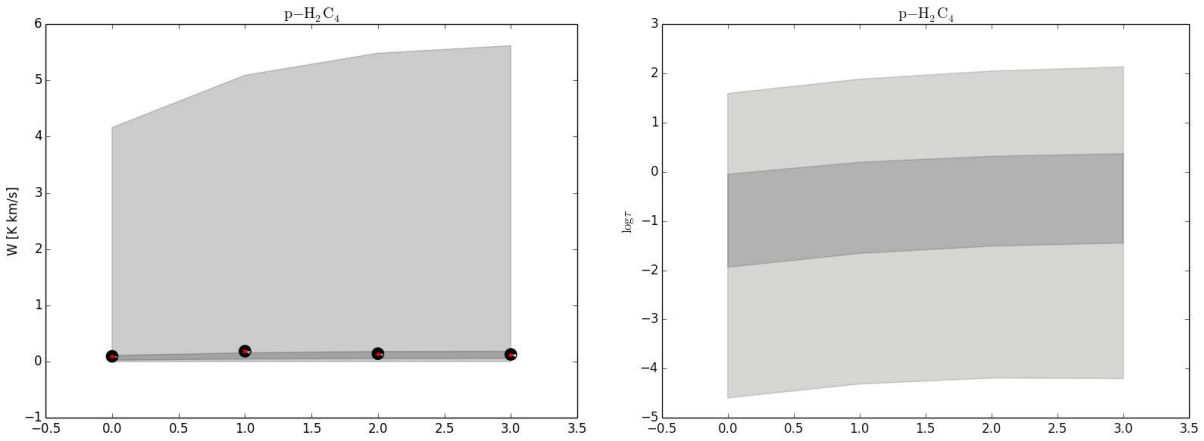
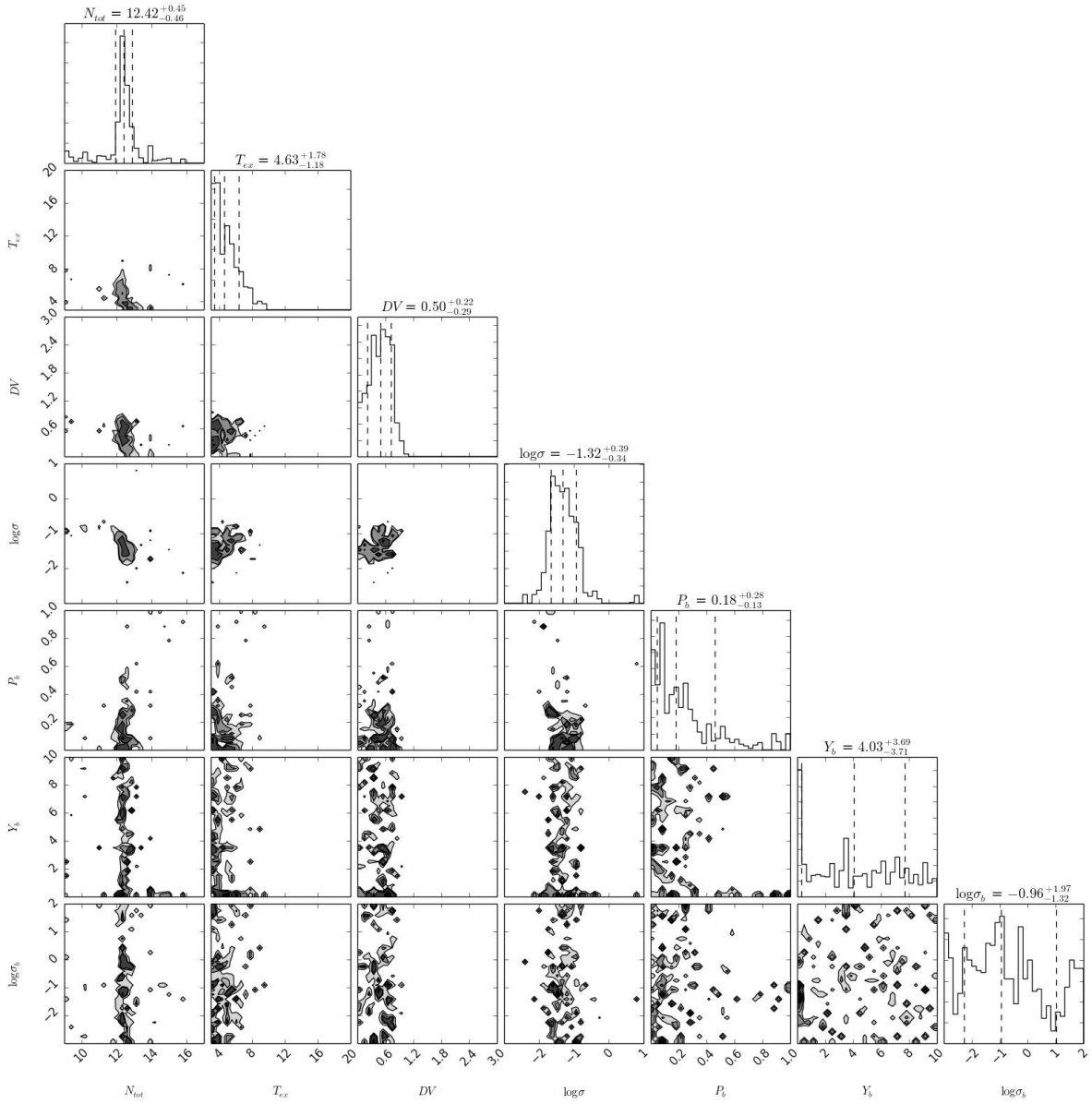
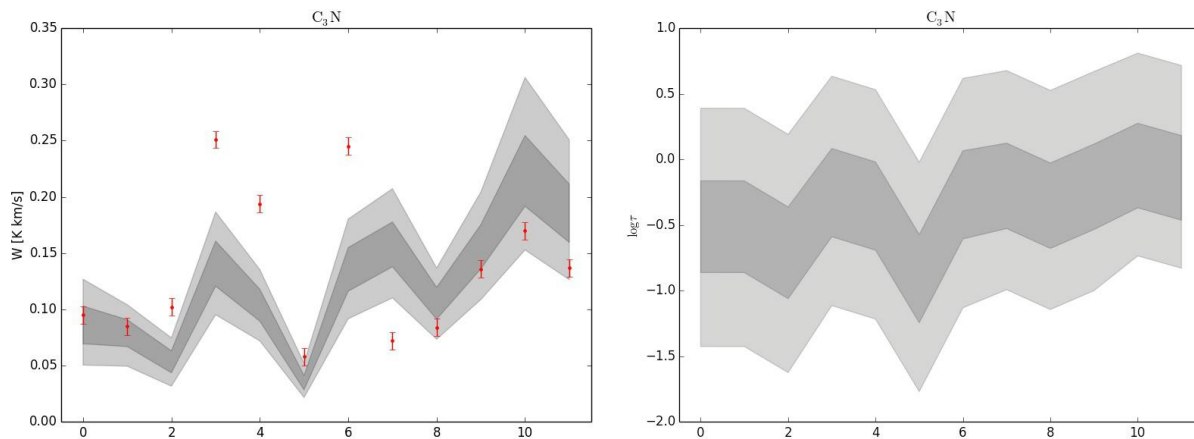
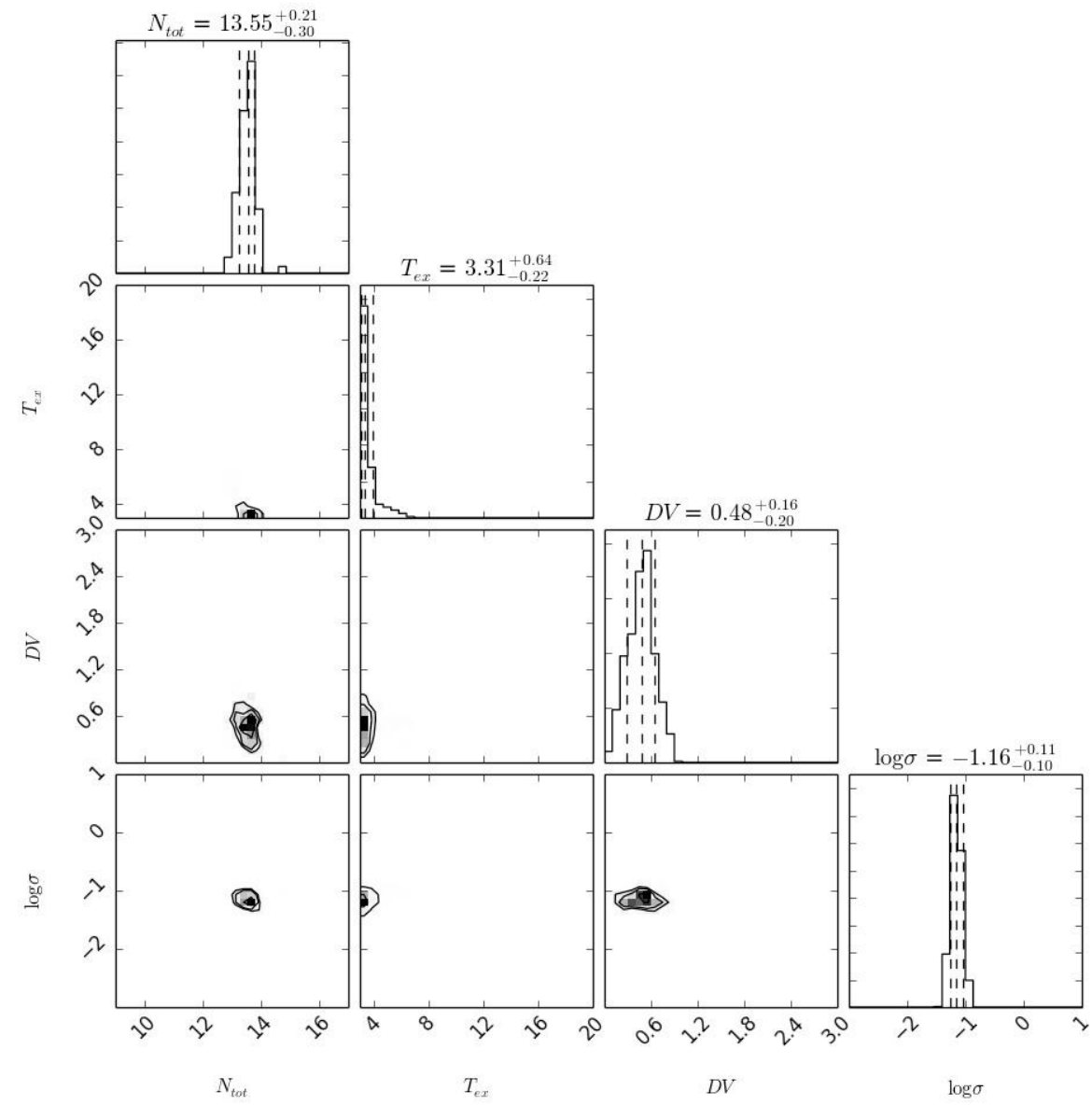
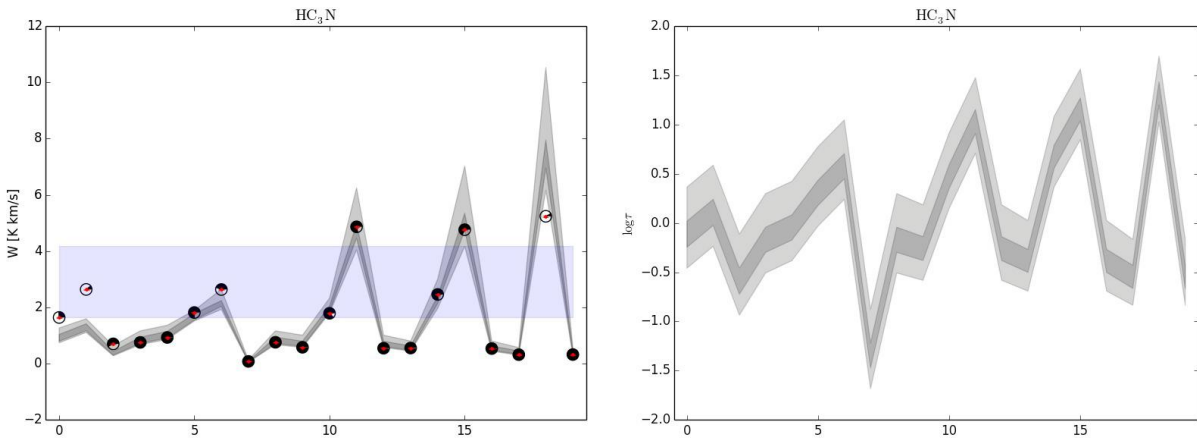
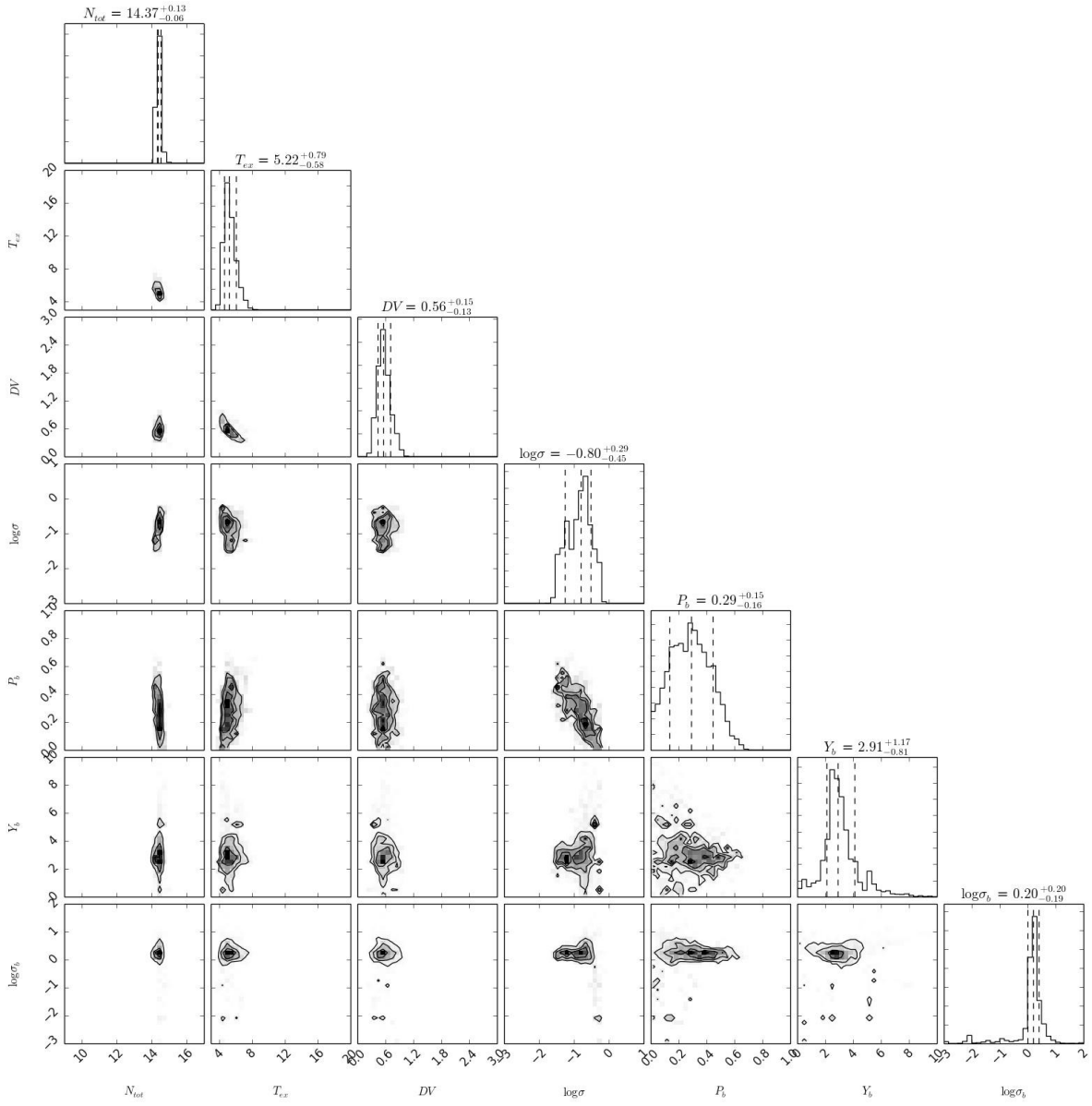


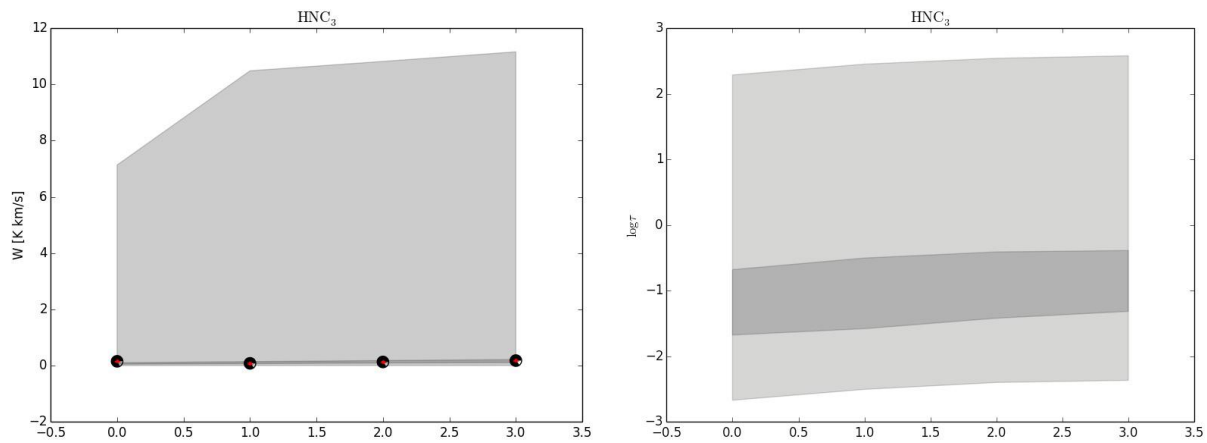
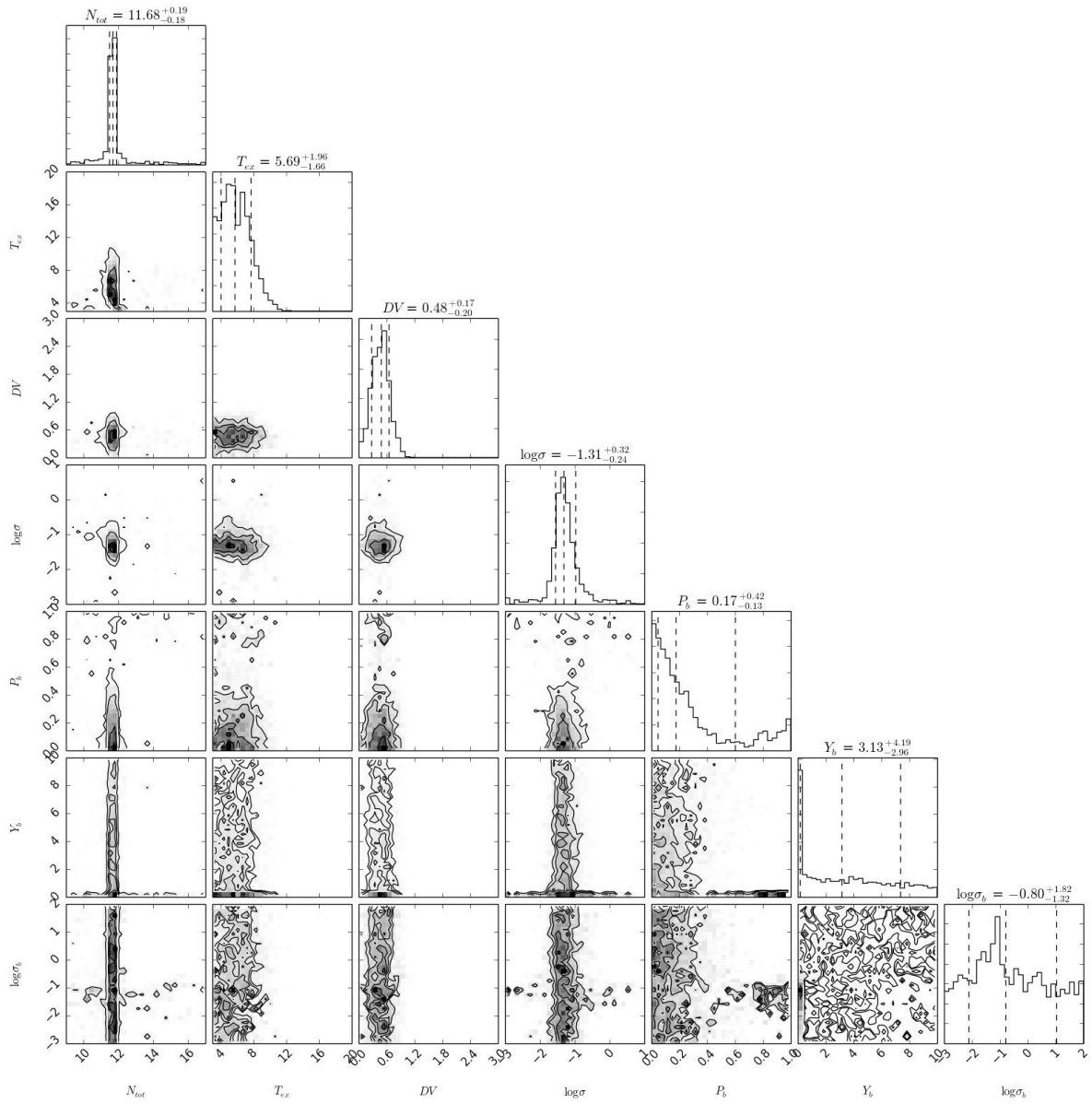
FIG. B25.— $\text{o-C}_4\text{H}_2$

FIG. B26.— ^{34}SO

FIG. B27.— p-C₄H₂

FIG. B28.— C_3N

FIG. B29.— HC₃N

FIG. B30.— HNC_3

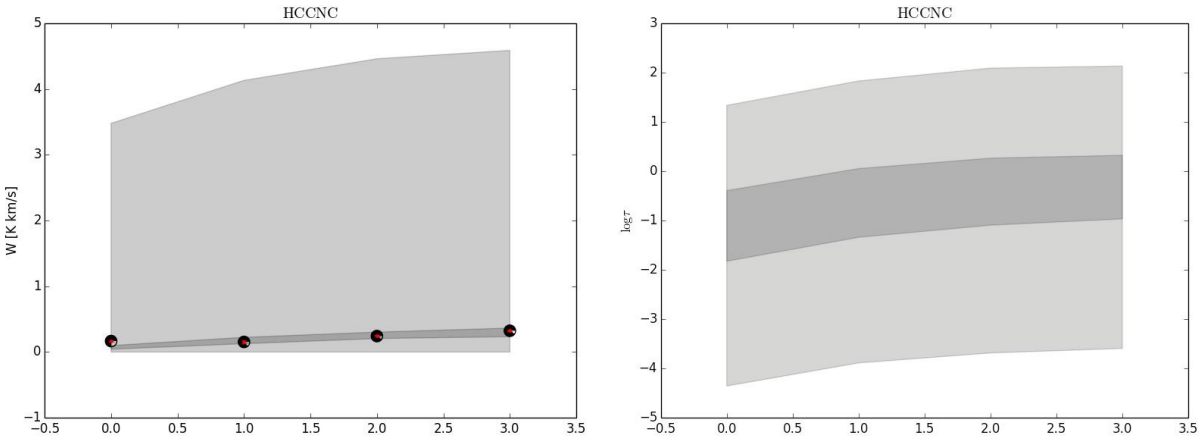
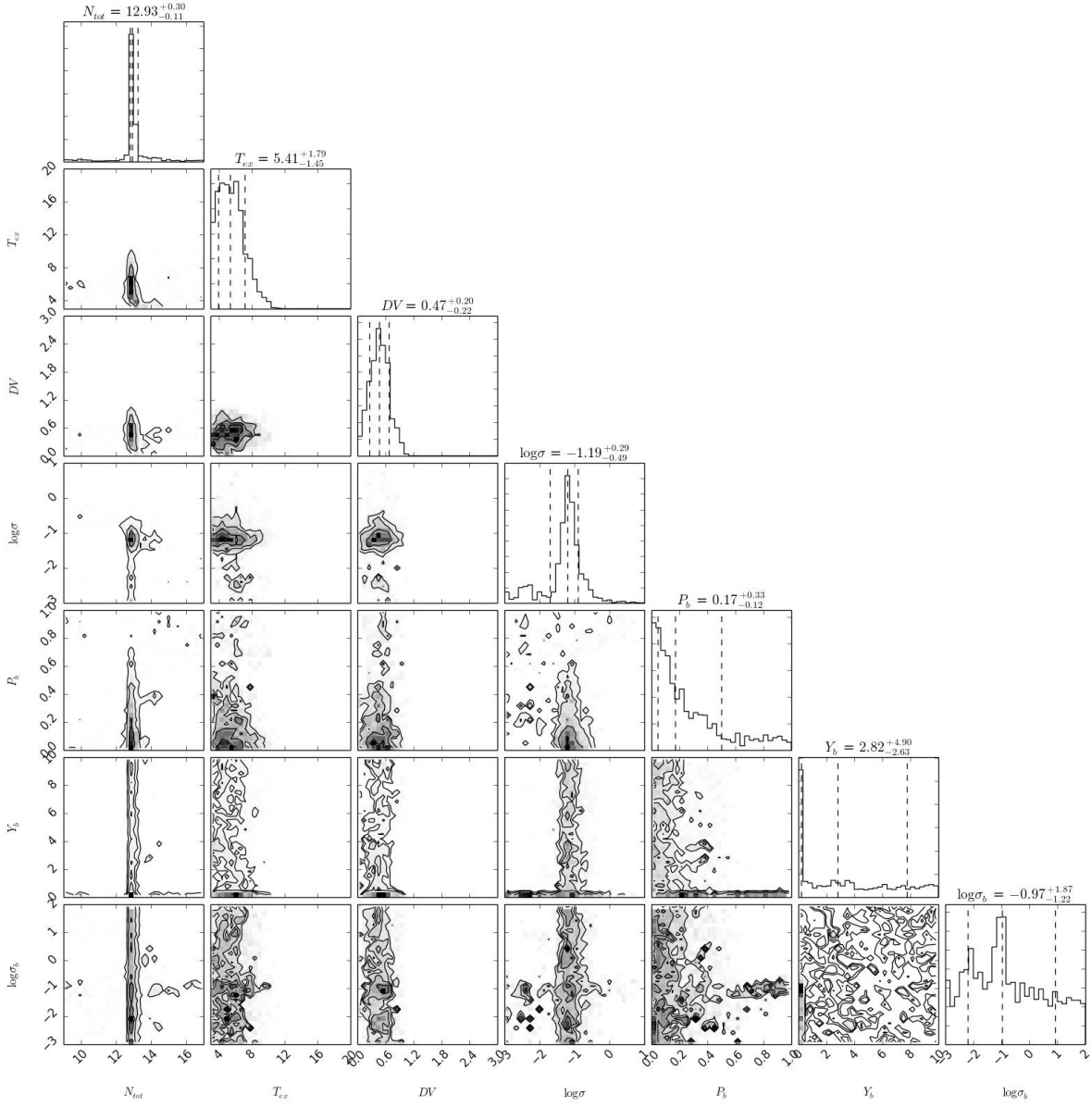
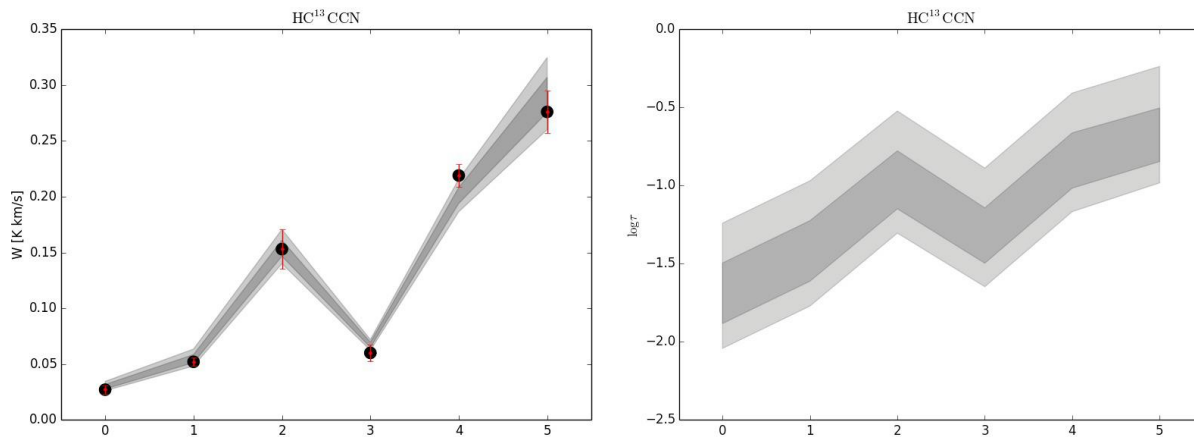
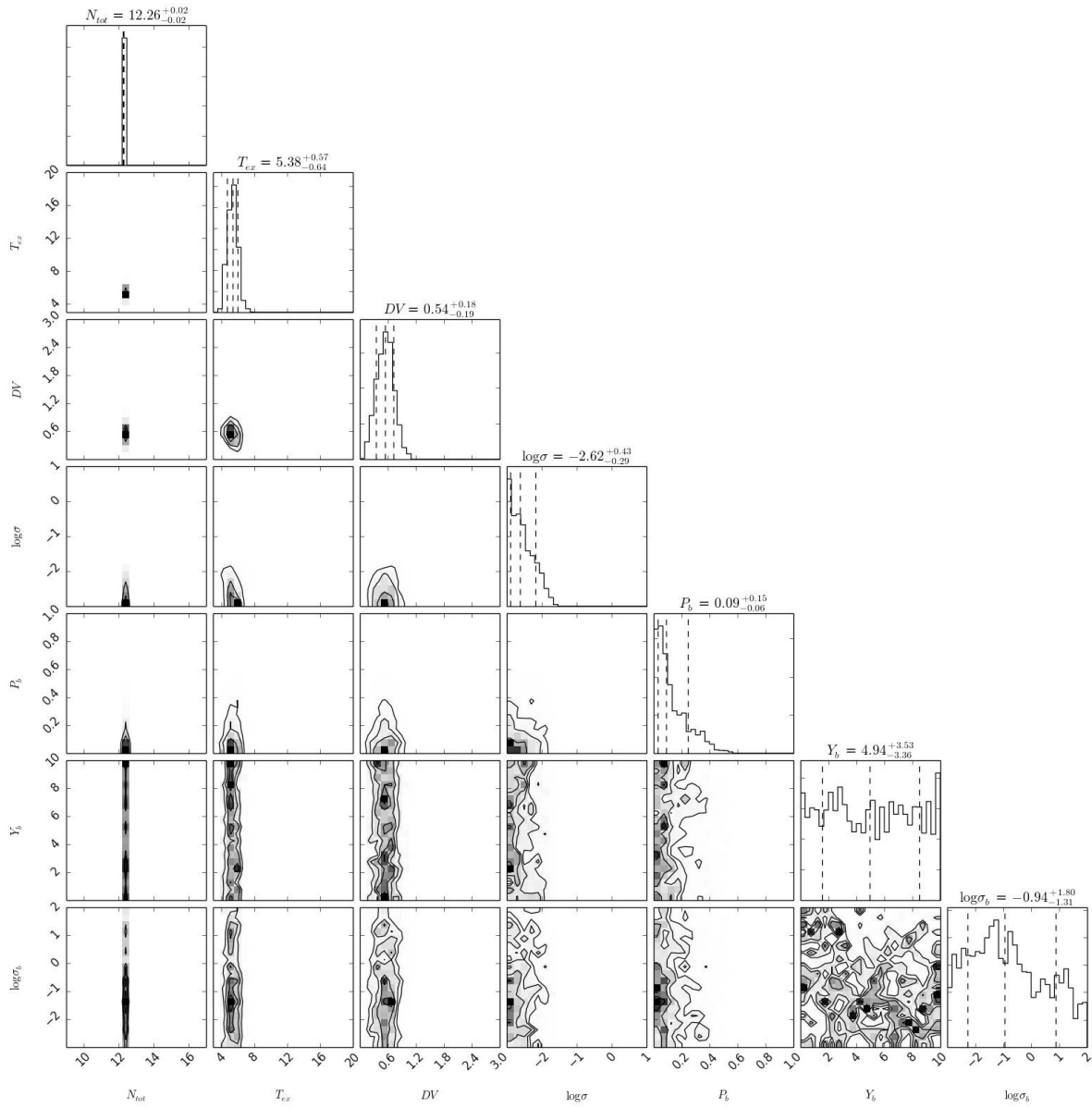


FIG. B31.— HCCNC

FIG. B32.— HC¹³CCN

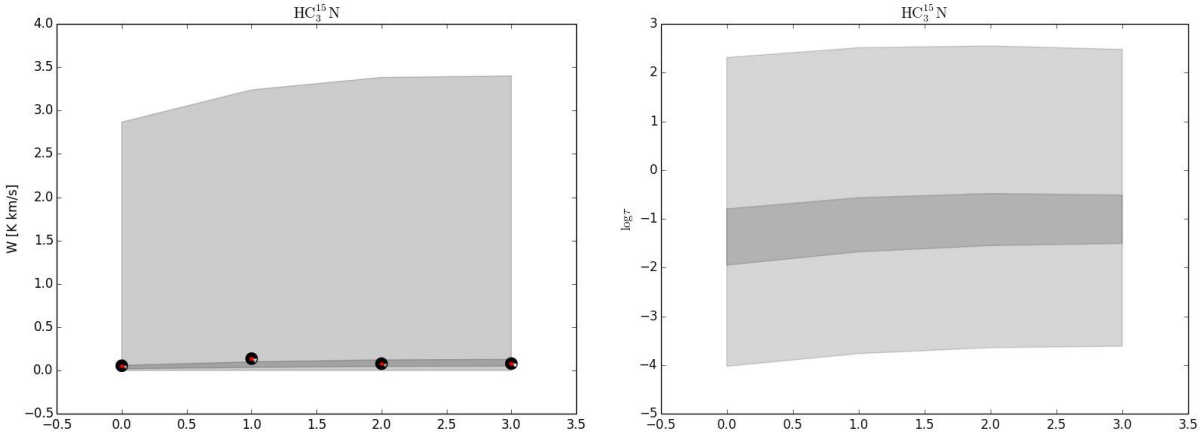
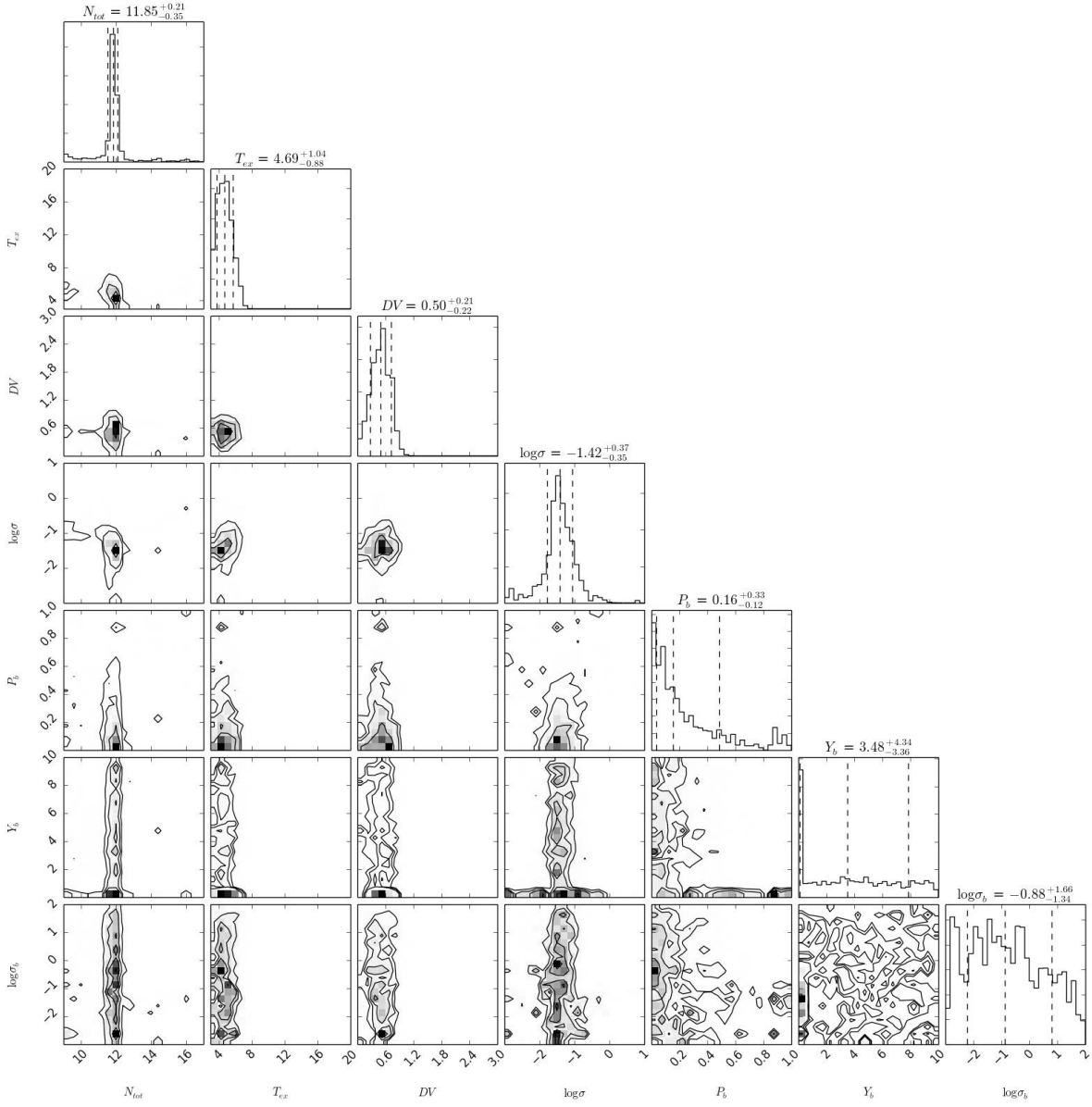
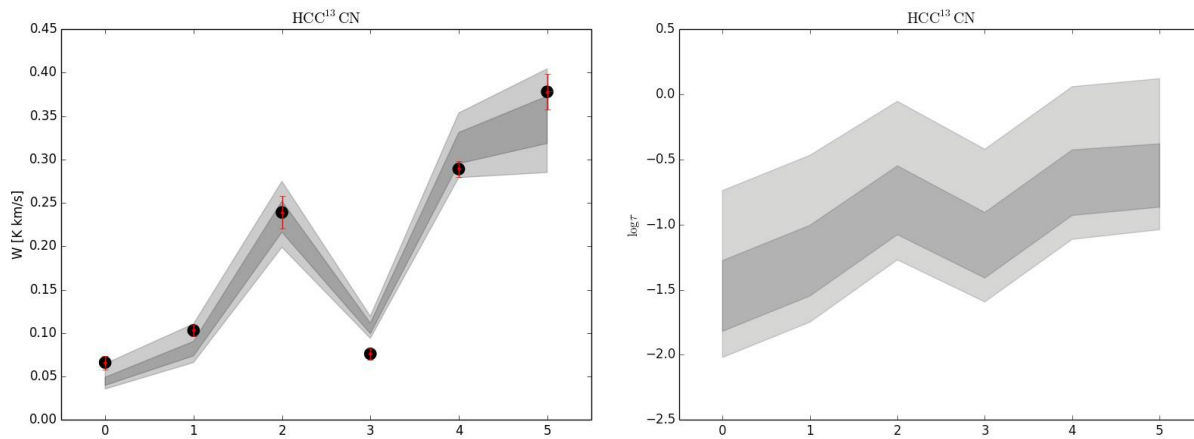
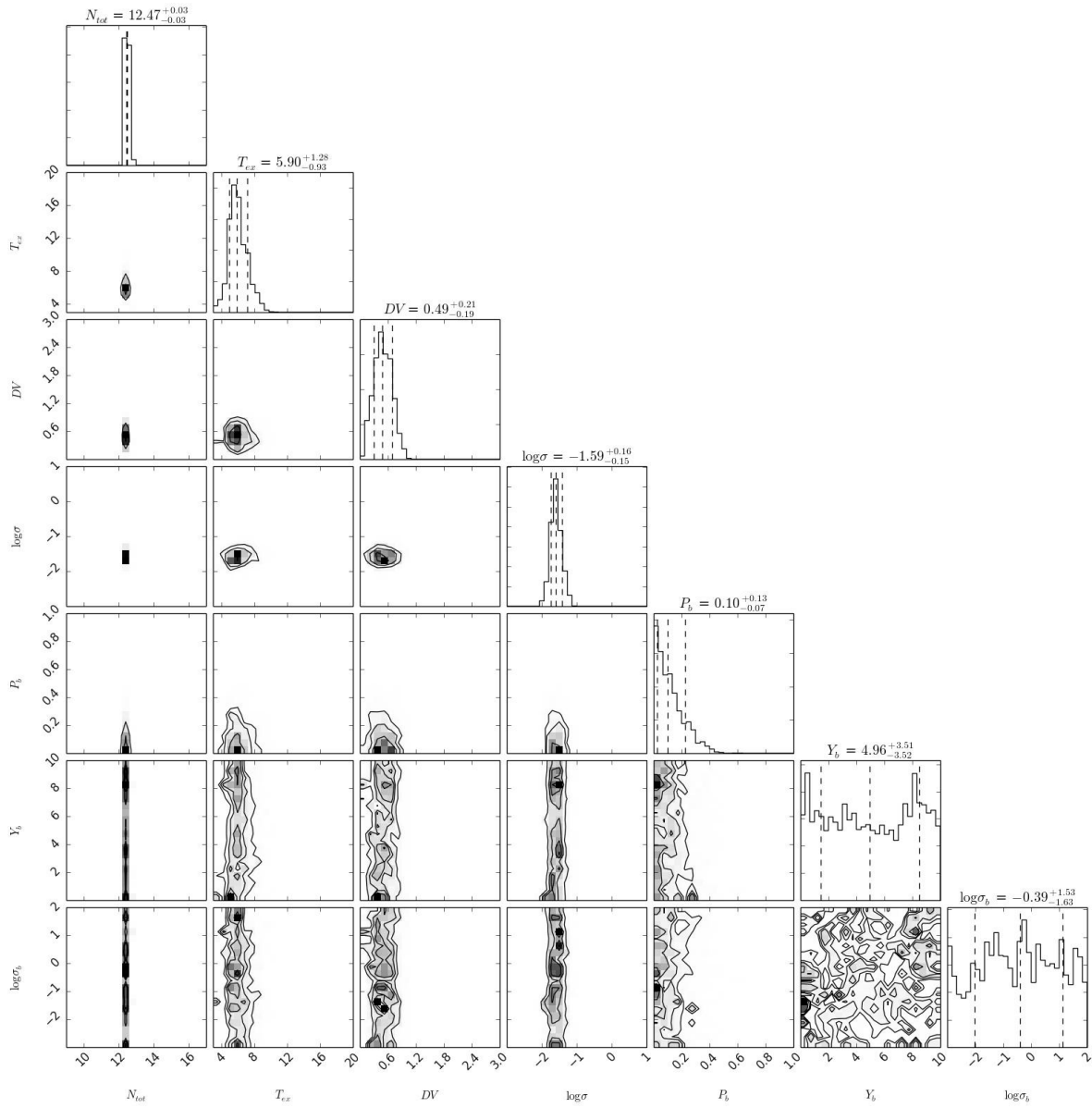


FIG. B33.— HC_3^{15}N

FIG. B34.— $\text{HC}_2^{13}\text{CN}$

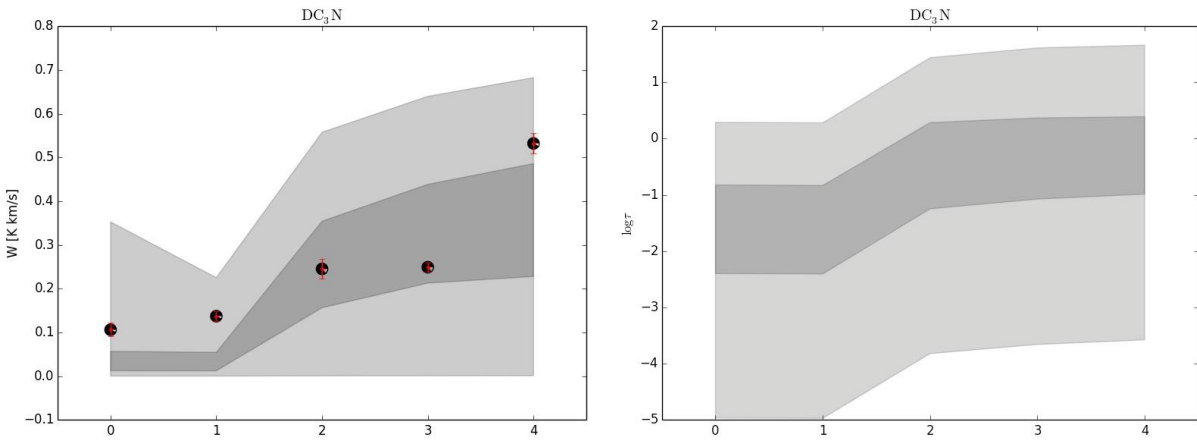
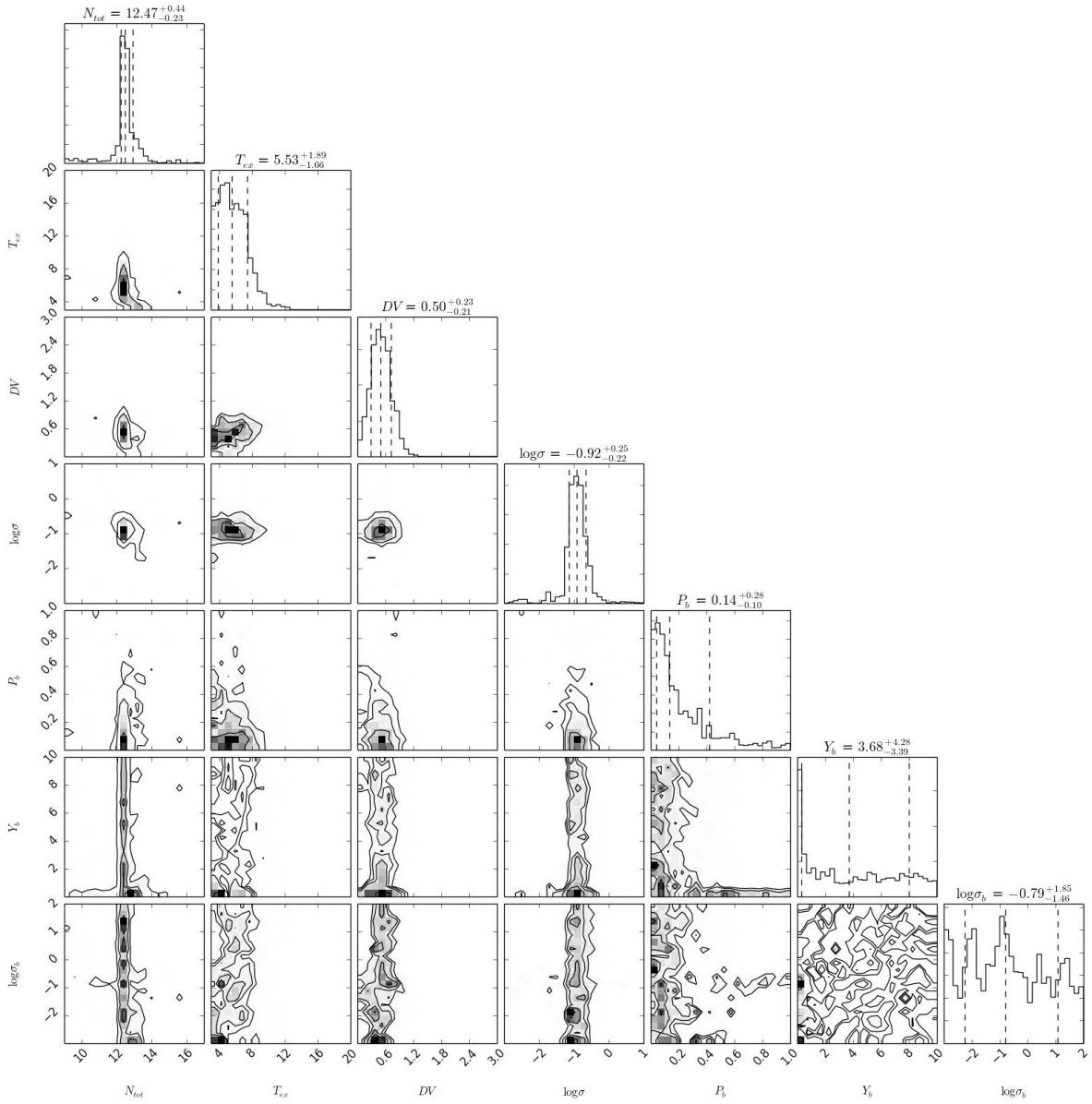
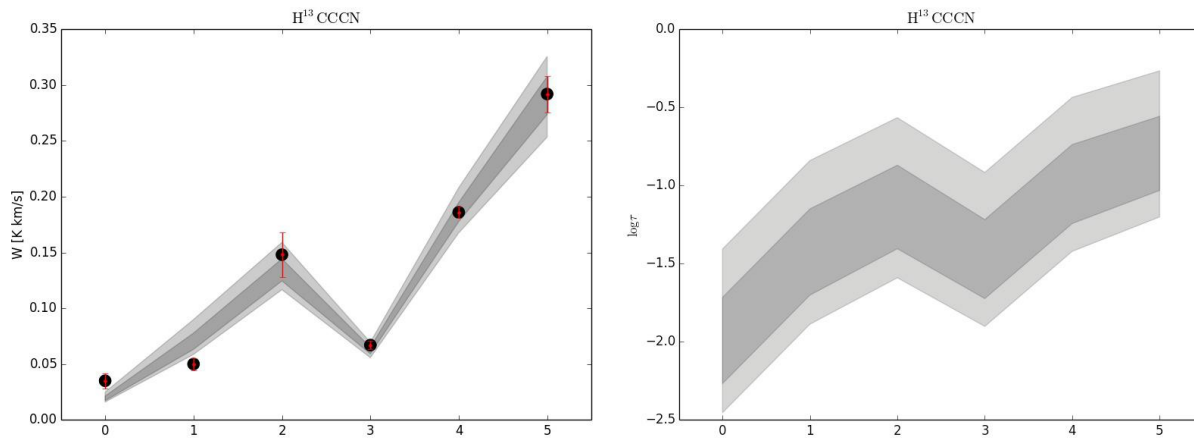
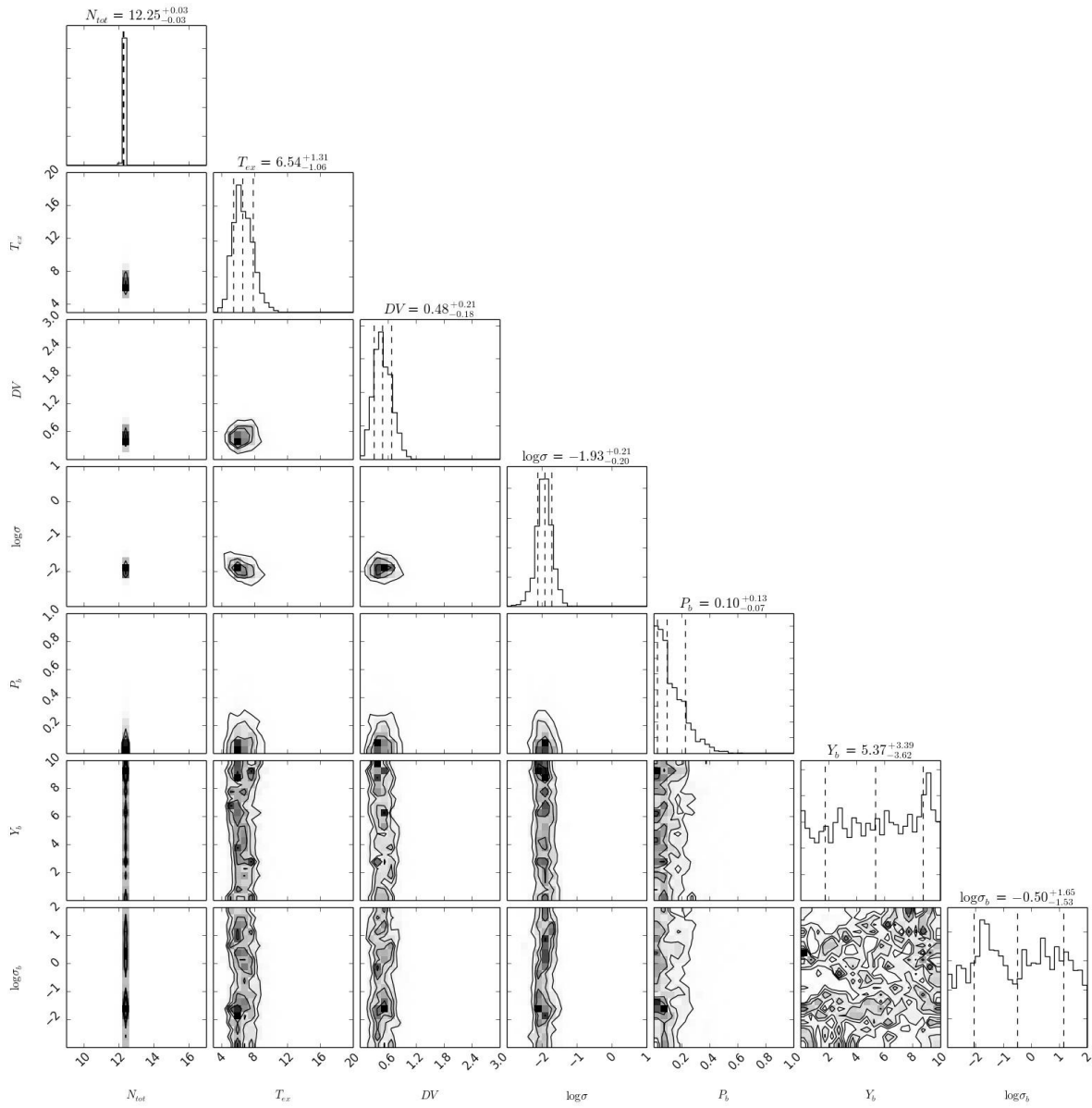
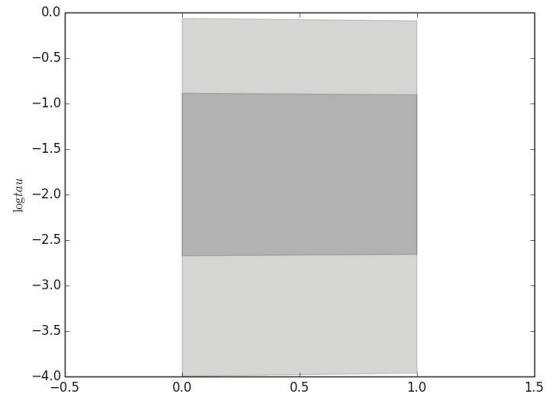
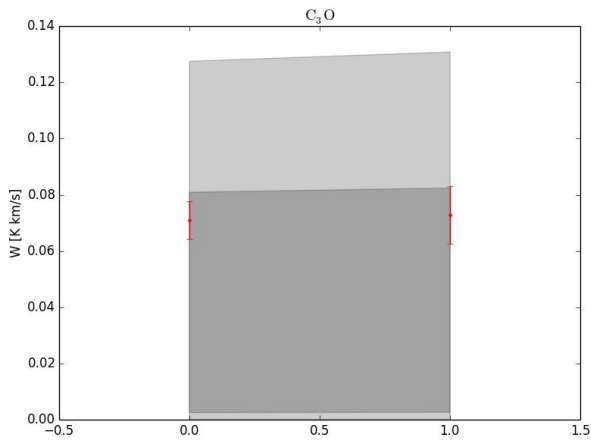
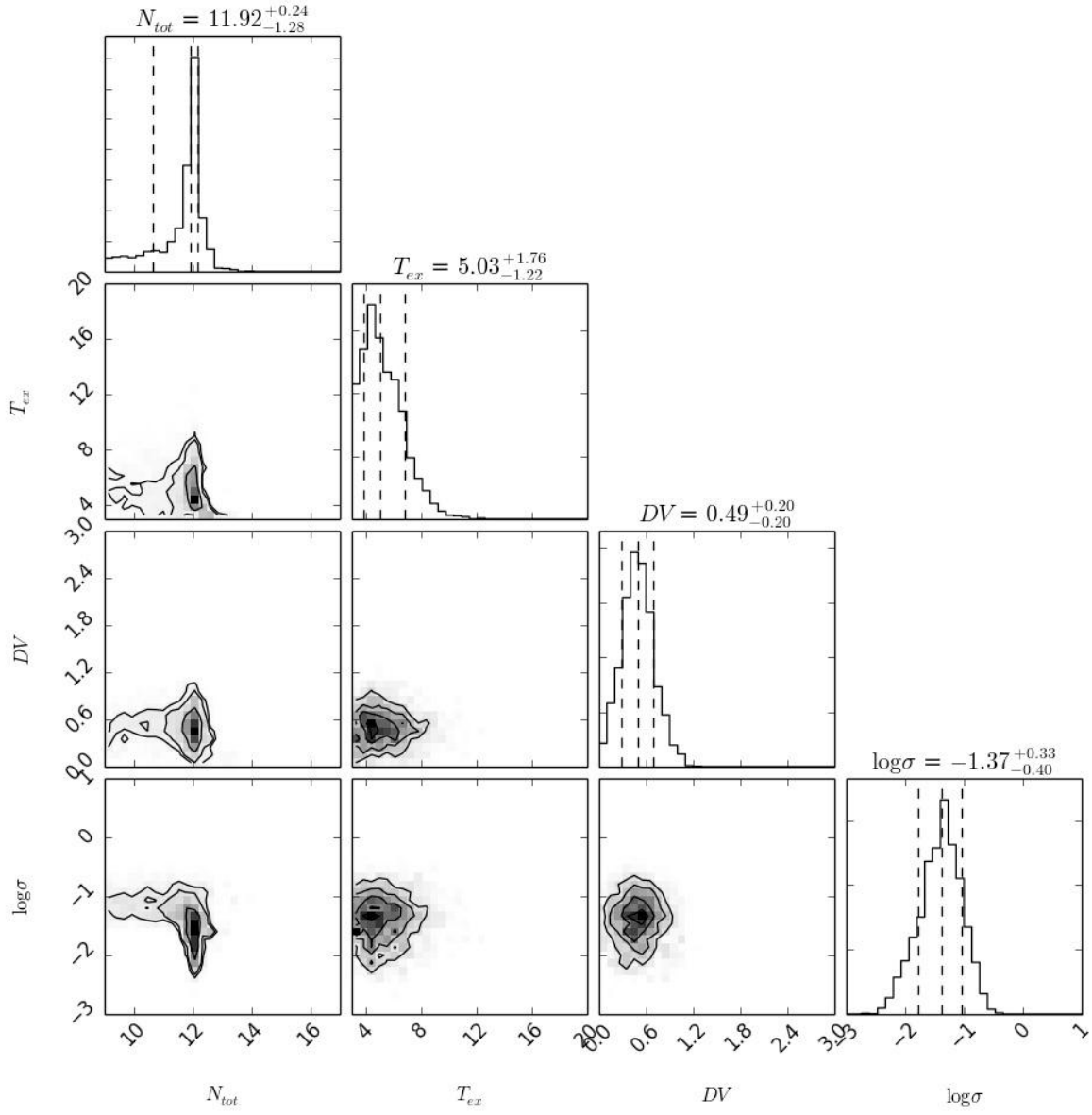
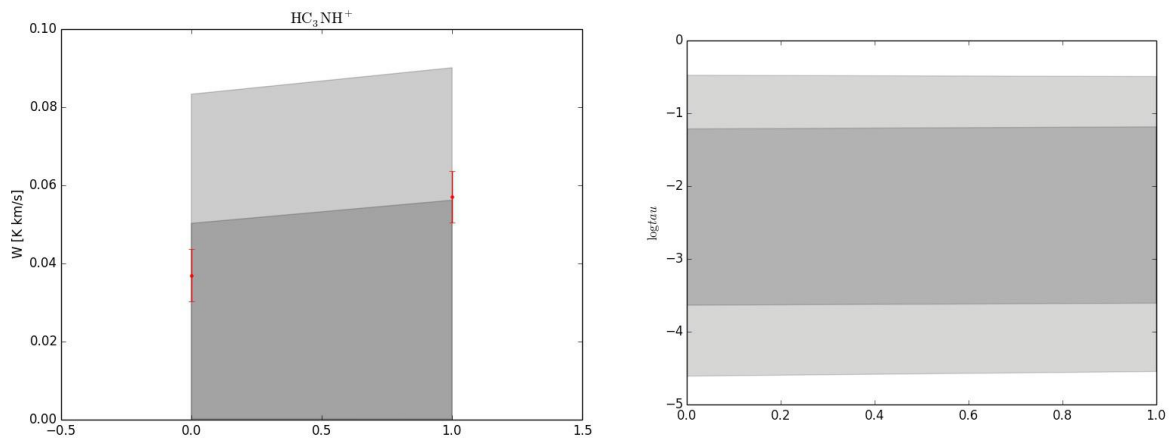
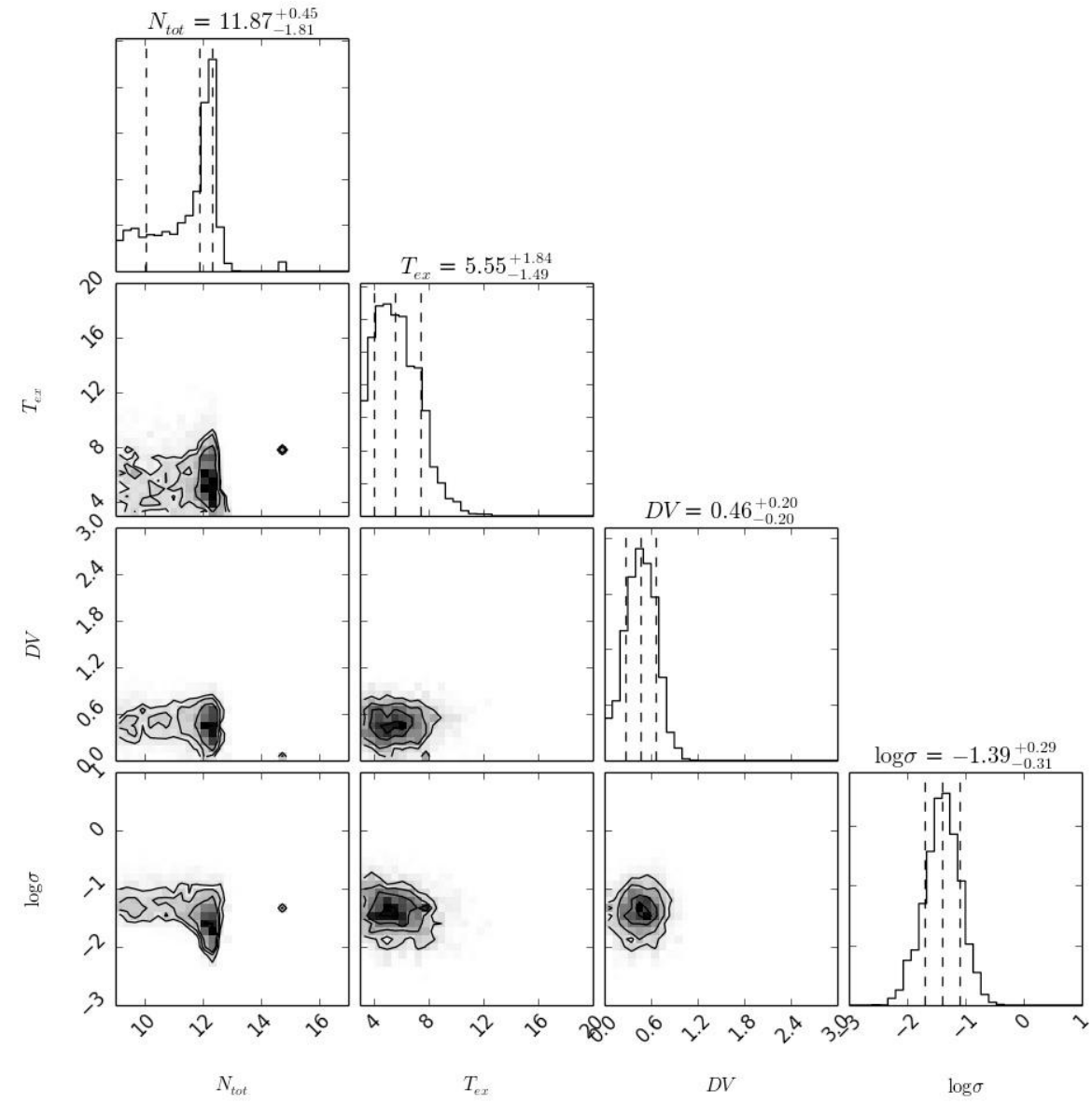
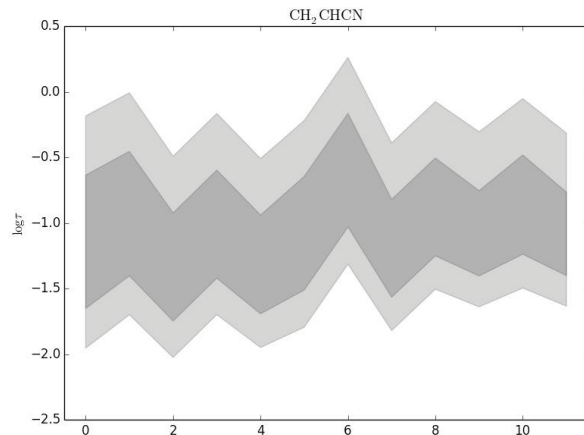
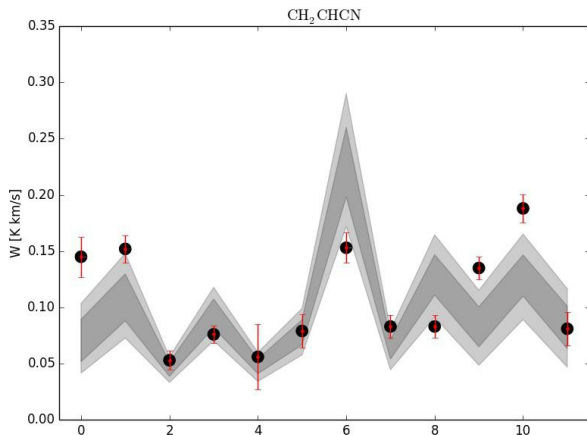
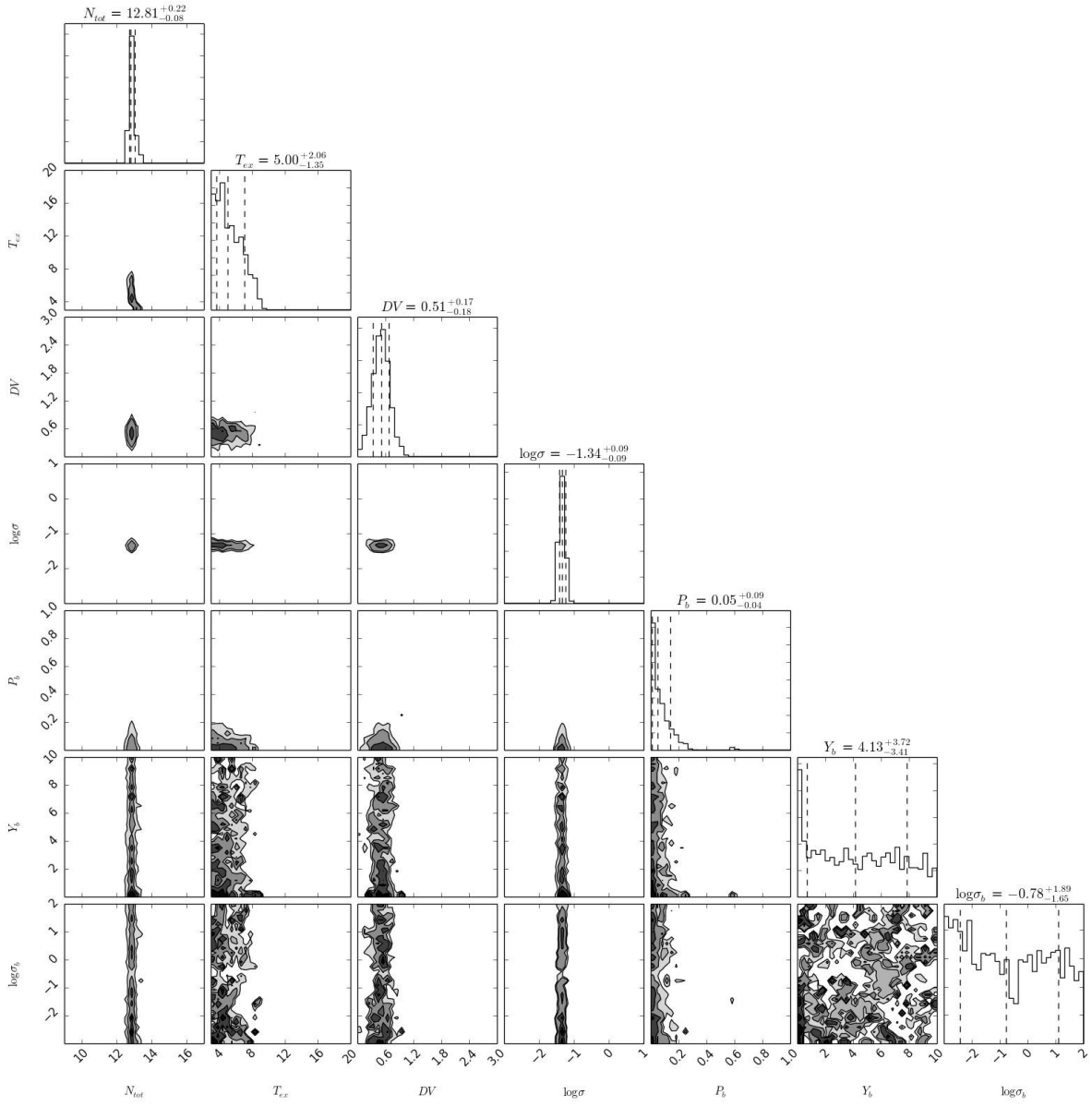


FIG. B35.— DC₃N

FIG. B36.— $\text{H}^{13}\text{CC}_2\text{N}$

FIG. B37.— C_3O

FIG. B38.— HC_3NH^+

FIG. B39.— CH_2CHCN

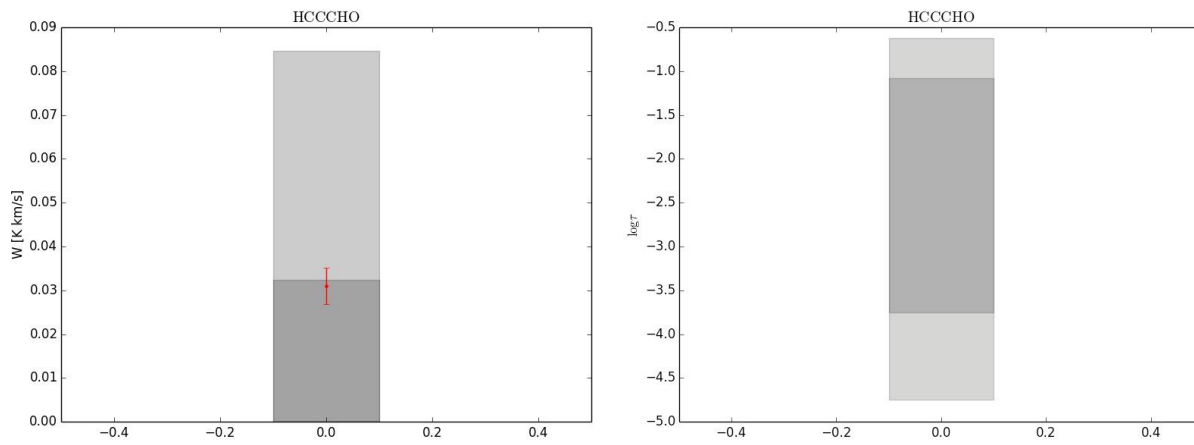
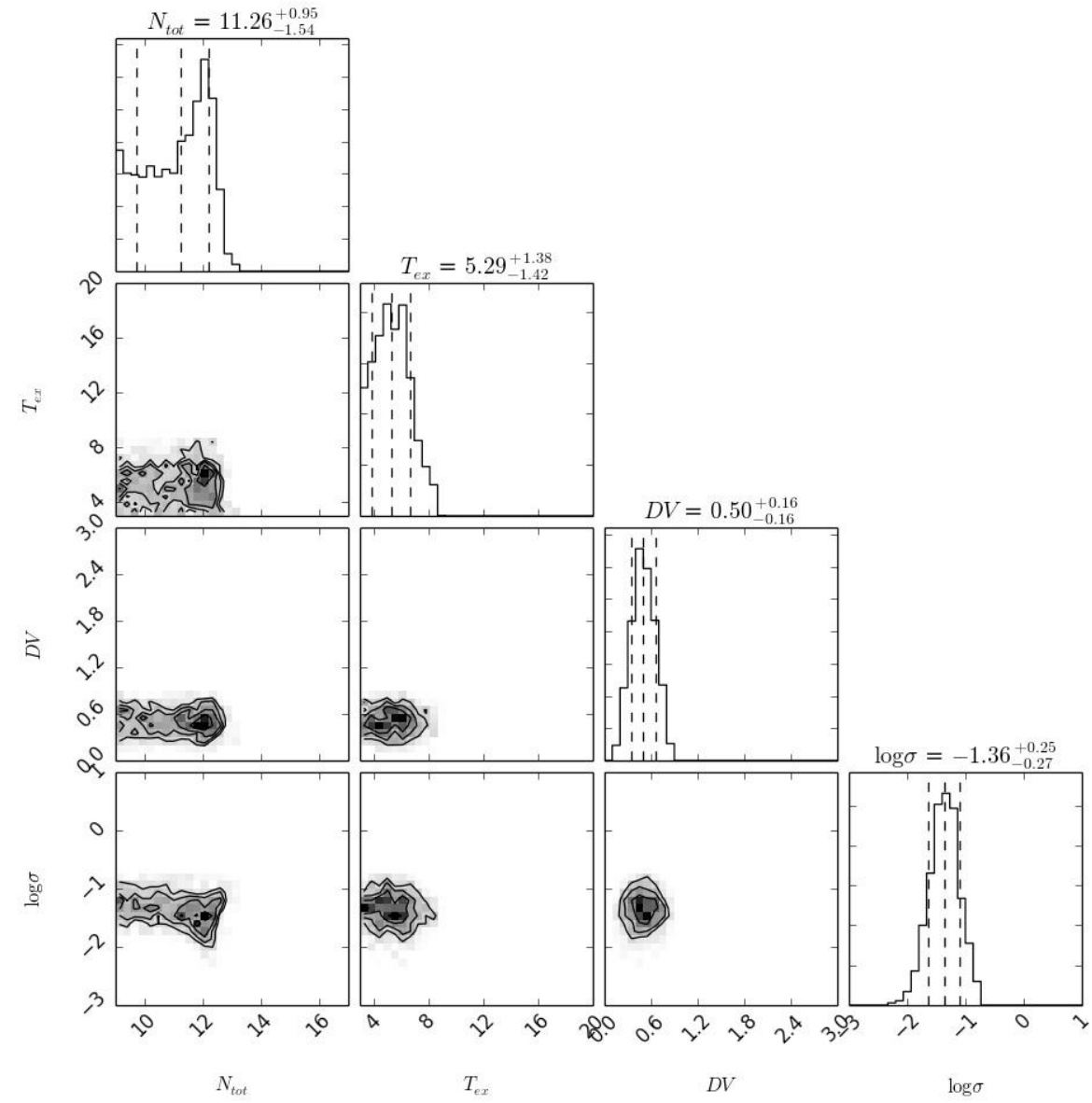
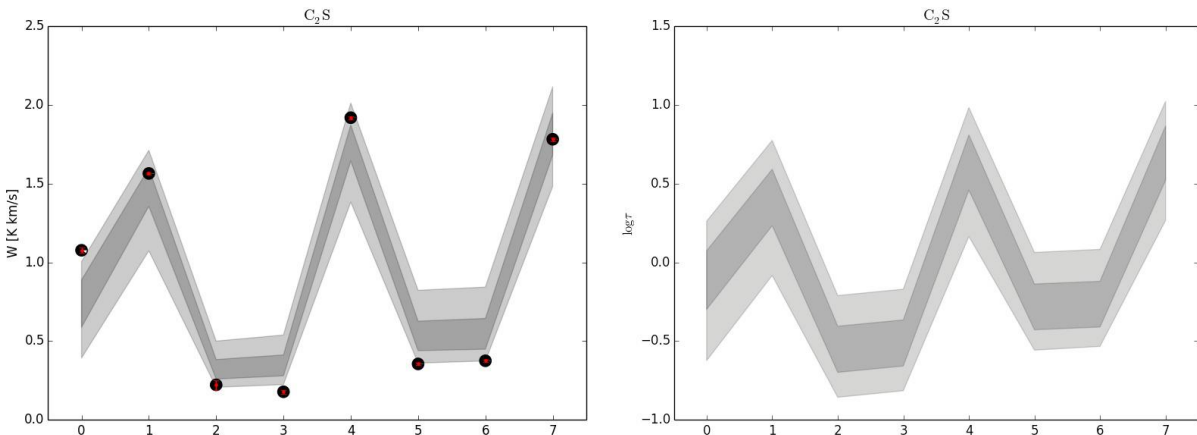
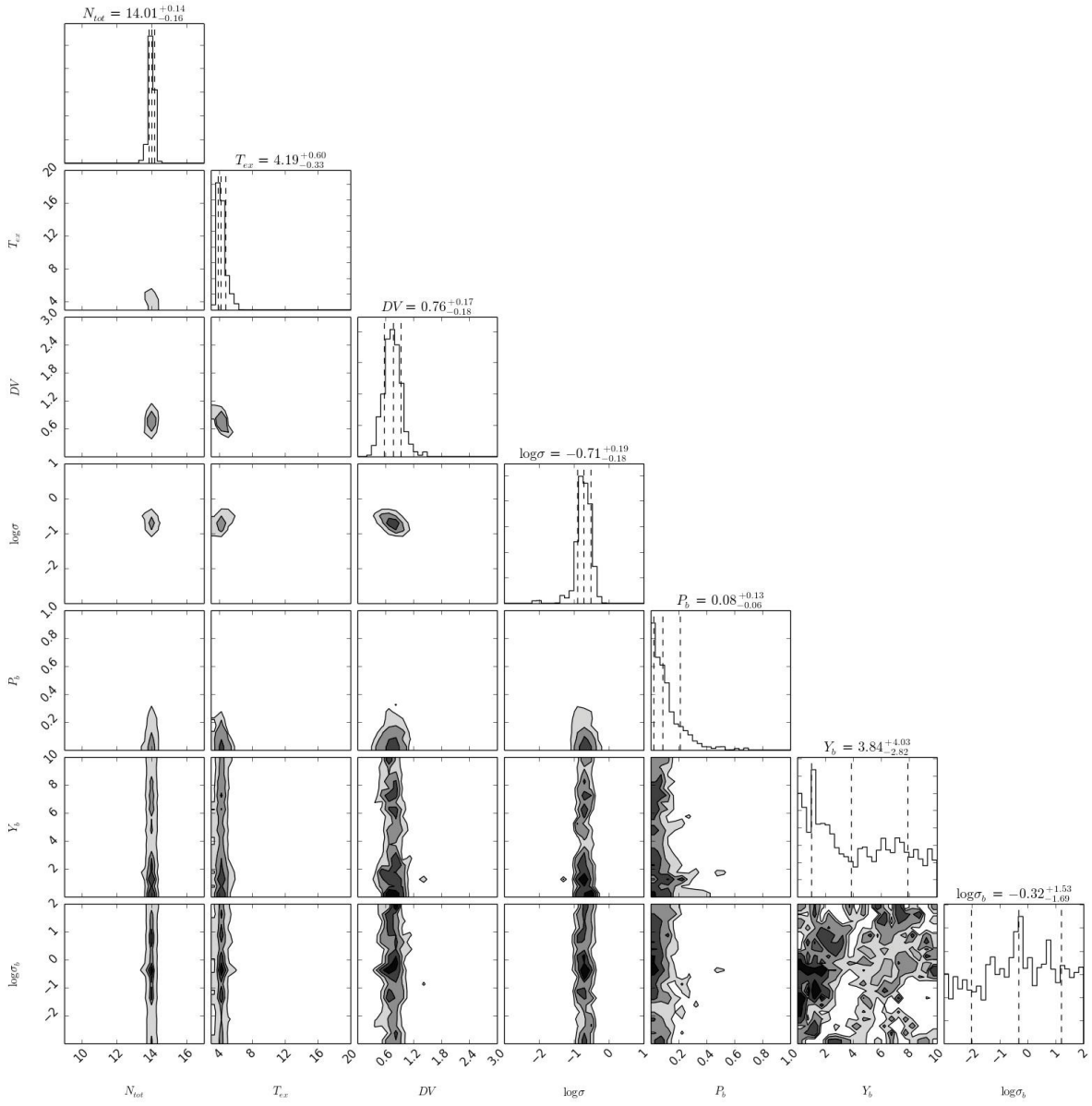


FIG. B40.— HCCCHO

FIG. B41.— C₂S

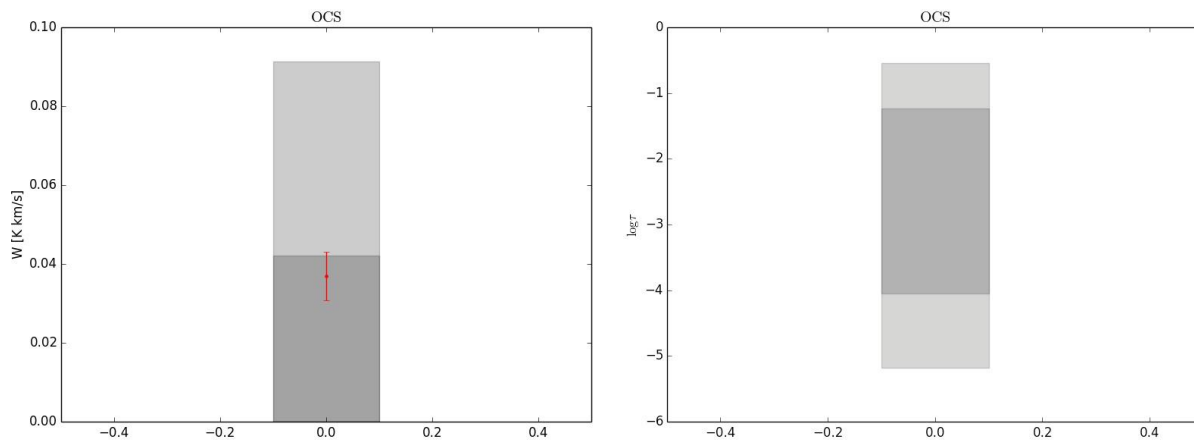
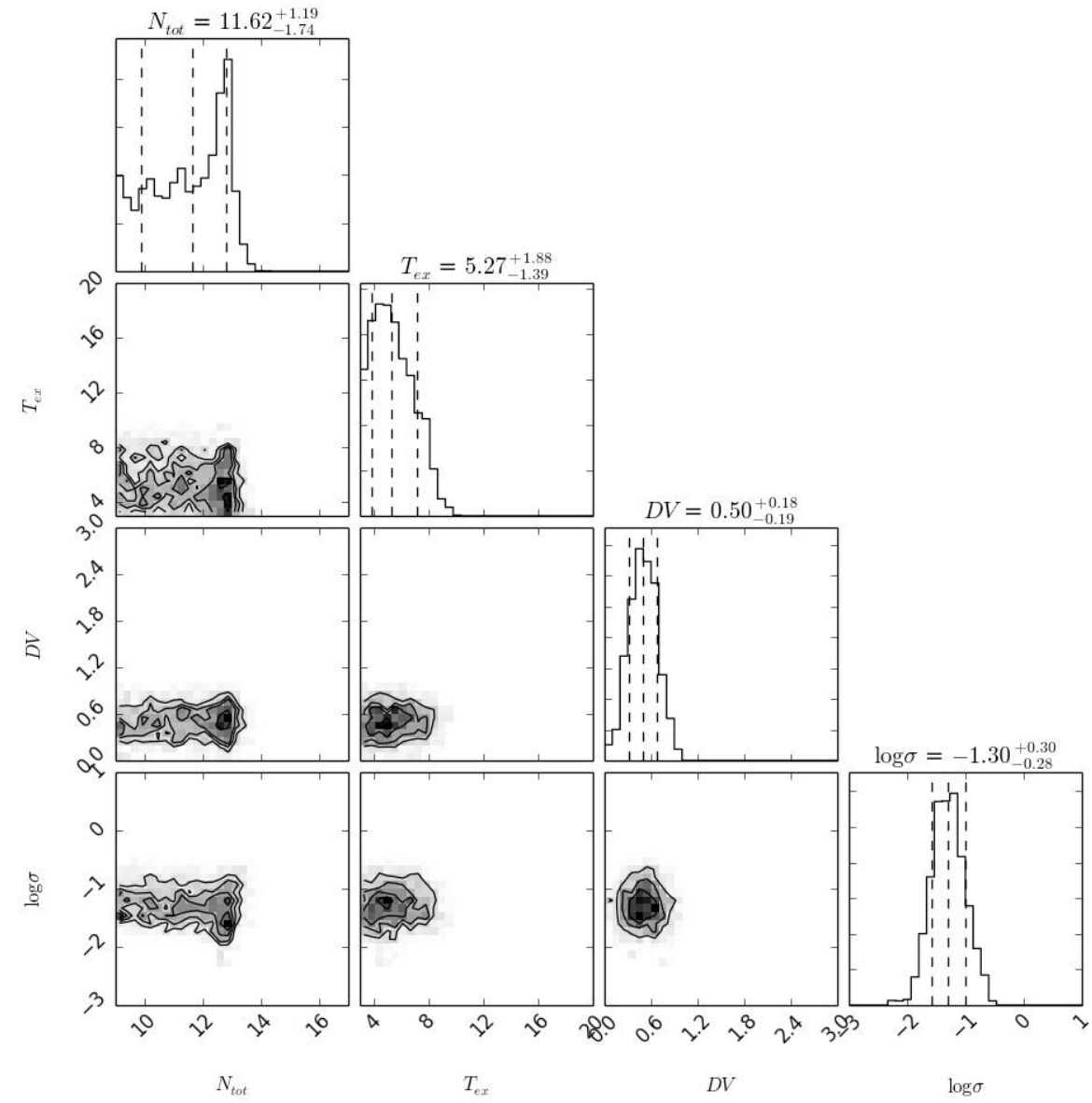
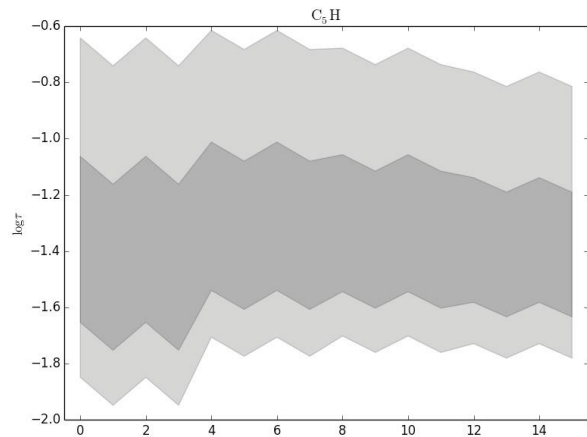
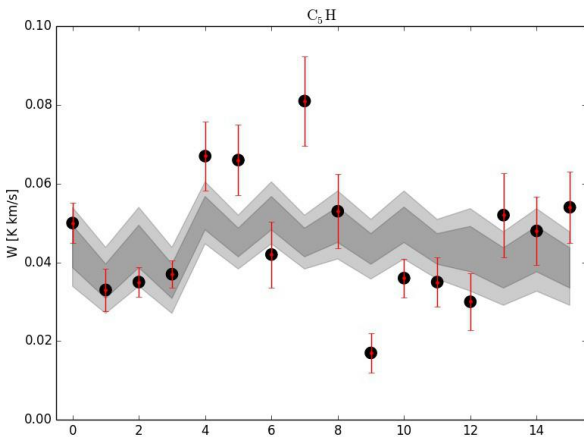
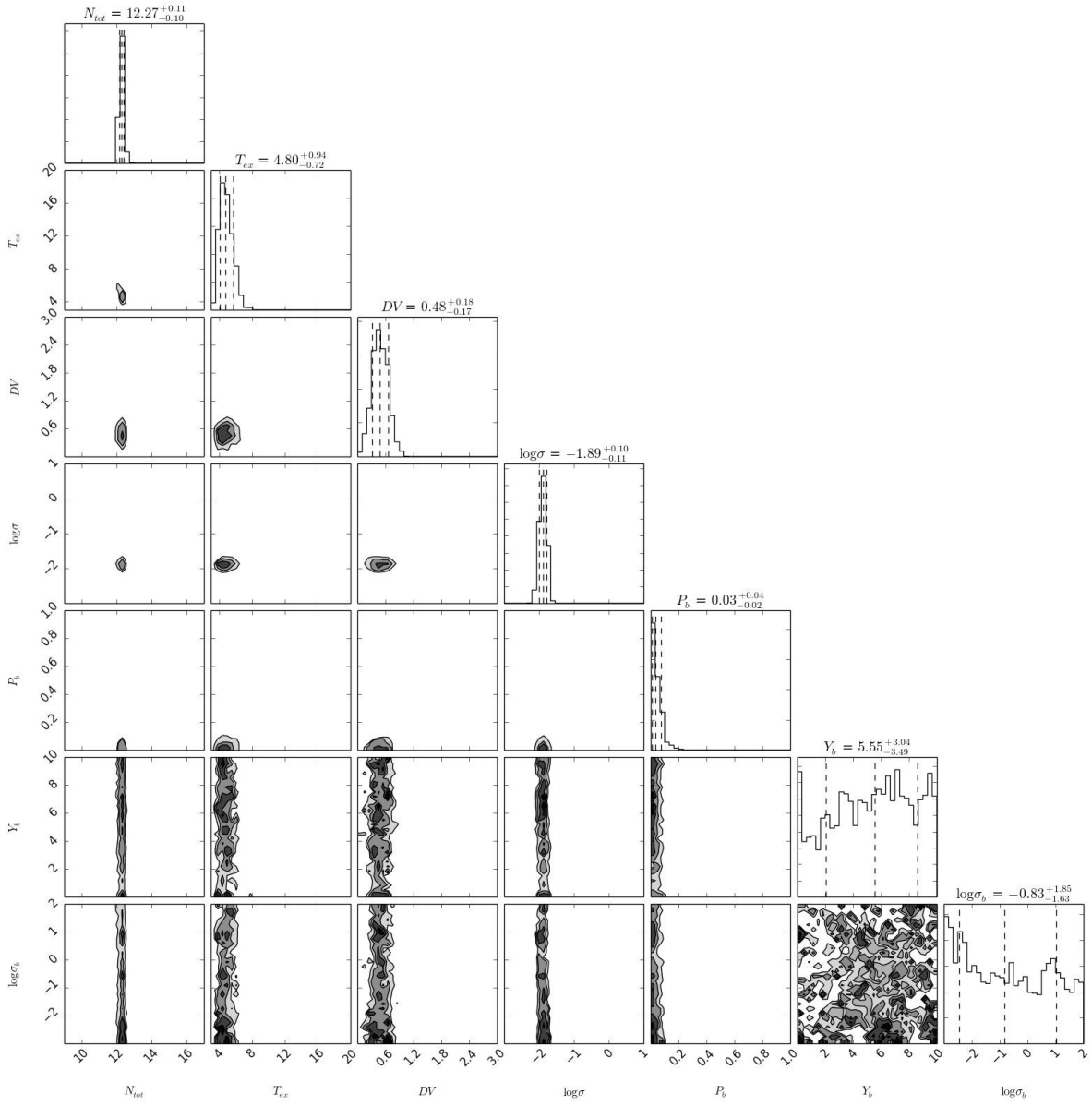
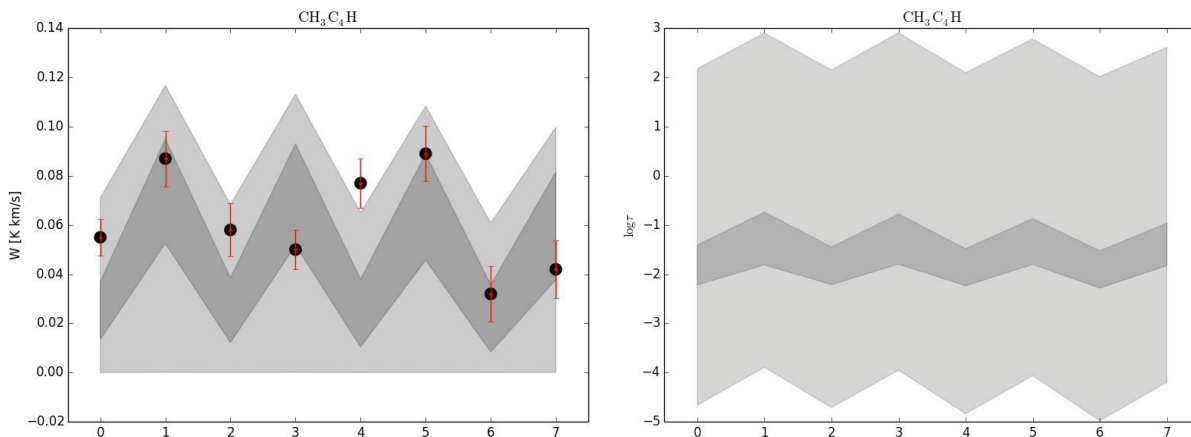
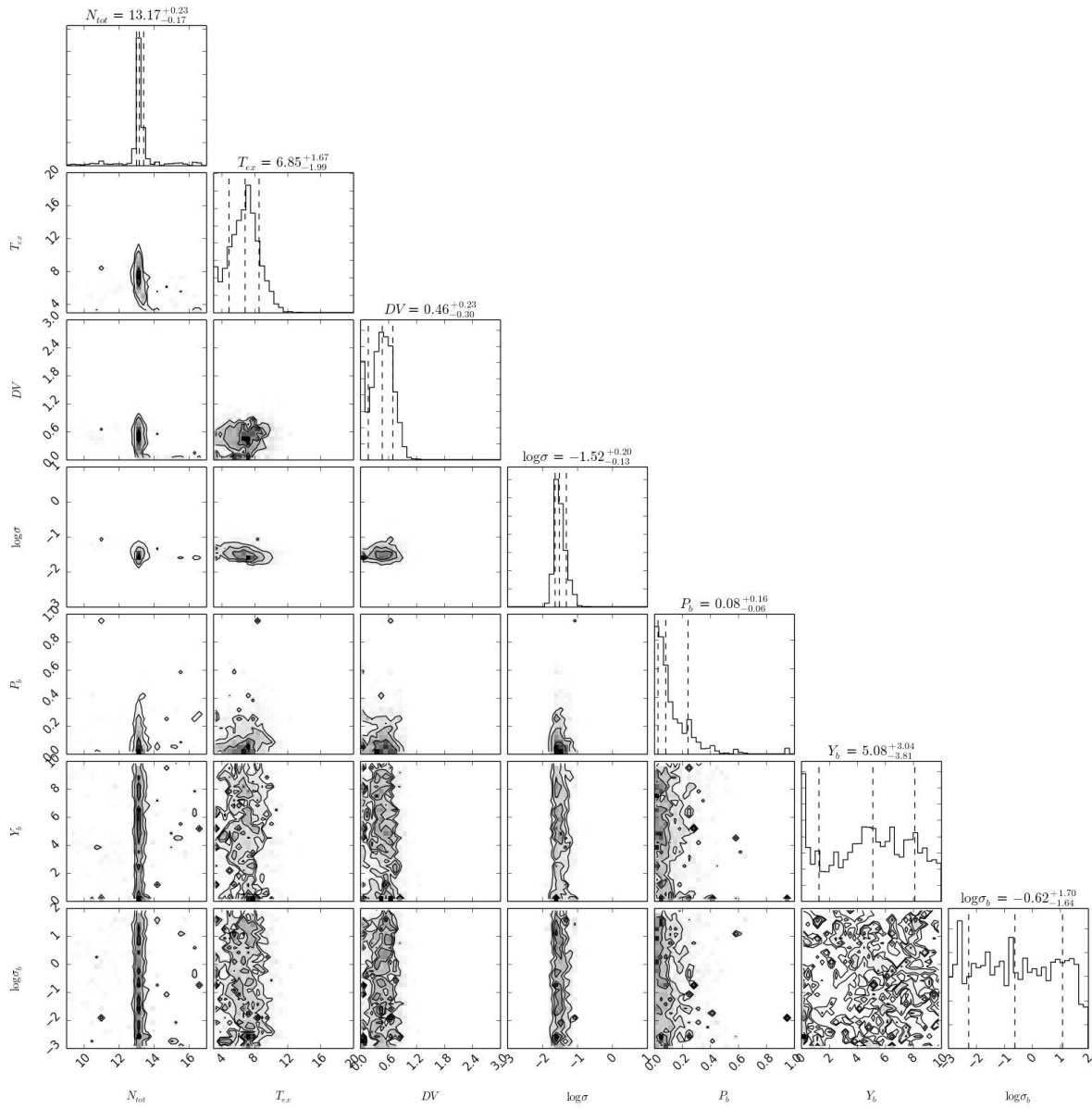
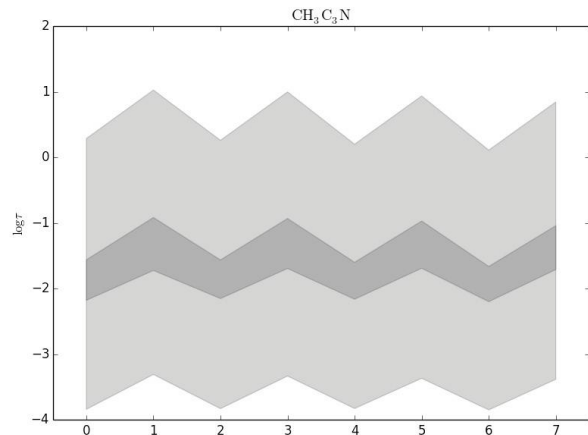
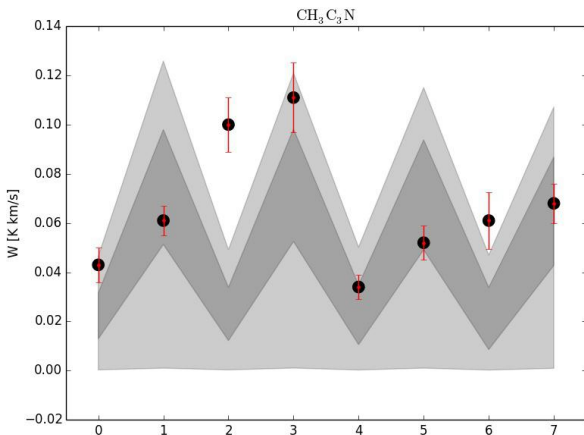
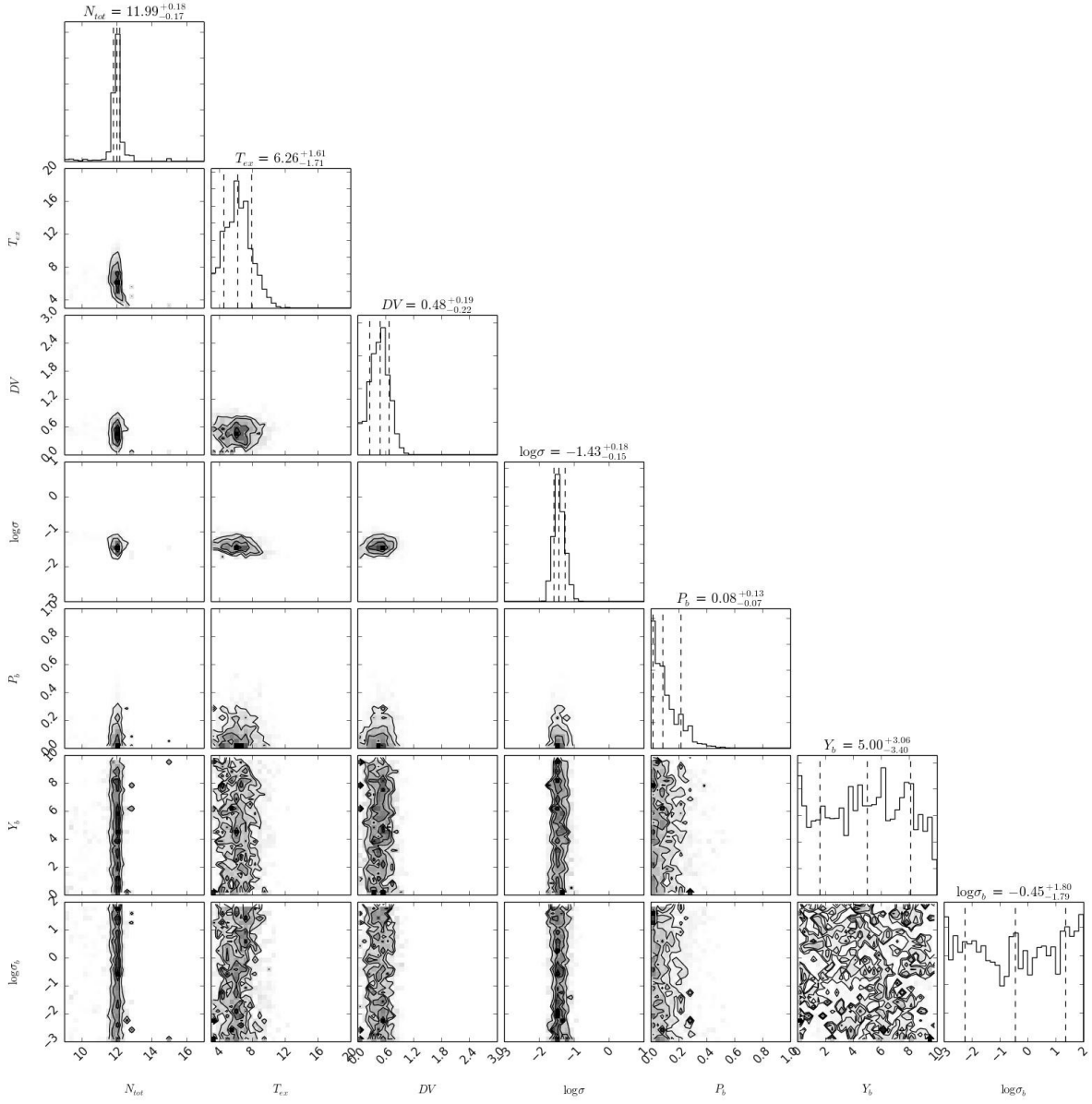
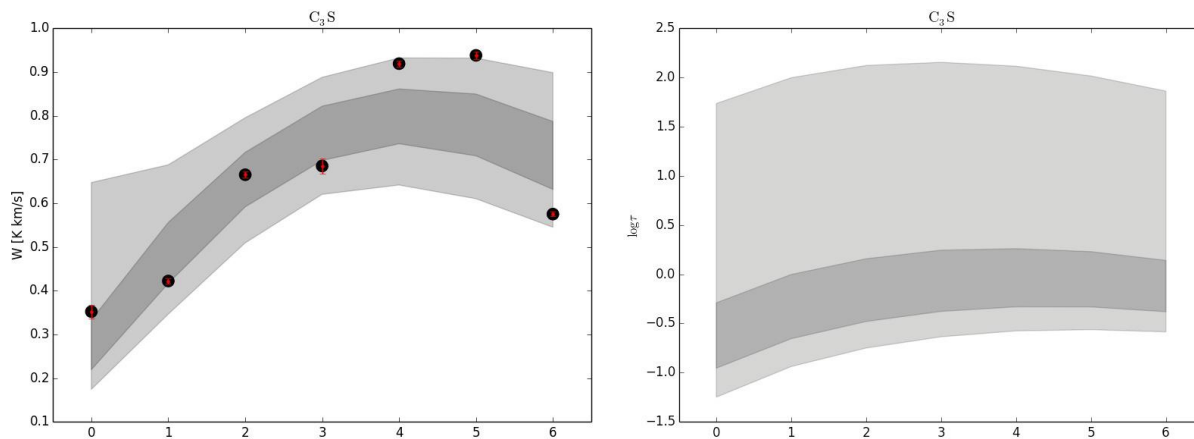
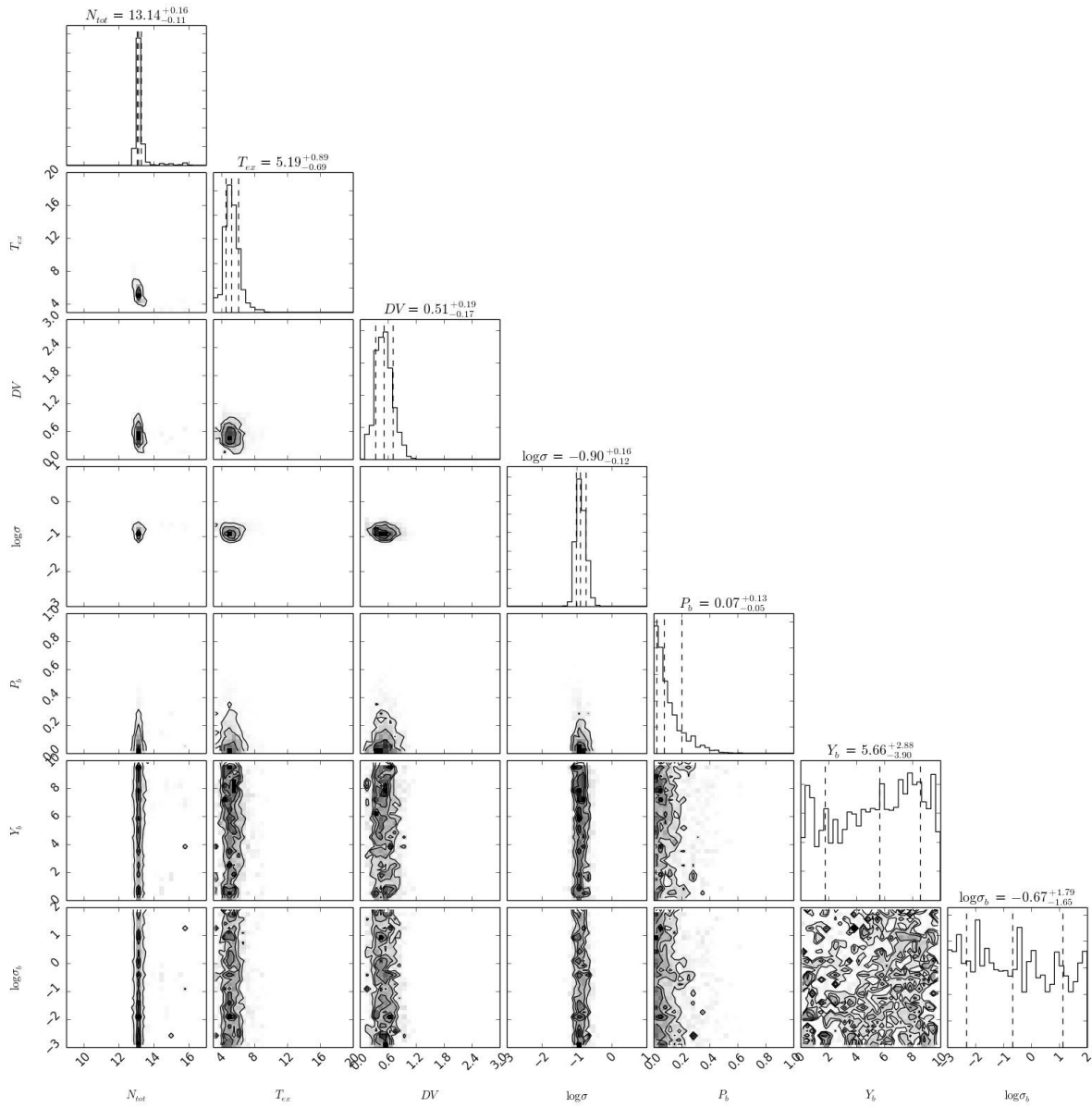


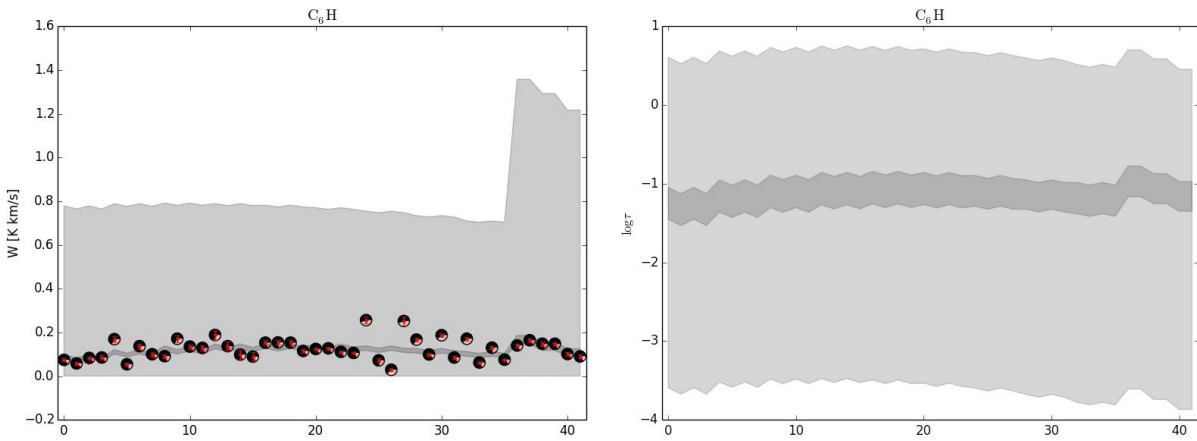
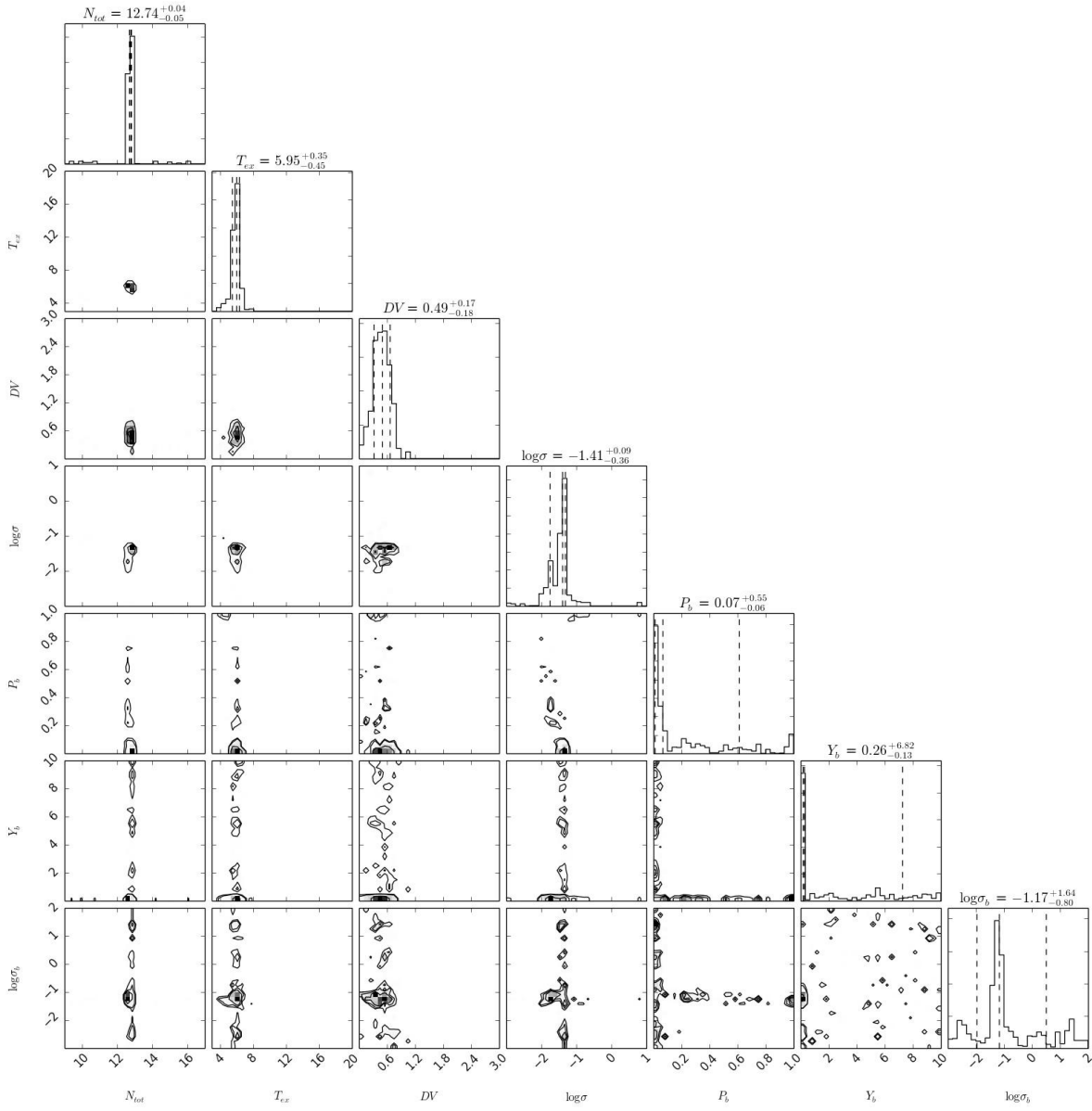
FIG. B42.— OCS

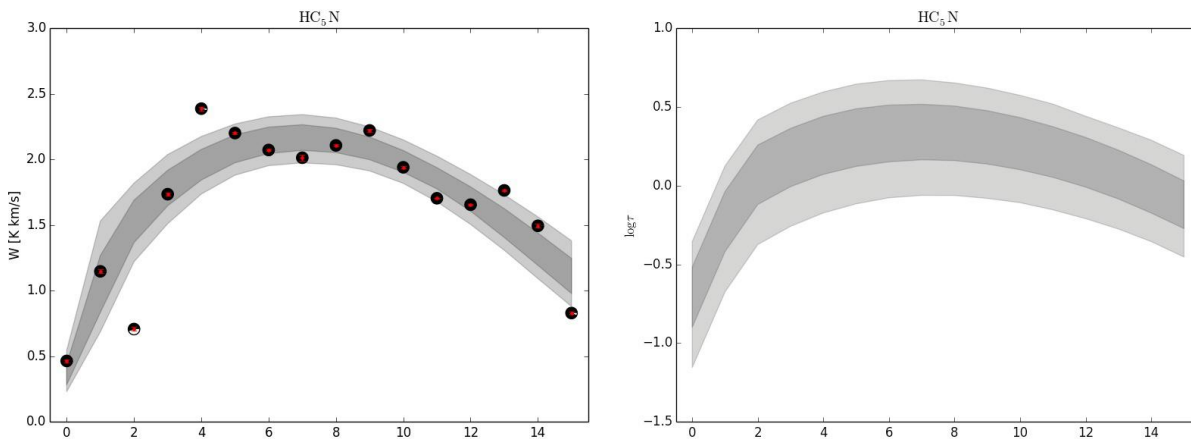
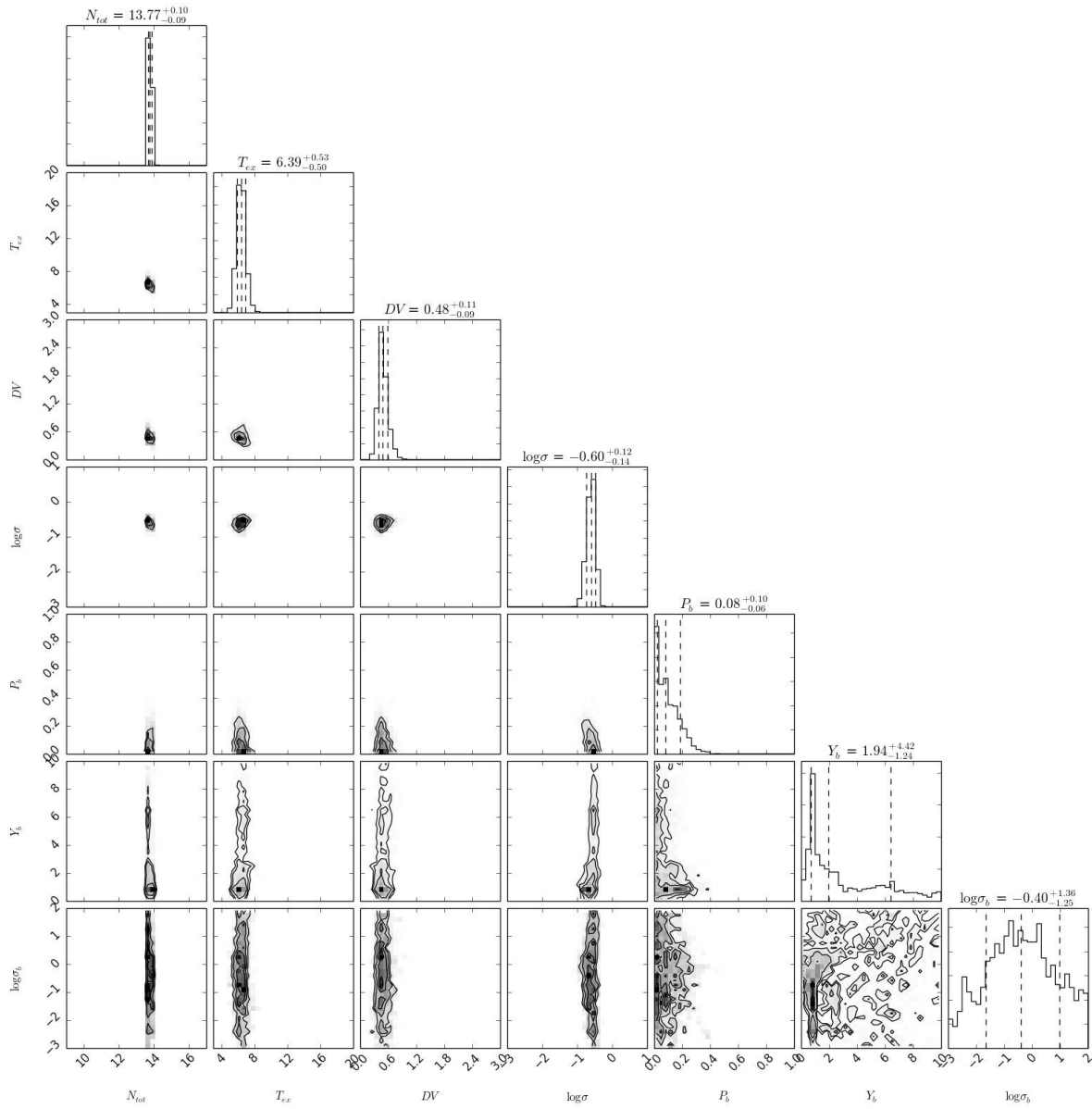
FIG. B43.— C_5H

FIG. B44.— $\text{CH}_3\text{C}_4\text{H}$

FIG. B45.— $\text{CH}_3\text{C}_3\text{N}$

FIG. B46.— C_3S

FIG. B47.— C₆H

FIG. B48.— HC_5N

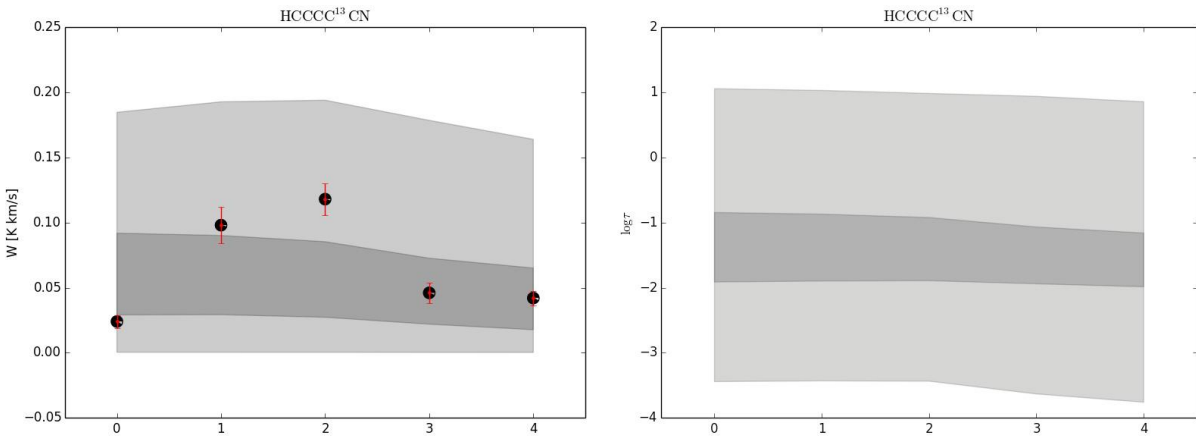
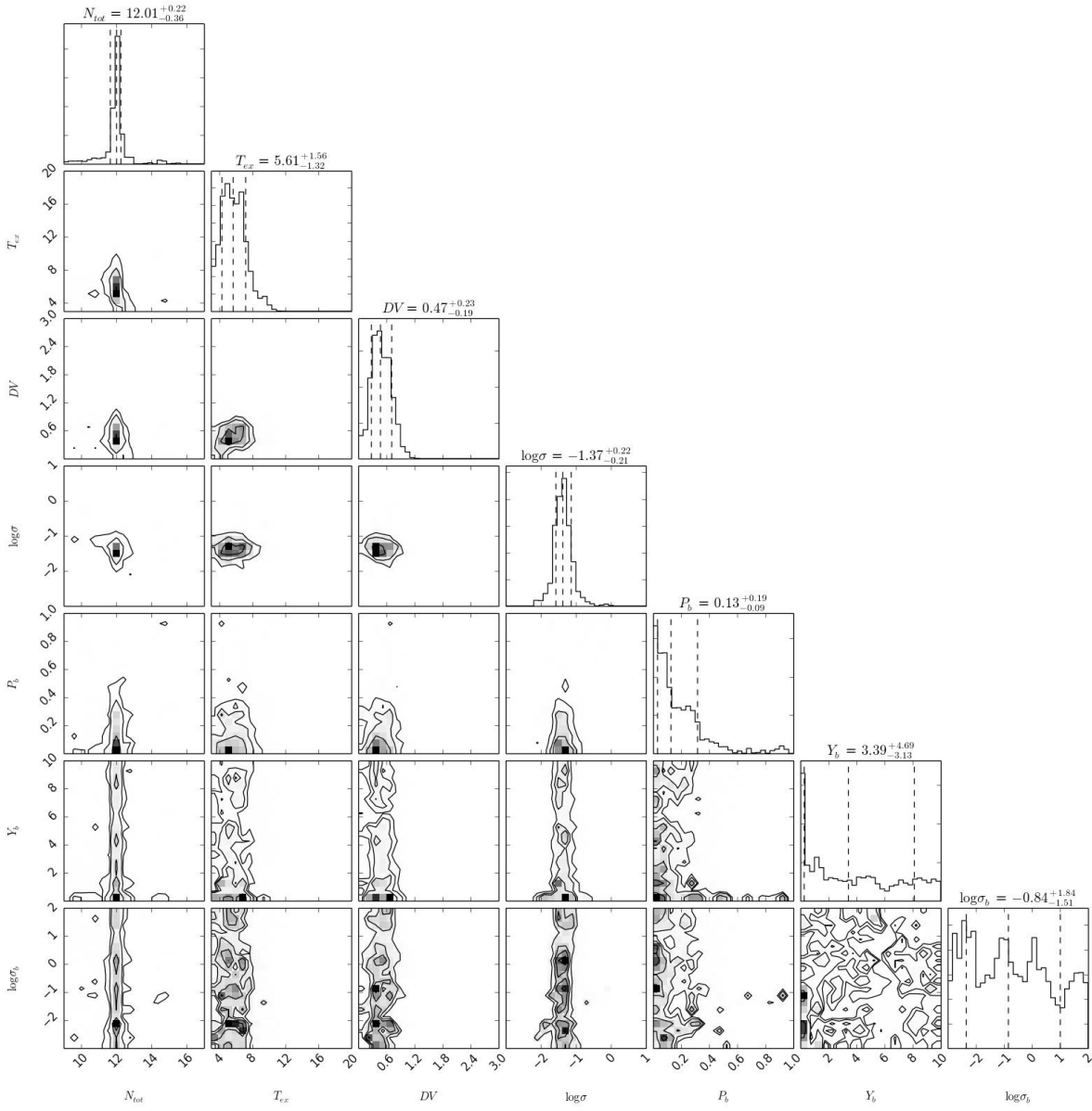
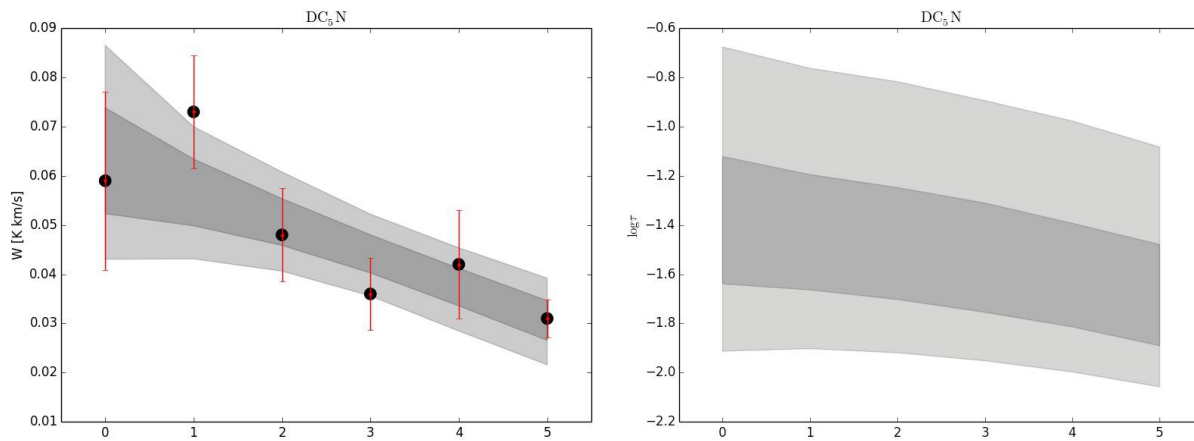
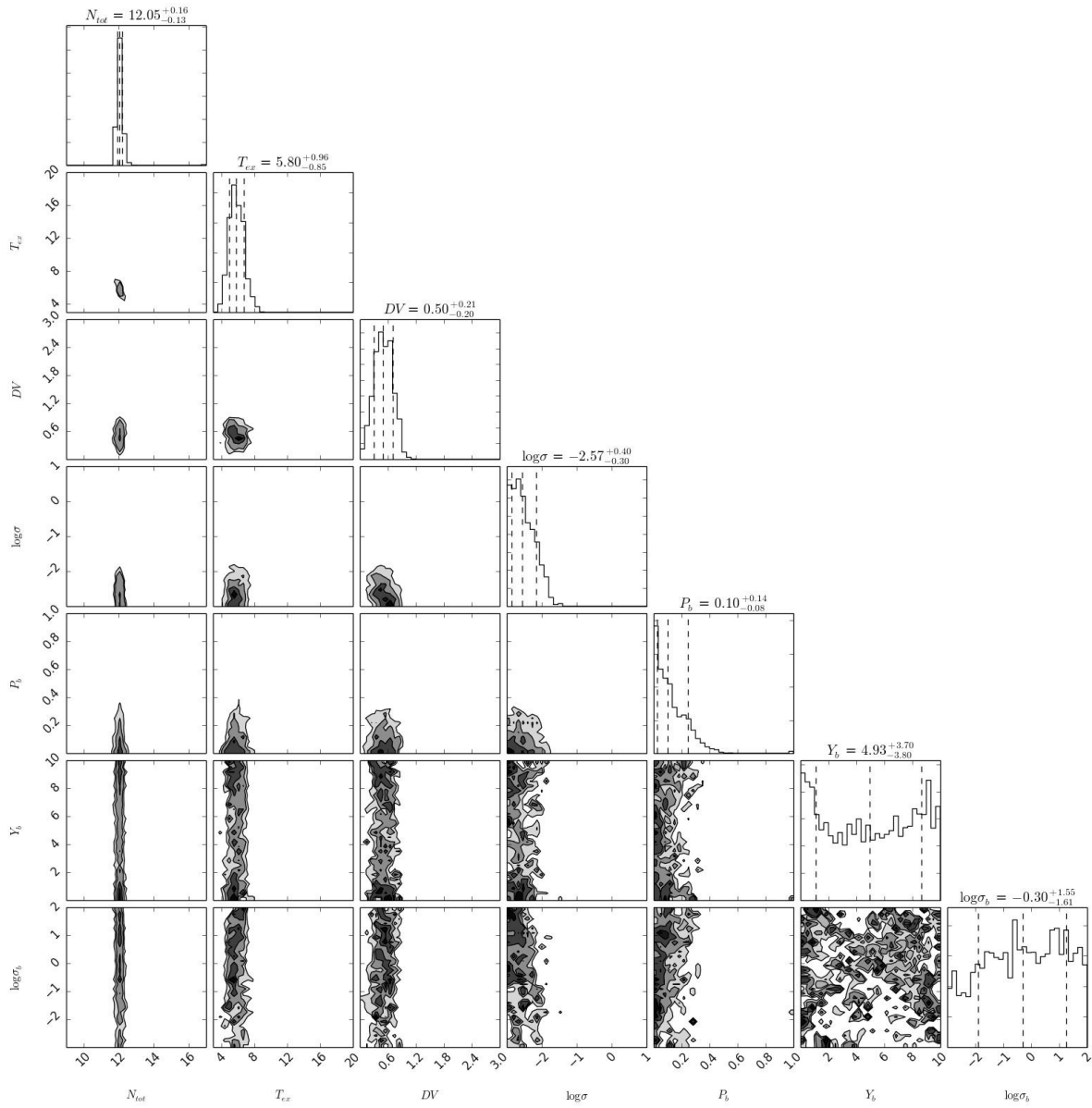
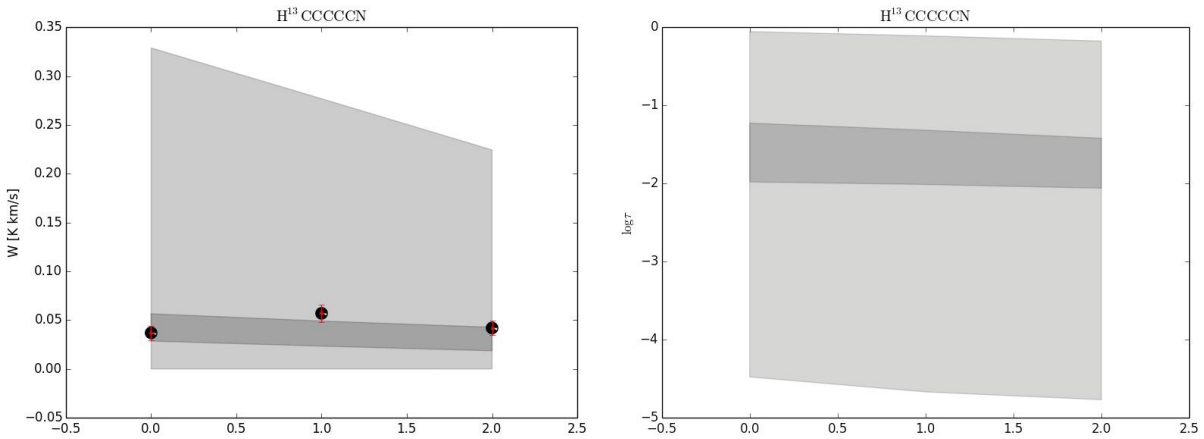
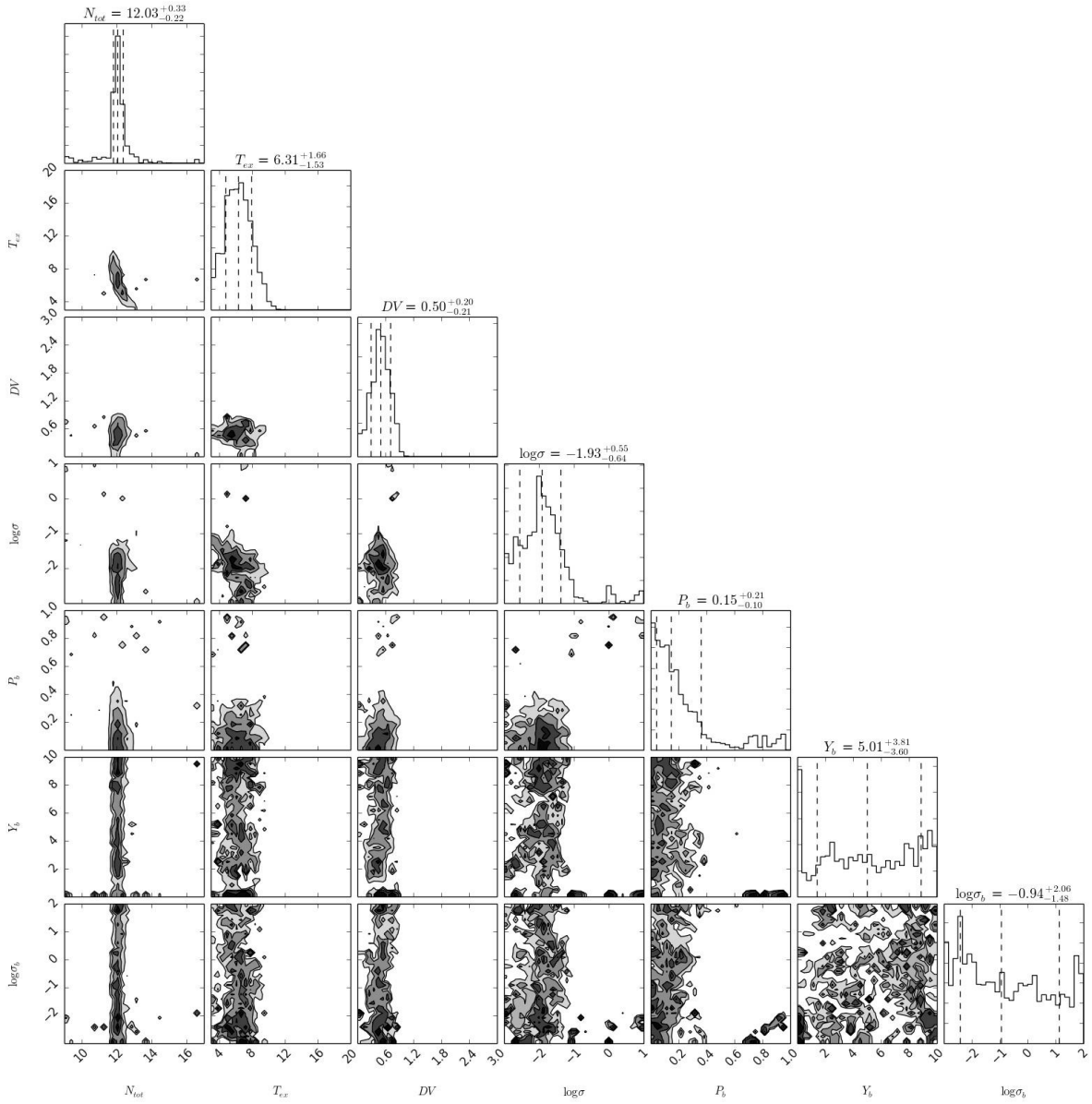
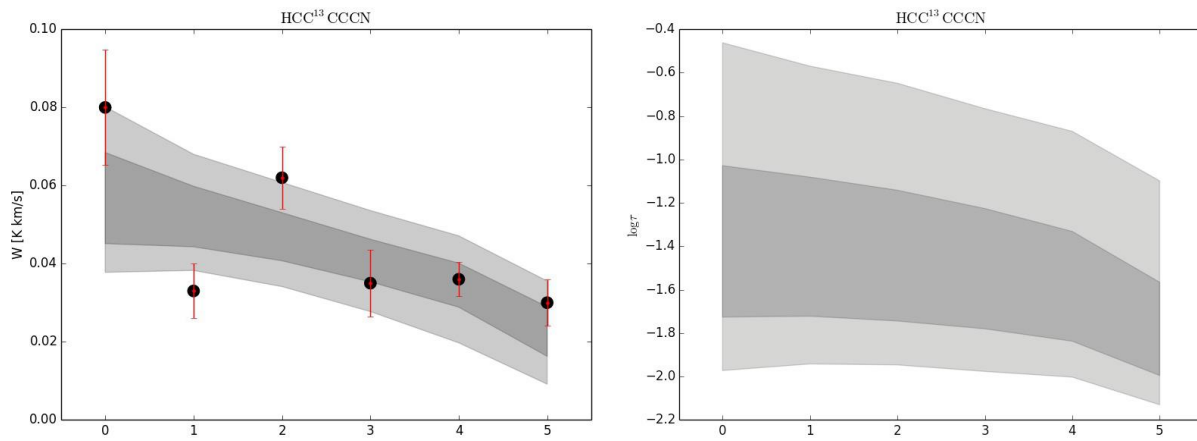
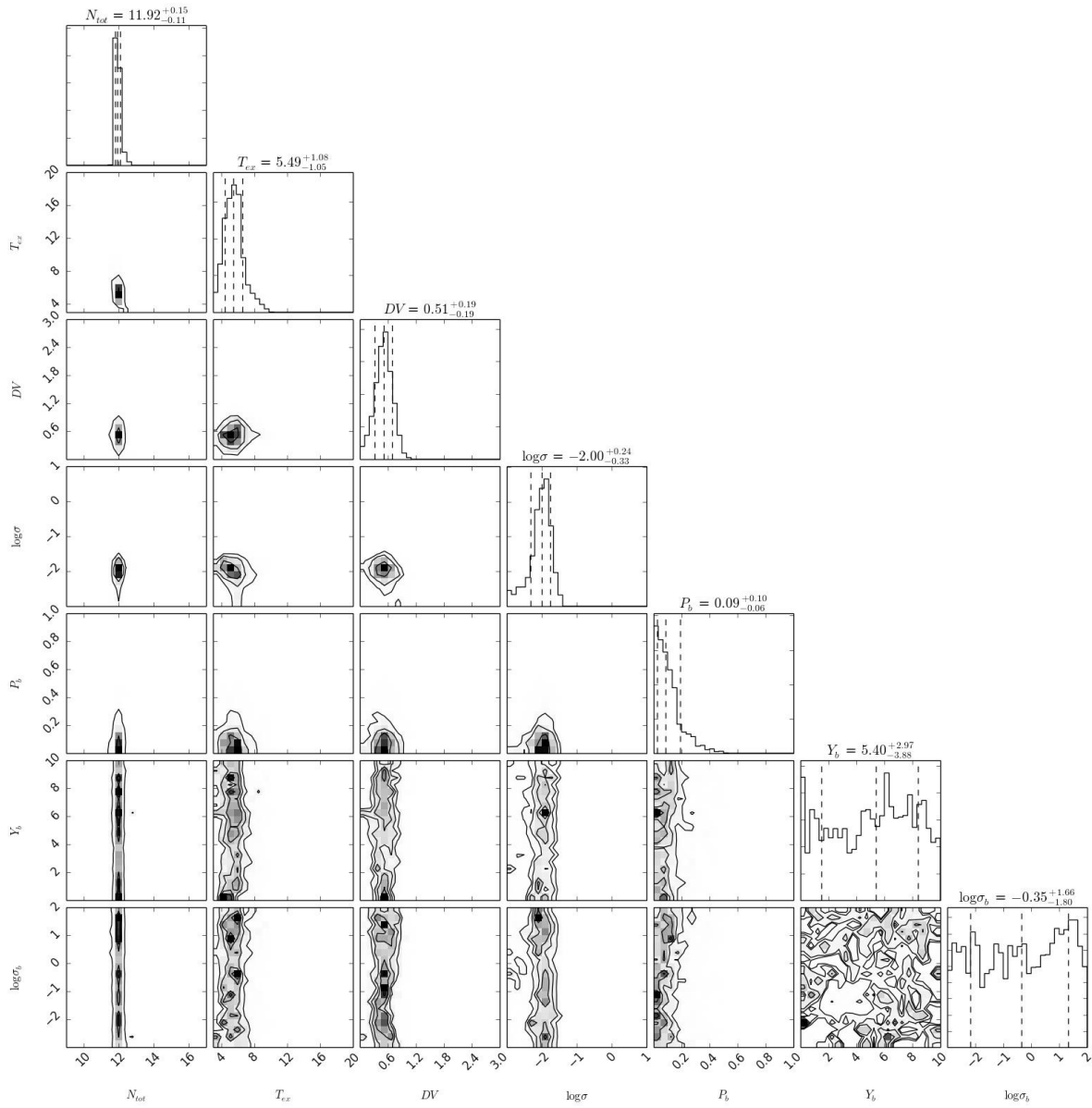
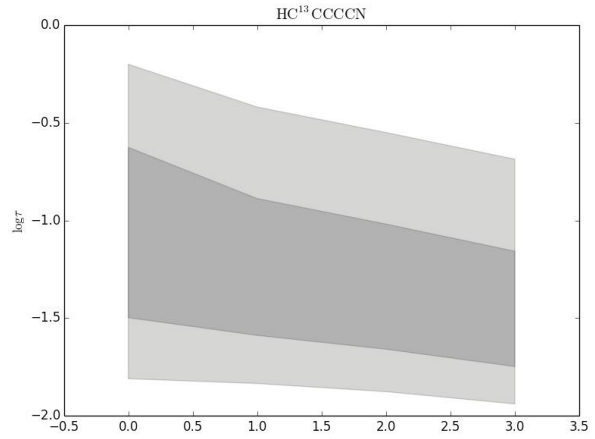
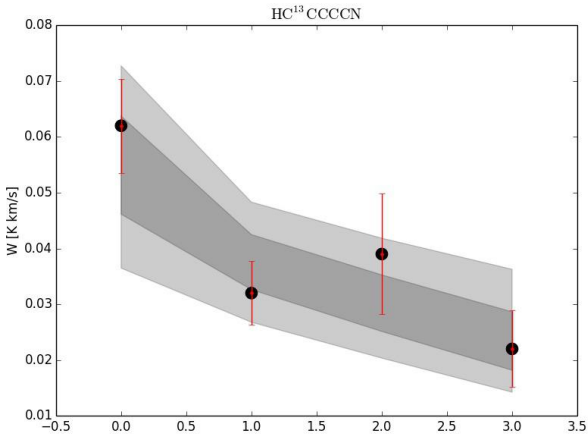
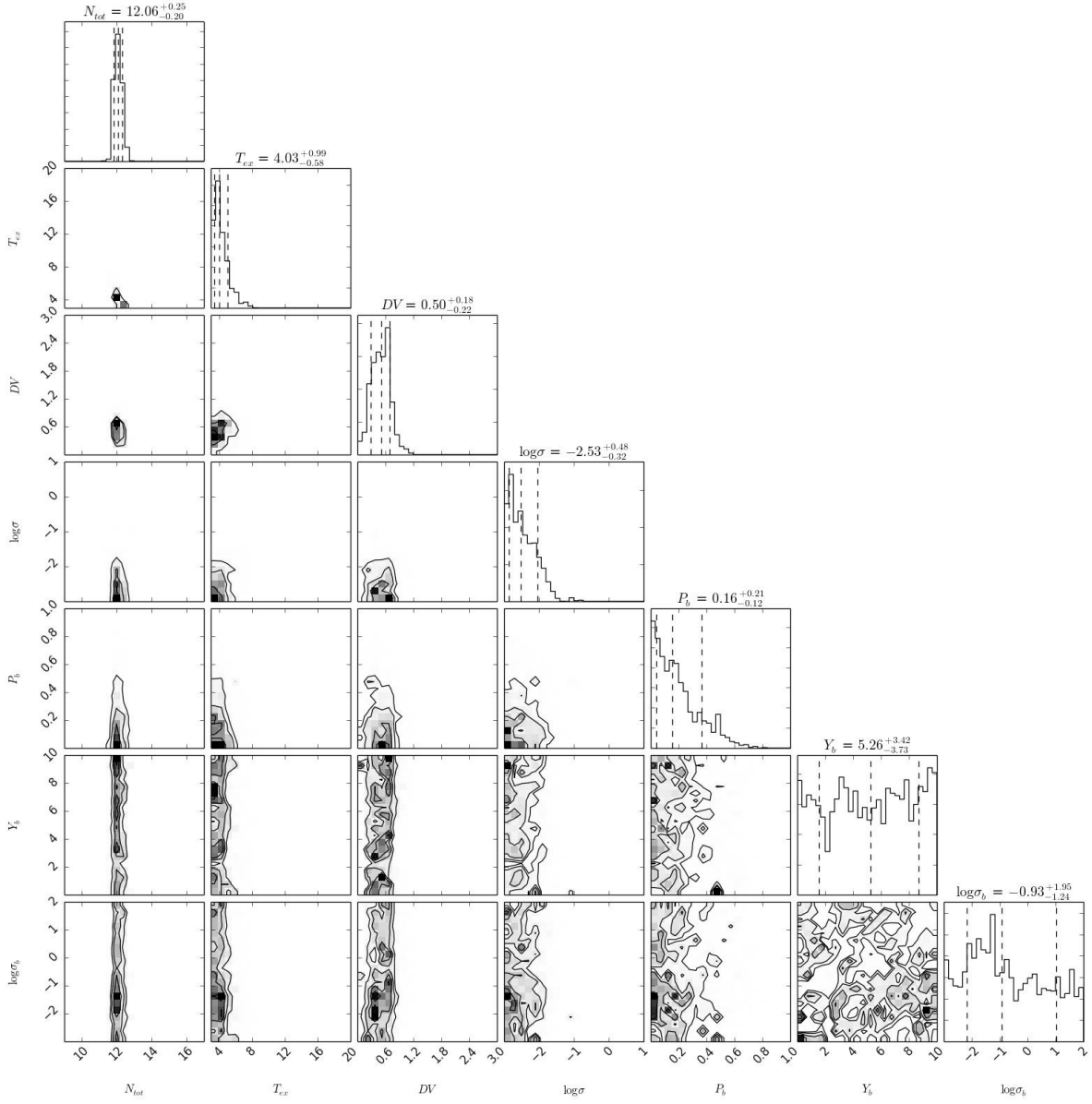


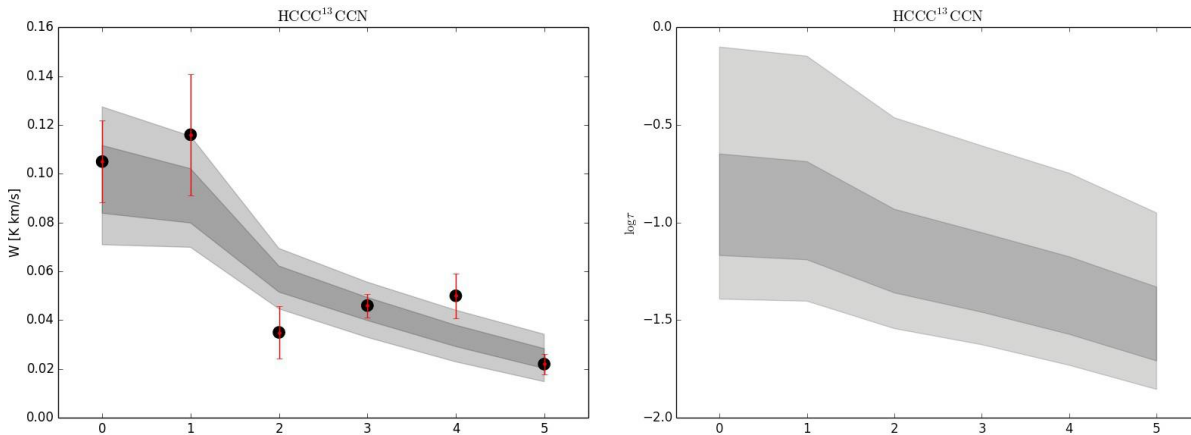
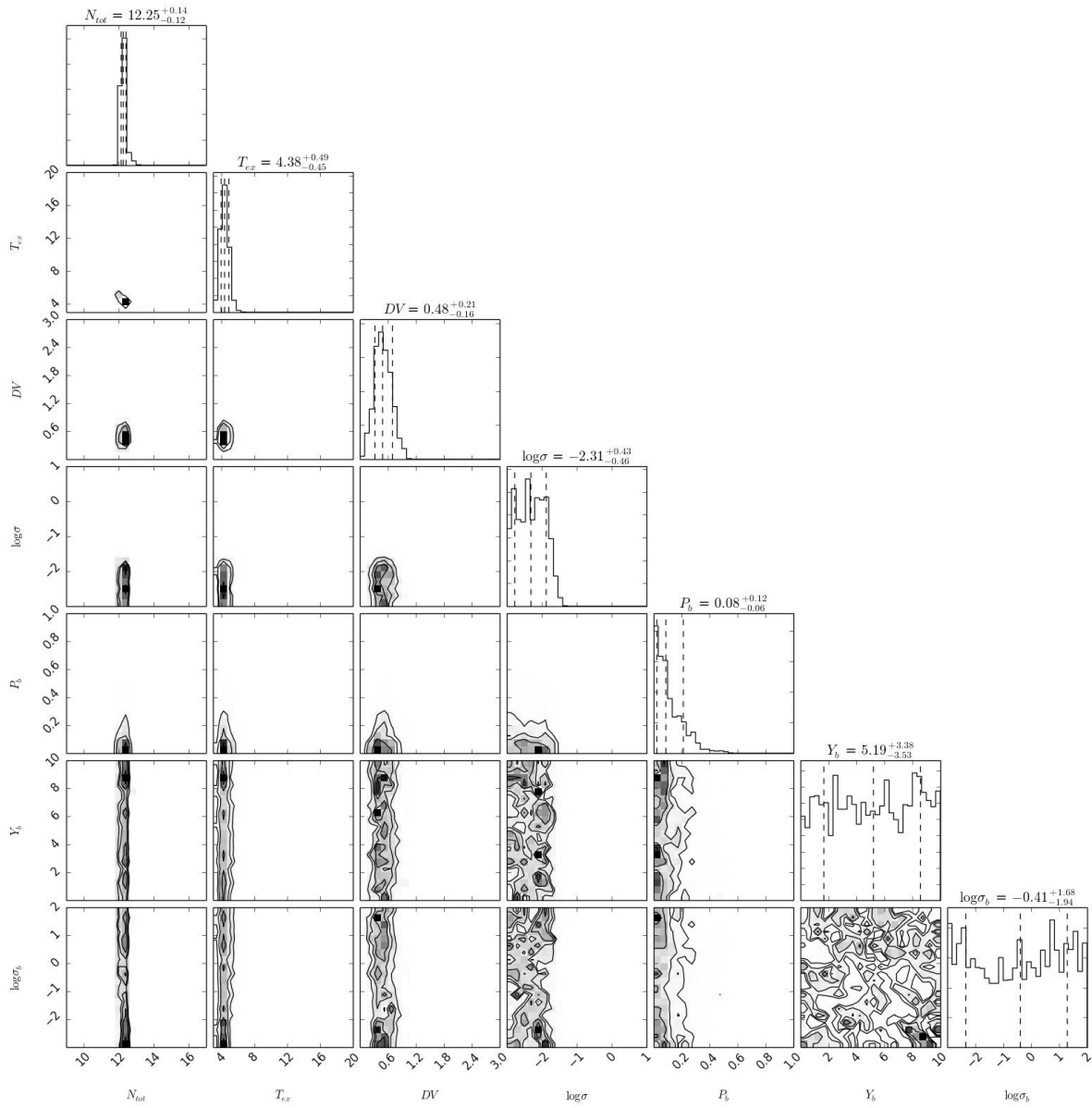
FIG. B49.— $\text{HC}_4^{13}\text{CN}$

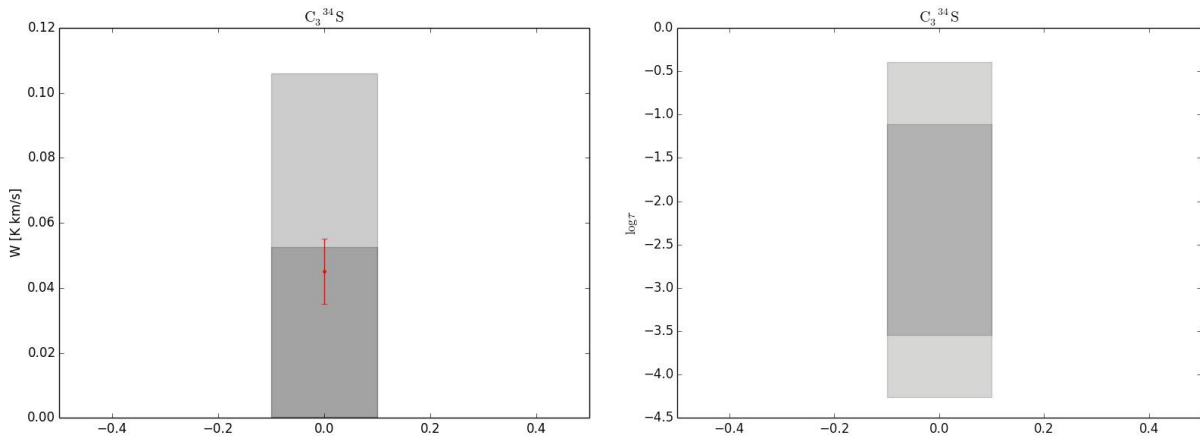
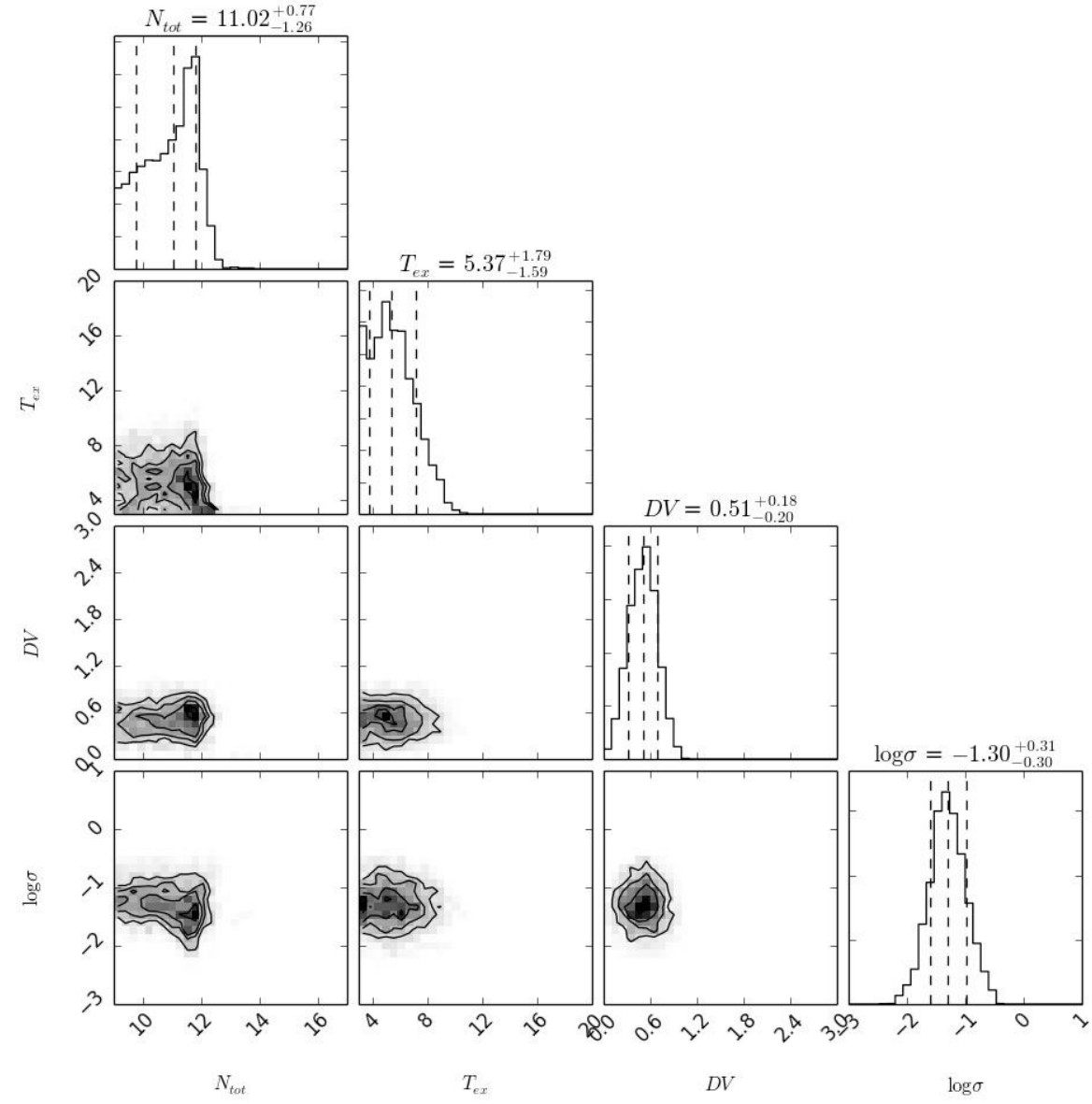
FIG. B50.— $DC_5 N$

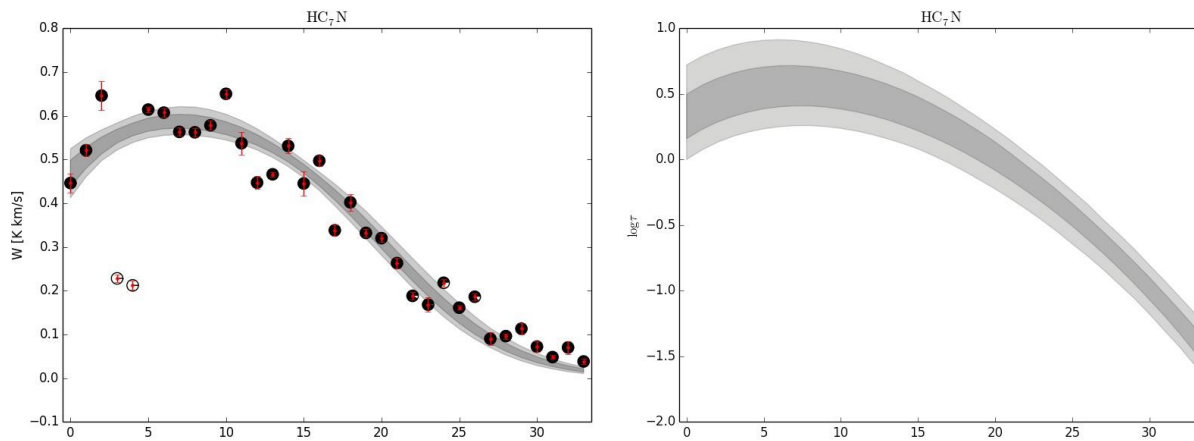
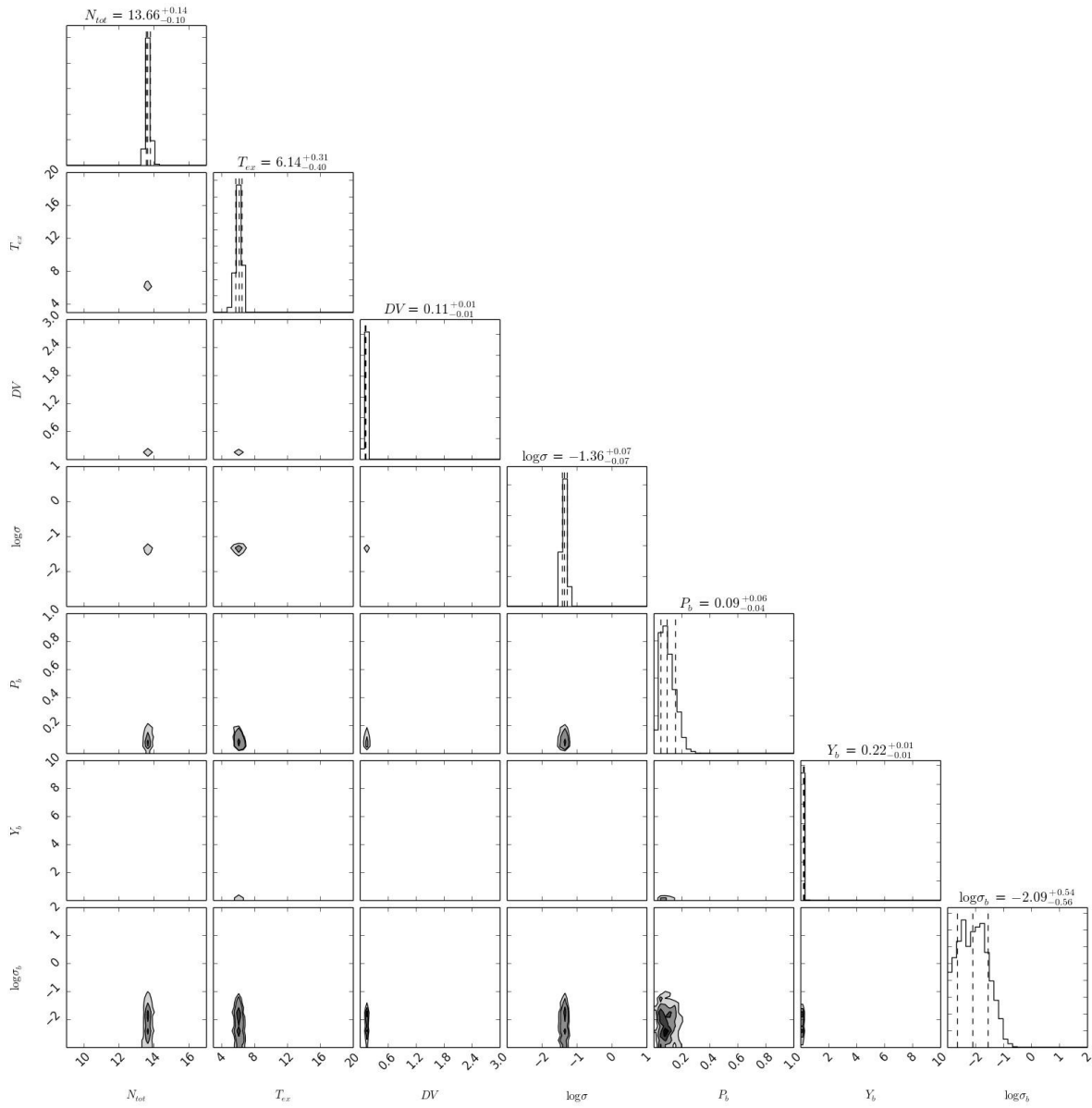
FIG. B51.— $\text{H}^{13}\text{CC}_4\text{N}$

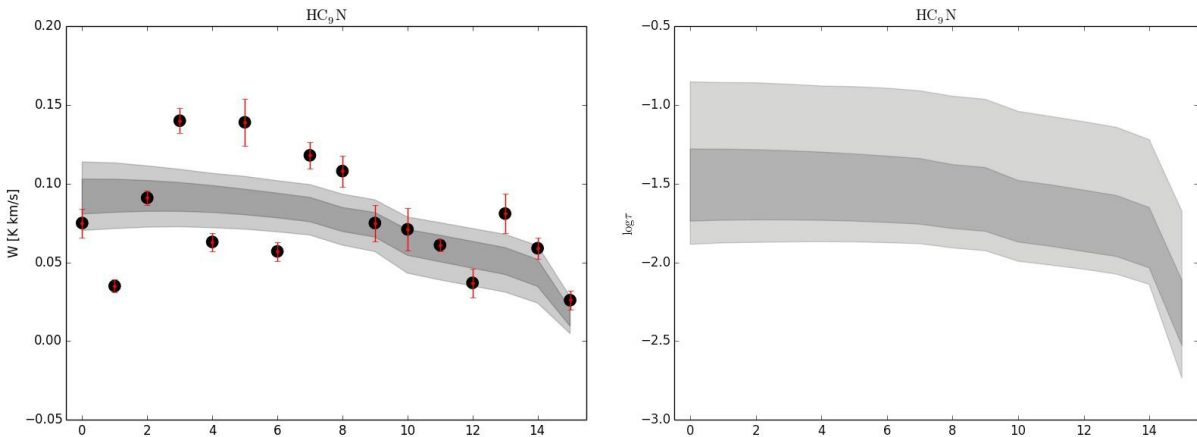
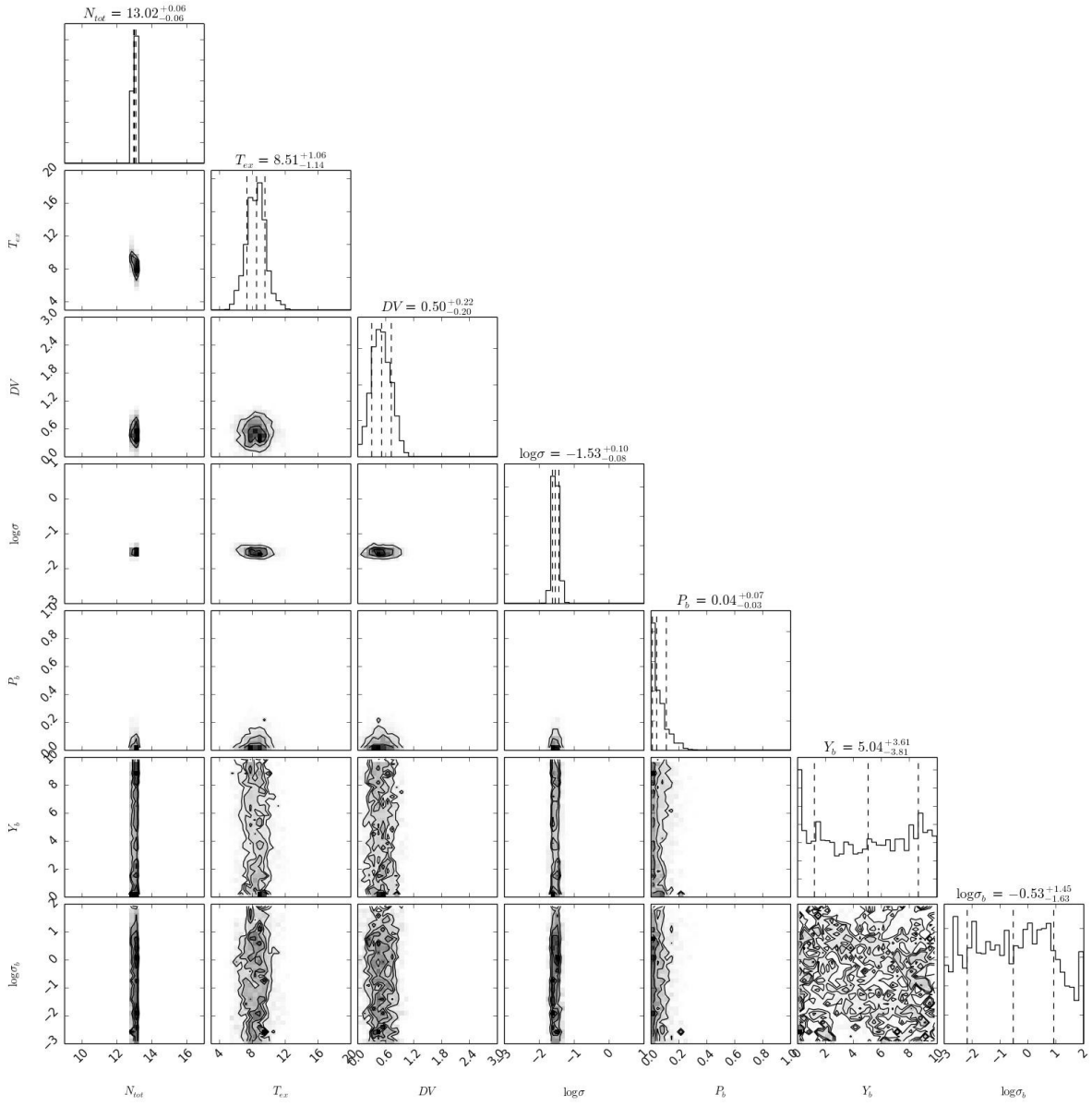
FIG. B52.— $\text{HC}_2^{13}\text{CC}_2\text{N}$

FIG. B53.— $\text{HC}^{13}\text{CC}_3\text{N}$

FIG. B54.— $\text{HC}_3^{13}\text{CCN}$

FIG. B55.— $C_3^{34}S$

FIG. B56.— HC₇N

FIG. B57.— HC₉N

REFERENCES

- Agúndez, M., & Wakelam, V. 2013, *Chemical Reviews*, 113, 8710
- Albertsson, T., Semenov, D. A., Vasyunin, A. I., Henning, T., & Herbst, E. 2013, *ApJS*, 207, 27
- Bacmann, A., Taquet, V., Faure, A., Kahane, C., & Ceccarelli, C. 2012, *A&A*, 541, L12
- Bell, M. B., Feldman, P. A., Travers, M. J., et al. 1997, *ApJ*, 483, L61
- Berglund, M., & Wieser, M. 2011, *Pure Appl. Chem.*, 83, 397
- Blake, G. A., Sutton, E. C., Masson, C. R., & Phillips, T. G. 1987, *ApJ*, 315, 621
- Bottinelli, S., Ceccarelli, C., Lefloch, B., et al. 2004, *ApJ*, 615, 354
- Cernicharo, J., Marcelino, N., Roueff, E., et al. 2012, *ApJ*, 759, L43
- Cummins, S. E., Linke, R. A., & Thaddeus, P. 1986, *ApJS*, 60, 819
- Dismuke, K. I., Graham, W. R. M., & Weltner, W. 1975, *Journal of Molecular Spectroscopy*, 57, 127
- Elias, J. H. 1978, *ApJ*, 224, 857
- Foreman-Mackey, D. 2014, *blog Post: Mixture Models*, doi:10.5281/zenodo.15856
- Foreman-Mackey, D., Hogg, D. W., Lang, D., & Goodman, J. 2013, *PASP*, 125, 306
- Fossé, D., Cernicharo, J., Gerin, M., & Cox, P. 2001, *ApJ*, 552, 168
- Friberg, P., Hjalmarsen, A., Madden, S. C., & Irvine, W. M. 1988, *A&A*, 195, 281
- Garrod, R. T., & Herbst, E. 2006, *A&A*, 457, 927
- Goodman, J., & Weare, J. 2010, *Commun. Appl. Math. Comput. Sci.*, 5
- Gottlieb, C. A., Gottlieb, E. W., Thaddeus, P., & Kawamura, H. 1983, *ApJ*, 275, 916
- Herbst, E., & Cuppen, H. M. 2006, *Proceedings of the National Academy of Science*, 103, 12257
- Herbst, E., & van Dishoeck, E. F. 2009, *ARA&A*, 47, 427
- Hogg, D. W., Bovy, J., & Lang, D. 2010, *ArXiv e-prints* (arXiv:1008.4686)
- Kaifu, N., Ohishi, M., Kawaguchi, K., et al. 2004, *PASJ*, 56, 69
- Kenyon, S. J., Dobrzycka, D., & Hartmann, L. 1994, *AJ*, 108, 1872
- Matthews, H. E., Friberg, P., & Irvine, W. M. 1985, *ApJ*, 290, 609
- Mazzotti, F. J., Raghunandan, R., Esmail, A. M., Tulej, M., & Maier, J. P. 2011, *J. Chem. Phys.*, 134, 164303
- Milam, S. N., Savage, C., Brewster, M. A., Ziurys, L. M., & Wyckoff, S. 2005, *ApJ*, 634, 1126
- Müller, H. S. P., Schlöder, F., Stutzki, J., & Winnewisser, G. 2005, *Journal of Molecular Structure*, 742, 215
- Ohishi, M., Irvine, W. M., & Kaifu, N. 1992, in *IAU Symposium*, Vol. 150, *Astrochemistry of Cosmic Phenomena*, ed. P. D. Singh, 171
- Ohishi, M., & Kaifu, N. 1998, *Faraday Discussions*, 109, 205
- Pickett, H. M., Poynter, R. L., Cohen, E. A., et al. 1998, *J. Quant. Spec. Radiat. Transf.*, 60, 883
- Ruud, M., Loison, J. C., Hickson, K. M., et al. 2015, *MNRAS*, 447, 4004
- Senent, M. L., & Hochlaf, M. 2010, *ApJ*, 708, 1452
- Shen, L. N., Doyle, T. J., & Graham, W. R. M. 1990, *J. Chem. Phys.*, 93, 1597
- Taniguchi, K., Ozeki, H., Saito, M., et al. 2016, *ApJ*, 817, 147
- Vastel, C., Ceccarelli, C., Lefloch, B., & Bachiller, R. 2014, *ApJ*, 795, L2
- Vasyunin, A. I., & Herbst, E. 2013, *ApJ*, 769, 34
- Watanabe, N., & Kouchi, A. 2002, *ApJ*, 571, L173
- Woon, D. E. 1995, *Chemical Physics Letters*, 244, 45